The Strong Interactions, Flavour Physics and Beyond

by

Saba Zuberi

A thesis submitted in conformity with the requirements
for the degree of Doctor of Philosophy
Graduate Department of Physics
University of Toronto

Abstract

The Strong Interactions, Flavour Physics and Beyond

Saba Zuberi

Doctor of Philosophy

Graduate Department of Physics

University of Toronto

2010

In this thesis we use effective field theories of the strong interactions to improve our understanding of several quantities in the Standard Model of particle physics (SM). We also examine constraints on an extension of the SM scalar sector and study the implications for the Higgs mass.

We first examine an approach to extracting the Cabibbo-Kobayashi-Maskawa matrix element $|V_{ub}|$ via the relationship between the B meson decays $B \to X_u \ell \nu_l$ and $B \to X_s \gamma$, where X_i is any final state hadron containing a quark of flavour i. Model dependence is reduced in this approach since the non-perturbative shape function at leading order is universal and drops out; however the perturbative expansion at next-to-leading order is found to be poorly behaved. We carry out a renormalon analysis of the relationship between these spectra to examine higher order perturbative corrections and compare the fixed-order and log expansions. Our analysis can be used to estimate the perturbative uncertainty in the extraction of $|V_{ub}|$, which we show to be relatively small.

Next we take a step towards the broader goal of summing large phase space logarithms from a variety of jet algorithms using Soft Collinear Effective Theory (SCET). We develop a consistent approach to implementing arbitrary phase space constraints in SCET and demonstrate the connection between cutoffs in SCET and phase space limits. By considering several jet algorithms at next-to-leading order, we gain some insight into factorization of final state jets. In particular, we point out the connection between the

ultraviolet regulator and factorization.

Finally we consider a scalar sector that contains a colour-octet electroweak-doublet scalar, in addition to the SM Higgs. This extension contains the only scalar representations that Yukawa-couple to quarks and are consistent with minimal flavour violation. We examine constraints from electroweak precision data, direct production from LEPII and the Tevatron, and from flavour physics. We find both the Higgs and new scalars can be simultaneously light, with masses of $\mathcal{O}(100\,\mathrm{GeV})$. The data also allows all the scalars to be heavy, with masses of $\mathcal{O}(1\,\mathrm{TeV})$. The presence of the additional scalars removes the preference for a light Higgs, which normally emerges from fits to electroweak precision data.

Acknowledgements

I owe my deepest thanks to my advisor Michael Luke for everything that I have learnt from him about physics, for his collaboration and for the encouragement and perspective he has provided. The work in this thesis would not have been possible without my other collaborators, from whom I have learnt a great deal: Cliff Burgess, Francisco Campanario, William Man-Yin Cheung and Michael Trott. I would also like to thank Brian Batell and Simon Freedman for many useful discussions. I am grateful to my committee members, Erich Poppitz and Pierre Savard, for their support.

Finally I'd like to thank my parents, my siblings and Chris for seeing me through.

Contents

Chapter 1

Introduction

In the last twenty years the Standard Model of particle physics (SM) has withstood rigourous precision tests, from measurements at LEP of the properties of W and Z gauge bosons to the exploration of the flavour sector at B factories and the Tevatron. However the mechanism for electroweak symmetry breaking remains to be established and many open questions remain, ranging from understanding neutrino mass generation to explaining the observed asymmetry between baryons and anti-baryons in the universe. As a result the search for new physics beyond the SM actively continues with, broadly speaking, two complementary approaches. There are direct production searches, for example at the new energy frontier at the Large Hadron Collider (LHC), and indirect ones, where deviations from SM predictions are sought in lower energy precision measurements. Both approaches demand reliable theoretical predictions with quantifiable error estimates and in both a central challenge is controlling quantum chromodynamics (QCD) effects.

QCD has the property of asymptotic freedom, whereby the coupling of quarks and gluons, which varies as a function of energy, becomes large at low energies or long distances. In this regime quantitative predictions based on a perturbative expansion break down and strongly interacting particles bind together to form hadrons. High energy processes involving coloured particles, such as the energetic underlying collisions at col-

liders, can be well described by perturbation theory. However, even in such processes low energy QCD effects can spoil theoretical predictions since the final states that are observed experimentally are hadrons and not free quarks and gluons, therefore the details of hadronization can creep into the calculation of a given observable.

In order to restore predictive power, it is important to separate perturbative affects from non-perturbative ones. Consider the example of the total cross-section for hadron production in e^+e^- annihilation, to which the leading contribution in the strong coupling constant is given by e^+e^- annihilating to a quark anti-quark pair. For large centre of mass energy, Q, the quark anti-quark pair are created and move apart at a time scale of $\mathcal{O}(1/Q)$. The details of the much longer time scale low-energy or soft dynamics, which we do not know how to calculate, do not effect the $q\bar{q}$ production probability. Furthermore we know that the probability for the quark and anti-quark to hadronize is unity, therefore to leading order $\sigma(e^+e^- \to \text{hadrons}) = \sigma(e^+e^- \to q\bar{q})$, given sufficient smearing over resonances. Here we have separated the non-perturbative part from the perturbative underlying cross-section. The non-perturbative contribution is unity with corrections in powers of $1/Q$, where the complicated details of hadronization enter. There are also perturbative corrections to this relation such as $e^+e^- \to q\bar{q}g$. This illustrates the idea of factorization, which is the separation of a measured quantity into well-defined components that each depend on physics at a single scale to all orders in the strong coupling constant and is at the heart of calculating reliably in QCD.

For observables with more complicated constraints such as $\sigma(e^+e^- \to n-\text{jets})$ defined by some jet algorithm, or observables with hadrons in the initial state, such as in proton collisions, the form of the factorization theorem and the hadronic contribution can become much more complicated than the unity at leading order in the above example. In proton collisions to some final state Y, where the underlying hard process is $q\bar{q} \to Y$ the

factorized cross-section take the form

$$\sigma\left(pp \to Y + anything\right) = \int_0^1 \mathrm{d}x_1 \int_0^1 \mathrm{d}x_2 \sum_i f_i(x_1) f_i(x_2) \cdot \sigma\left(q_i(x_1 P)\bar{q}_i(x_2 P) \to Y\right) \quad (1.1)$$

This is a convolution over the fraction, x_1, x_2, of total momentum P, carried by the proton, with a sum over quark flavours i. The long distance non-perturbative physics of the proton is given by the parton distribution functions, $f_i(x)$. Quantitative predictions can still be made because the parton distribution function is a property of the proton and not the hard scattering process of interest. This non-perturbative contribution can therefore be measured in other processes.

The proof of factorization theorems is clearly important to making reliable quantitative predictions for processes involving the strong interactions. Effective field theories (EFTs) of QCD are useful because they make the separation of scales manifest at the level of the effective Lagrangian. As a result the proof of factorization theorems are much more tractable using EFTs than with traditional diagrammatic techniques; furthermore the EFT approach is systematically improvable.

In this thesis we use EFT techniques to systematically deal with QCD effects and improve our understanding of a variety of SM quantities. In particular, we first consider the Cabibbo-Kobayashi-Maskawa (CKM) matrix element $|V_{ub}|$, which is relevant to indirect precision constraints on new physics. We analyse the behaviour of the perturbative piece of factorized B meson decay rates and use this to estimate the perturbative uncertainty in a particular approach to extracting $|V_{ub}|$. Next we take a step towards understanding the form of the factorized expression for final state jet production for a given jet algorithm, an important process in the LHC environment. Finally we consider an extension of the SM scalar sector motivated by the flavour structure of the SM and use electroweak precision measurements as well as current direct production data to constrain the model.

1.1 Flavour Sector of the Standard Model

The flavour structure of the Standard Model arises from the Higgs Yukawa interaction, which generates quark masses when the Higgs gets a vacuum expectation value

$$\mathcal{L}_{\text{Yukawa}} = g_U^{ij} \bar{u}_R^i H^T \epsilon \, Q_L^j - g_D^{ij} \bar{d}_R^i H^\dagger Q_L^j + \text{h.c.} \tag{1.2}$$

where $g_{U,D}$ are the Yukawa matrices, $i\,j$ are flavour indices and

$$\epsilon = \begin{pmatrix} 0 & 1 \\ -1 & 0 \end{pmatrix}. \tag{1.3}$$

Since the mass and weak eigenstates are not diagonal in the same basis, the weak interaction allows for the flavour changing charged current transition between left handed up and down type quarks of the following form

$$\mathcal{L}_{int} = -\frac{g_2}{\sqrt{2}} \, \bar{u}_L^j \, \gamma_\mu \, V_{\text{CKM}}^{j\,k} \, d_L^k \, W^\mu + h.c. \tag{1.4}$$

where V_{CKM} is the CKM matrix, a 3×3 unitary matrix, j labels the generation and g_2 is the $SU(2)$ gauge coupling. There are, however, no flavour changing neutral currents at tree-level in the SM. With three generations, the CKM matrix can be expressed in terms of three angles and one complex phase, which gives rise to charge-parity (CP) violation. These are free parameters of the SM and it is therefore of interest to determine them accurately. Furthermore, it is experimentally very well established that a hierarchy exists in the entries of V_{CKM}. This non-trivial flavour structure provides important constraints on physics beyond the SM.

The flavour structure in the CKM matrix is made clear by the Wolfenstein parameterization [1], which expresses the matrix as an expansion in λ, the charged weak current coupling of the up to the strange type quark. To $\mathcal{O}(\lambda^4)$ it is given by

$$V_{\text{CKM}} = \begin{pmatrix} V_{ud} & V_{us} & V_{ub} \\ V_{cd} & V_{cs} & V_{cb} \\ V_{td} & V_{ts} & V_{tb} \end{pmatrix} = \begin{pmatrix} 1 - \frac{\lambda^2}{2} & \lambda & A\,\lambda^3(\rho - i\eta) \\ -\lambda & 1 - \frac{\lambda^2}{2} & A\,\lambda^2 \\ A\,\lambda^3(1 - \rho - i\eta) & -A\lambda^2 & 1 \end{pmatrix} \tag{1.5}$$

where $\lambda = 0.2257^{+0.0009}_{-0.0010}$ [2]. The unitarity of the CKM matrix gives rise to six vanishing constraints, each of which can be represented by a triangle in the complex plane. A convenient representation is obtained from

$$V_{ud}V_{ub}^* + V_{cd}V_{cb}^* + V_{td}V_{tb}^* = 0, \tag{1.6}$$

illustrated in Fig. 1.1. To test the consistency of this picture it is important to overconstrain the unitarity triangle with independent measurements. The angle $\sin 2\beta$ has been well measured, with $\sin 2\beta = 0.681 \pm 0.025$ [2]. It is therefore of particular interest to accurately determine the side opposite the angle β which depends on both V_{cb} and V_{ub}. The consistency of the independent determinations of the angle β and the side opposite would provide an important check of the CKM picture and would serve to constrain new physics.

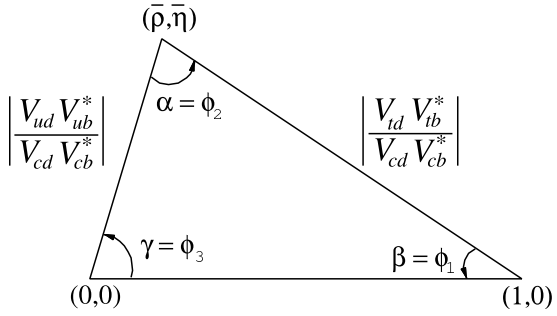

Figure 1.1: Representation of the unitarity triangle. The apex is $(\bar{\rho}, \bar{\eta}) = (\rho, \eta)(1 - \lambda^2/2) + \mathcal{O}(\lambda^4)$ [2].

B mesons provide an excellent testing ground of the flavour structure of the SM, because the separation of scales $m_b \gg \Lambda_{\rm QCD}$ allows short distance physics to be consistently separated from the details of hadronization using heavy quark effective theory (HQET) and the operator product expansion (OPE), discussed in Chapter 2. With these techniques, $|V_{cb}|$ has been determined with a 2% uncertainty from inclusive decays $B \to X_c \ell \nu_\ell$, where X_c denotes any state originating from the decay to a charm quark [3]. The extraction of $|V_{ub}|$ from inclusive decays $B \to X_u \ell \nu_\ell$ is more theoretically involved [4, 5]

and has a larger uncertainty, of order 10% [2]. The situation is even worse for exclusive decays such as $\bar{B} \to \pi \ell \bar{\nu}_\ell$, due to theoretical uncertainties in determining form factors. The difficulty for $|V_{ub}|$ arises because B mesons decay predominantly via the $b \to c$ quark level transition, making it challenging to measure the fully inclusive $B \to X_u \ell \nu_\ell$ decay rate. Eliminating charm background severely restricts the phase space in which $B \to X_u \ell \nu_\ell$ can be measured and increases the sensitivity of the rate to non-perturbative effects. As will be described in Chapter 2.2, the techniques used so effectively for $|V_{cb}|$ are no longer valid and instead a non-perturbative distribution function, called the shape function, arises at leading order. The shape function [6] is universal in B decays and it can either be modelled or eliminated by relating $B \to X_u \ell \nu_\ell$ to another inclusive rare B decay, $B \to X_s \gamma$. In Chapter 3 we focus on the latter approach since it minimizes model dependence.

1.2 Final State Jet Production

The hadron collider environment requires an understanding of QCD over a wide range of scales, from partonic hard scattering to the description of initial state protons and the evolution of final state jets. Factorization is critical to this understanding because it allows us to separate measured quantities that depend on physics at different scales into components that each depend on a single scale. As a result a controlled perturbative expansion is obtained and non-perturbative effects can be isolated.

While calculating QCD effects at colliders is a long-standing and challenging program with many developments from traditional QCD techniques (see for example [7, 8, 9]), there has been recent demonstrated potential for soft-collinear effective theory (SCET) to extend previous results, from event shape variables to event generators [10, 11, 12]. SCET is an effective theory of the strong interactions, which provides a model independent, systematically improvable framework to describe the interactions of energetic jets and

soft quarks and gluons [6, 13, 14, 15, 16]. The effective theory naturally separates physics at hard, collinear and soft scales, and consequently is useful in proving factorization, resumming large logarithms and parameterizing non-perturbative corrections.

A necessary ingredient in controlling QCD effects at colliders is proving factorization for final state jet production defined by a jet algorithm. A jet algorithm is a prescription by which final state particles in an event are grouped together. At each order in perturbation theory this corresponds to a division of phase space into different numbers of jets. Observables that integrate over the phase space given by a jet definition typically give rise to logarithms of the ratio of scales associated with the jet algorithm, of the form $\alpha_s^n \ln^m$, $m \leq 2n$. These phase space logarithms can be large, for example when the jets are constrained to be in narrow cones, and can spoil the perturbative expansion. We would therefore like to be able to resum them.

It is difficult to extend traditional QCD techniques to resum large logarithms to arbitrary order in the log expansion. Furthermore there are a class of observables, called non-global observables [17], in which cuts are placed on restricted angular regions of phase space, for which it is not known how to analytically resum logarithms beyond leading order with perturbative QCD. The two-jet rate defined with the Sterman-Weinberg cone algorithm [18] is one such example. We would therefore like to be able to address these questions using EFT techniques. In particular we would like to be able to factorize the n-jet cross section and resum the large logarithms of phase space cuts for a given jet algorithm using SCET. In Chapter 4 we take a step towards this broader goal by developing a consistent approach to implementing jet algorithm phase space constraints in the effective theory.

1.3 Flavour Constraints and the Scalar Sector

The quadratic dependence of the Higgs mass on the scale of new physics, Λ, leads, from considerations of naturalness, to the perspective that $\Lambda \sim \mathcal{O}(\text{TeV})$ and that the SM is a low energy effective theory [19]

$$\mathcal{L}_{\text{eff}}(E < \Lambda) = \mathcal{L}_{SM} + \sum_{i,p} \frac{c_i}{\Lambda^p} O_i^{(4+p)}. \tag{1.7}$$

However the excellent agreement between the SM and data, particularly in the flavour sector, restricts the scale of new physics for generic operators to be parametrically larger than the electroweak scale. This leads to the expectation that new physics will have a non-trivial structure and will respect the approximate symmetries that we observe experimentally, such as custodial SU(2). However flavour $\text{SU}(3)_{U_R} \times \text{SU}(3)_{D_R} \times \text{SU}(3)_{Q_L}$ is not a symmetry of the SM. It is broken by the Yukawa couplings of the quarks and the Higgs field, Eq. (1.2). Instead we assume that the underlying theory has this flavour symmetry and that it is broken to generate the Yukawa matrices. This is implemented by the Minimal Flavour Violation (MFV) criteria [20, 21, 22, 23, 24, 25]. It requires that by promoting the Yukawa matrices to spurions which transform as $g_U \sim (\mathbf{3_U}, \bar{\mathbf{3}}_\mathbf{Q})$ and $g_D \sim (\mathbf{3_D}, \bar{\mathbf{3}}_\mathbf{Q})$, all new physics terms must be invariant under the flavour group. Satisfying MFV leads to the fact that all new physics Yukawa couplings must be proportional to the SM Yukawas, which are proportional to the quark mass matrices. It follows that all Yukawa matrices will be diagonal in the same basis as the quark mass matrices. This naturally suppresses tree-level flavour changing neutral currents and generates structure in the effective theory for new physics without requiring parameters in the theory to be small. Such an approach can be viewed as an extension of the work of Glashow and Weinberg [26].

It has been shown [27] that there is only one other scalar representation, in addition to the SM Higgs, that can Yukawa couple to quarks and is consistent with MFV. It is $(\mathbf{8}, \mathbf{2})_{\mathbf{1/2}}$ under the SM gauge group $\text{SU}(3) \times \text{SU}(2) \times \text{U}(1)$. In Chapter 5 we consider

an extension of the SM proposed by Manohar and Wise [27], which contains one such colour octet electroweak doublet scalar. By examining electroweak precision data, flavour measurements and direct production bounds, we ask whether such a theory consistent with MFV satisfies current data constraints and what the implications are for the Higgs mass.

1.4 Organization of this thesis

We begin in Chapter 2 by reviewing HQET, as well as the tools used to calculate inclusive B meson decays. We continue our review by discussing the other effective theory of the strong interactions used in this thesis, SCET. In Chapter 3 we study an approach to extracting the CKM matrix element $|V_{ub}|$ by examining higher order peturbative corrections using a renormalon analysis. This material originally appeared in "Higher order peturbative corrections to the determination of $|V_{ub}|$ from the P_+ spectrum in $B \to X_u \ell \nu_\ell$" [28]. In Chapter 4 we move on to study jet algorithms in SCET, where we use the explicit calculation of several next-to-leading order two-jet cross sections to gain some useful insights into the factorization of final state jets. The contents of this chapter were published in "Phase Space and Jet definitions in SCET" [29].

We then shift from work aimed at improving our understanding of SM quantities to studying constraints on an extended scalar sector model, motivated by the flavour structure of the SM, in Chapter 5. In particular, we examine constraints on the model and the implications for the Higgs from electroweak precision data, flavour and direct production bounds. Chapter 5 was published in "Light Octet Scalars, a Heavy Higgs and Minimal Flavour Violation" [30]. Finally in Chapter 6 we conclude.

Chapter 2

Effective Theories of the Strong Interactions

QCD is asymptotically free and at long distances perturbation theory breaks down and strongly interacting particles bind together to form hadrons. The factorization of physics at different scales into separate well-defined components is therefore critical to making reliable predictions for processes involving hadrons. Factorization enables us to parameterize our ignorance by separating short distance perturbatively calculable effects from long distance non-perturbative ones and prevents the perturbative expansion from being spoiled by the presence of large logarithms of the ratio of scales in the problem.

The EFT approach to the strong interactions is useful because it provides a systematically improvable framework with which to factorize physics at different scales. It is formulated by utilizing the separation of scales in a physical process to construct a small parameter in which to expand the full theory, QCD. This leads to a simplification of the theory at leading order in the expansion.

In this chapter we will discuss the two EFTs of QCD that we make use of in this thesis, HQET and SCET. We also discuss the techniques used to calculate inclusive B meson decays, which rely on the use of HQET and the OPE, which we will exploit in

Chapter 3 when we consider a method to extract $|V_{ub}|$.

2.1 Heavy Quark Effective Theory

HQET describes the interaction of a single heavy quark, bottom or charm, that interacts with light quarks and gluons. It has been extensively and successfully applied to the study of B meson decays [31]. The typical momentum of the light degrees of freedom is $\Lambda_{\rm QCD} \sim 300\,{\rm MeV}$, which is much smaller than the mass of the heavy quark, m_Q. Therefore in the limit the Compton wavelength of the heavy quark, $1/m_Q$, goes to zero the low energy degrees of freedom cannot resolve the structure of the heavy quark; it appears simply as a static colour source. The heavy quark has spin 1/2 and therefore a chromomagnetic moment of $\mu_Q = g/(2m_Q)$. In the $m_Q \to \infty$ limit, $\mu_Q \to 0$ and therefore the interaction between the spin of the heavy quark and light degrees of freedom is suppressed. This leads to heavy quark spin-flavour symmetry, which we expect will be broken at $\mathcal{O}(1/m_Q)$. As we shall see, the effective theory makes this explicit.

Since interactions with light degrees of freedom have momentum transfers of $\mathcal{O}(\Lambda_{\rm QCD})$, it is useful to decompose the momentum of the heavy quark in to a small piece, the residual momentum $k \sim \Lambda_{\rm QCD}$, and a large piece which is unchanged by the interactions

$$p_Q^\mu = m_Q v^\mu + k^\mu. \tag{2.1}$$

In the heavy quark limit v^μ is conserved and acts like a label, while k^μ is dynamical. We therefore redefine the QCD heavy quark field to remove the large momentum component

$$\begin{aligned} Q(x) &= \sum_v e^{-im_Q v\cdot x} Q_v(x) = \sum_v e^{-im_Q v\cdot x}(P_+ Q_v(x) + P_- Q_v(x)) \\ &= \sum_v e^{-im_Q v\cdot x}(h_v(x) + H_v(x)) \end{aligned} \tag{2.2}$$

where we have defined the projection operators $P_{+(-)} = (1 \pm \not{v})/2$, which project out the upper (lower) two components of the spinor. The quark part of the QCD Lagrangian

becomes

$$\begin{aligned}\mathcal{L}_{QCD} &= \bar{Q}(x)\left(i\not{D} - m_Q\right)Q(x) = \bar{Q}_v(x)\left(i\not{D} + m_Q\not{v} - m_Q\right)Q_v(x) \\ &= \bar{h}_v(x) iv\cdot D h_v(x) - \bar{H}_v(x)\left(iv\cdot D + 2m_Q\right)H_v(x) \\ &\quad + \bar{H}_v(x) i\not{D}_\perp h_v(x) + \bar{h}_v(x) i\not{D}_\perp H_v(x) \end{aligned} \tag{2.3}$$

where we have used $P_\pm \gamma^\mu P_\pm = \pm\, v^\mu$ and $P_\pm \gamma^\mu P_\mp = \gamma_\perp^\mu$. The kinetic term of the H_v field is suppressed by $\Lambda_{\rm QCD}/m_Q$ relative to the leading quadratic piece and so is not dynamical in the effective theory and can be removed using its equation of motion

$$\mathcal{L} = \bar{h}_v(x) iv\cdot D h_v(x) + \bar{h}_v(x) i\not{D}_\perp \frac{1}{iv\cdot D + 2m_Q} i\not{D}_\perp h_v(x). \tag{2.4}$$

The heavy quark field of the effective theory, h_v, annihilates heavy quarks with velocity v, but does not create antiquarks. We can now expand the quark part of the QCD Lagrangian in powers of $1/m_Q$ to obtain the HQET Lagrangian to order $\mathcal{O}(1/m_Q^2)$

$$\mathcal{L}_{HQET} = \bar{h}_v(x) iv\cdot D h_v(x) + \frac{1}{2m_Q}\bar{h}_v(x)(iD_\perp)^2 h_v(x) - \frac{g}{4m_Q}\bar{h}_v(x)\sigma_{\alpha\beta}G^{\alpha\beta}h_v(x) \tag{2.5}$$

where $\sigma^{\alpha\beta} = i[\gamma^\alpha, \gamma^\beta]/2$ and $igG^{\alpha\beta} = [D^\alpha, D^\beta]$. We can see from Eq. (2.5) that the leading term in the HQET Lagrangian has an additional spin-flavour symmetry as expected, with $\mathcal{O}(1/m_Q)$ kinetic and spin corrections.

The key point is that the formulation of the effective theory as an expansion in small parameter $\Lambda_{\rm QCD}/m_b$ makes this approximate symmetry manifest and allows corrections to this limit to be calculated systematically. The enhanced symmetry is a vaulable tool, and in the next section we will describe how HQET is used along with the OPE to calculate inclusive B meson decays. We will use the results outlined below in Chapter 3 when we consider a method to extract $|V_{ub}|$.

2.2 Inclusive B Decays and the Operator Product Expansion

In order to calculate B meson decays the effective weak Hamiltonian is used, in which the W propagator as been expanded in powers of $1/M_W$. For $b \to u$ transitions it is

$$H_{\text{eff}} = \frac{4G_F}{\sqrt{2}} V_{ub}\, \bar{u}_L \gamma^\mu b_L \bar{\ell}_L \gamma_\mu \nu_L \tag{2.6}$$

and for $b \to s$ processes it is given by [32]

$$H_{\text{eff}} = \frac{4G_F}{\sqrt{2}} V_{tb} V_{ts}^* \sum_{i=1}^{8} C_i(\mu) O_i(\mu) \tag{2.7}$$

where

$$\begin{aligned}
O_1 &= (\bar{c}_{L\beta}\gamma^\mu b_{L\alpha})(\bar{s}_{L\alpha}\gamma_\mu c_{L\beta}) & O_2 &= (\bar{c}_{L\alpha}\gamma^\mu b_{L\alpha})(\bar{s}_{L\beta}\gamma_\mu c_{L\beta}) \\
O_3 &= \sum_q (\bar{s}_{L\alpha}\gamma^\mu b_{L\beta})(\bar{q}_{L\beta}\gamma_\mu q_{L\beta}) & O_4 &= \sum_q (\bar{s}_{L\alpha}\gamma^\mu b_{L\beta})(\bar{q}_{L\beta}\gamma_\mu q_{L\alpha}) \\
O_5 &= \sum_q (\bar{s}_{L\alpha}\gamma^\mu b_{L\alpha})(\bar{q}_{R\beta}\gamma_\mu q_{R\beta}) & O_6 &= \sum_q (\bar{s}_{L\alpha}\gamma^\mu b_{L\beta})(\bar{q}_{R\beta}\gamma_\mu q_{R\alpha}) \\
O_7 &= \tfrac{e}{16\pi^2} m_b \bar{s}_{L\alpha} \sigma^{\mu\nu} b_{R\alpha} F_{\mu\nu} & O_8 &= \tfrac{g}{16\pi^2} m_b \bar{s}_{L\alpha} \sigma^{\mu\nu} T^a_{\alpha\beta} b_{r\beta} G^a_{\mu\nu}
\end{aligned}$$

The dominant contribution to $B \to X_s\gamma$ is given by O_7, which is the only operator that contributes at tree-level, however under renormalization it mixes with all seven other operators.

Decays with photons and leptons in the final state are useful to consider since the final state particles do not interact strongly so the matrix element of H_{eff} may be factorized into a hadronic matrix element and a perturbatively calculable leptonic piece, $L_{\alpha\beta}$. For example, for $B \to X_u \ell \nu_\ell$

$$d\Gamma \sim \sum_{X_u} \langle B | J_{bu}^{\dagger\alpha} | X_u \rangle \langle X_u | J_{bu}^{\beta} | B \rangle L_{\alpha\beta}. \tag{2.8}$$

The hadronic matrix element can be related to the imaginary part of the forward scattering amplitude of the time ordered product of currents, $T^{\alpha\beta}$, by the optical theorem,

where

$$T^{\alpha\beta} = -i \int d^4x e^{-iq.x} \langle B|T\{J_{bu}^{\dagger\alpha}(x), J_{bu}^{\beta}(0)\}|B\rangle. \tag{2.9}$$

The forward scattering matrix element develops an imaginary piece along a branch cut when real intermediate states go on-shell. The locations of the branch cuts are determined by kinematics. Let p_X be the momentum of the hadronic products and q the momentum of the leptons. The rest frame of the B meson can be used to define a four velocity such that its momentum is $p_B^\mu = m_B v^\mu$. The forward scattering amplitude $T^{\mu\nu}$ is then a function of both q^2 and $v \cdot q$. Its analytic structure is shown in Fig. 2.1. The branch cut on the left corresponds to the decay of interest $B \to X_u \ell \nu_\ell$ and the other involves the scattering process $B\ell\nu_\ell \to X_{bb}$.

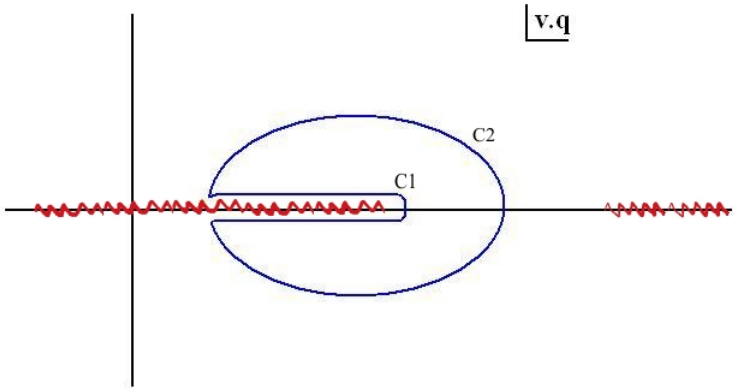

Figure 2.1: The analytic structure of the forward scattering matrix element for fixed q^2 in the complex $v \cdot q$ plane. The branch cut on the left corresponds to the decay process of interest which arises for $v \cdot q < \frac{m_B^2 + q^2 - m_{\rm Xmin}^2}{2m_B}$.

The integral over phase space for the decay rate is given by an integral over intermediate physical bound states, contour C_1, where $T^{\mu\nu}$ is non-local and perturbation theory breaks down. The contour C_1 can however be deformed to contour C_2, a large distance away from the cuts, where the large scale is set by $m_b \gg \Lambda_{\rm QCD}$. Along this contour the intermediate states are constrained to be far off-shell and these virtual, $\mathcal{O}(m_b)$, degrees of freedom can be integrated out. The time ordered product of currents is replaced by

an OPE in powers of $1/m_b$ [33]

$$-i\int \mathrm{d}^4x e^{-iq\cdot x} T\{J_{bu}^{\dagger\alpha}(x), J_{bu}^{\beta}(0)\} \sim \frac{1}{m_b}\left(O_0 + \frac{1}{2m_b}O_1 + \frac{1}{4m_b^2}O_2 + \cdots\right). \tag{2.10}$$

Since all hadronic momentum transfers are now below m_b, HQET may be used in the OPE and the coefficients of these operators are calculated perturbatively using matching calculations.

The validity of the OPE relies on being able to deform the contour away from the physical cut. This clearly fails in the region where contours C_1 and C_2 meet, however it is expected that the smearing effect of integrating over a large enough region of phase space will yield reliable results. The contour can also not be sufficiently deformed when the endpoints of the two branch cuts in Fig. 2.1 approach each other, which is the case when $q^2 \to m_B^2$.

As discussed in Chapter 1.1, rare decays require cuts on the overwhelming background from $b \to c$ transitions, restricting for example $B \to X_u \ell \nu_\ell$ to be measured in regions with small M_{X_u} which are less populated by the heavier charm states. The impact on the OPE of the restriction on phase space depends on the observable. In Chapter 3 we consider the partial rate with a cut on P_+ [34]

$$P_+ = E_X - |\vec{P}_X| = (m_B v - q)\cdot n, \qquad P_- = E_X + |\vec{P}_X| = (m_B v - q)\cdot \bar{n} \tag{2.11}$$

where q is the lepton neutrino four momentum, n and $\bar{n}$ are light-like four vectors in the $\pm\vec{q}$ direction and v is the four velocity of the B meson. The P_+ spectra has been measured by BaBar and Belle [35]. The cut used in these measurements, and the one we consider in Chapter 3, removes final states with $M_X^2 = P_+P_- < M_D^2$, in particular $P_+ < M_D^2/M_B^2 \sim 0.66\text{GeV}$. This corresponds to a region of large $P_- \sim \mathcal{O}(m_B)$ and small $P_+ \sim \mathcal{O}(\Lambda_{\text{QCD}})$

The convergence of the OPE for this spectra can be illustrated by considering the expansion of the tree-level forward scattering matrix element in the effective theory, see

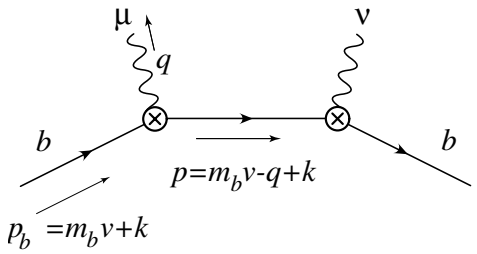

Figure 2.2: The tree level diagram for the forward scattering matrix element.

Fig. 2.2. The hadronic variables $P_\pm$ can be easily related to the following partonic ones

$$p_+ = (m_b v - q)\cdot n, \qquad p_- = (m_b v - q)\cdot \bar{n} \tag{2.12}$$

by $P_\pm = p_\pm + \Lambda$, where $\Lambda = m_B - m_b$. In terms of these variables the forward scattering matrix becomes

$$\frac{\bar{b}_v \gamma^\mu P_L (m_b \not{v} - \not{q} + \not{k}\gamma^\nu P_L b_v}{(m_b v - q + k)^2 + i\epsilon} = \frac{\bar{b}_v \gamma^\mu P_L (p_- \not{n}/2 + p_+ \not{\bar{n}}/2 + \not{k})\gamma^\nu P_L b_v}{p_+\, p_- + k\cdot\bar{n}\, p_+ + k\cdot n\, p_- + k^2 + i\epsilon}. \tag{2.13}$$

Expanding in $\Lambda_{\rm QCD}/m_b$ with p_- of order m_b and p_+ and the residual momenta, k, of order $\Lambda_{\rm QCD}$ gives

$$\bar{b}_v \gamma^\mu P_L \frac{p_- \not{n}/2}{p_+\, p_- + k\cdot n\, p_- + i\epsilon}\gamma^\nu P_L b_v + \mathcal{O}\left(\frac{\Lambda_{QCD}}{m_b}\right). \tag{2.14}$$

The imaginary piece is given by

$$\mathrm{Im}\frac{1}{p_+ + k\cdot n + i\epsilon} = -\pi\,\delta(p_+ + k\cdot n). \tag{2.15}$$

The leading order operator in the OPE that gives this contribution is clearly not a local operator. It is instead given by the shape function [6]

$$f(w) \equiv \langle B|\bar{b}_v\,\delta(p_+ + in\cdot D)\,b_v|B\rangle \tag{2.16}$$

in which the b quarks are separated along a light-cone. This is seen more clearly in position space where we obtain a Wilson line

$$\tilde{f}(s) \equiv \langle B|\bar{b}_v(0)\,P\exp\left(\int_0^s \mathrm{d}s\, n\cdot A(s\,n)\right)\,b_v(s)|B\rangle. \tag{2.17}$$

In this region, which corresponds to $M_X^2 \sim m_b\,\Lambda_{\rm QCD}$, the differential decay rate is given by a nonlocal OPE of the form

$$\mathrm{d}\Gamma \sim \int_{-\infty}^{\infty} \mathrm{d}w\, C(w) f(w) + \mathcal{O}\left(\frac{\Lambda_{QCD}}{m_b}\right). \tag{2.18}$$

The leading order shape function describes the non-perturbative distribution of the light-cone component of the residual momentum inside the B meson. It is universal, unlike the subleading operators that arise, and can either be modelled using constraints from processes such as $B \to X_s\gamma$ or it can be removed by directly relating $B \to X_u\ell\nu_\ell$ to $B \to X_s\gamma$ [36, 37, 38]. We consider the latter approach in Chapter 3. Notice that if $M_X^2 \sim \mathcal{O}(\Lambda_{\rm QCD}^2)$, which means both P_+ and P_- are of order $\Lambda_{\rm QCD}$, there would be no expansion of the terms in Eq. (2.13) and the OPE would break down as expected, since the decay would be dominated by a small number or resonances.

2.3 Soft Collinear Effective Theory

SCET is an effective theory of QCD that describes states with large energy, Q, and small invariant mass [6, 13, 14, 15, 16]. To construct the theory it is useful to first define null vectors n^μ and $\bar{n}^\mu$, such that $n^2 = 0, \bar{n}^2 = 0$ and $n\cdot\bar{n} = 2$. Any vector can be decomposed as

$$p^\mu = p^+\frac{\bar{n}^\mu}{2} + p^-\frac{n^\mu}{2} + p_\perp^\mu \tag{2.19}$$

where $p^+ \equiv n\cdot p$, $p^- \equiv \bar{n}\cdot p$ and for short-hand we write $p = (p^+, p^-, p_\perp)$. Since energetic particles with small mass travel close to the light-cone there is a large separation between the light-cone components, we therefore construct the small parameter $\lambda \sim p_\perp/p^-$ in which to expand the full theory. It follows that a particle collinear to the n-direction has $p^- \sim Q$ and $p_\perp \sim \lambda\, Q$ and for fluctuations near the mass shell $p^+ \sim p_\perp^2/p^- \sim \lambda^2\, Q^2$. The collinear scaling in SCET is therefore $p_c = Q(\lambda^2, 1, \lambda)$. In order to correctly reproduce the infrared physics of QCD, the effective theory also requires soft particles with scaling

$p_s = Q(\lambda^2, \lambda^2, \lambda^2)$ [6]. The effective theory containing these soft and collinear modes is referred to as SCET_I and is the theory we shall focus on here and utilize in Chapter 4.

In order to obtain the SCET Lagrangian, we begin as in HQET by decomposing the quark momentum collinear in the n-direction into a large label piece, denoted by a tilde, and residual soft component

$$p^\mu = \tilde{p}^\mu + k^\mu \tag{2.20}$$

where $k \sim \lambda^2 Q$ and the label piece $\tilde{p}$ contains both $\tilde{p}^- \sim Q$ and $\tilde{p}_\perp \sim \lambda Q$. The QCD field is re-defined to explicitly separate label and residual momenta

$$Q(x) \;=\; \sum_{\tilde{p}} e^{-i\tilde{p}\cdot x} Q_{n,p}(x) \tag{2.21}$$

where the field subscript p refers to the label momenta and derivatives acting on $Q_{n,p}(x)$ give terms of order $\lambda^2 Q$. Projection operators, $P_n = \not{n}\bar{\not{n}}/4$ and $P_{\bar{n}} = \bar{\not{n}}\not{n}/4$, are used to separate the large (n) and small ($\bar{n}$) components of the re-defined QCD field

$$Q_{n,p}(x) = P_n Q_{n,p}(x) + P_{\bar{n}} Q_{n,p}(x) = \xi_{n,p}(x) + \xi_{\bar{n},p}(x) \tag{2.22}$$

such that $\not{n}\xi_{n,p} = 0$ and $\bar{\not{n}}\xi_{\bar{n},p} = 0$. With this re-definition the quark part of the QCD Lagrangian can then be written as

$$\begin{aligned}
\mathcal{L}_{QCD} &= \bar{Q}(x) i\not{D} Q(x) \\
&= \sum_{\tilde{p},\tilde{p}'} e^{-i(\tilde{p}-\tilde{p}')\cdot x} \left(\bar{\xi}_{n,p'}(x) + \bar{\xi}_{\bar{n},p'}(x)\right) (\not{\tilde{p}} + i\not{D}) \left(\xi_{n,p}(x) + \xi_{n,p}(x)\right) \\
&= \sum_{\tilde{p},\tilde{p}'} e^{-i(\tilde{p}-\tilde{p}')\cdot x} \Big[\bar{\xi}_{n,p'}(x) \frac{\bar{\not{n}}}{2} (in\cdot D)\, \xi_{n,p} + \bar{\xi}_{\bar{n},p'}(x) \frac{\not{n}}{2} \left(\tilde{p}^- + i\bar{n}\cdot D\right) \xi_{\bar{n},p}(x) \\
&\qquad\qquad + \bar{\xi}_{n,p'} (\not{\tilde{p}}_\perp + i\not{D}_\perp)\, \xi_{\bar{n},p} + + \bar{\xi}_{\bar{n},p'} (\not{\tilde{p}}_\perp + i\not{D}_\perp)\, \xi_{n,p} \Big] .
\end{aligned} \tag{2.23}$$

The kinetic term of the $\xi_{\bar{n},p}$ field is suppressed by λ^2 relative to the leading quadratic piece and therefore we can remove it from the Lagrangian using the equations of motion

$$\xi_{\bar{n},p}(x) = \frac{1}{\tilde{p}^- + i\bar{n}\cdot D} (\tilde{p}_\perp + i\not{D}_\perp) \frac{\bar{\not{n}}}{2} \xi_{n,p}(x), \tag{2.24}$$

and the quark Lagrangian then becomes

$$\mathcal{L} = \sum_{\tilde{p},\tilde{p}'} e^{-i(\tilde{p}-\tilde{p}')\cdot x} \bar{\xi}_{n,p'}(x) \left[(in\cdot D) + (\not{p}_\perp + i\not{D}_\perp) \frac{1}{\tilde{p}^- + i\bar{n}\cdot D} (\not{p}_\perp + i\not{D}_\perp) \right] \frac{\not{\bar{n}}}{2} \xi_{n,p}. \quad (2.25)$$

The n-collinear quark interacts with gluons with soft scaling, $A^s \sim Q(\lambda^2, \lambda^2, \lambda^2)$, and collinear scaling, $A^c \sim Q(\lambda^2, 1, \lambda)$. Both of these gluon fields are present in the covariant derivatives in Eq. (2.25) and in order to obtain a Lagrangian with a consistent expansion in λ, we must expand these terms.

As with the collinear quark field, the effective theory collinear gluon field is defined by removing the large momentum component

$$A^c = \sum_{\tilde{q}} e^{-i\tilde{q}\cdot x} A^c_{n,q}(x). \quad (2.26)$$

In order to be able to pull out the sum over label momenta of the collinear gluons in Eq. (2.25), it is useful to introduce a label operator [14], $\mathcal{P}^\mu = \bar{\mathcal{P}}\, n^\mu/2 + \mathcal{P}^\mu_\perp$, which acts on fields with labels to give factors of large label momenta

$$\begin{aligned} &\mathcal{P}^\mu(\phi^\dagger_{n,q1}\, \phi^\dagger_{n,q2} \dots \phi_{n,p1}\, \phi_{n,p2} \dots) \\ &\qquad = (\tilde{p}_1^\mu + \tilde{p}_2^\mu \cdots - \tilde{q}_1^\mu - \tilde{q}_2^\mu)(\phi^\dagger_{n,q1}\, \phi^\dagger_{n,q2} \dots \phi_{n,p1}\, \phi_{n,p2} \dots). \end{aligned} \quad (2.27)$$

The derivative can then be written as

$$\begin{aligned} i\partial^\mu \sum_{\tilde{p}} e^{-i\tilde{p}\cdot x} \phi_{n,p}(x) &= \sum_{\tilde{p}} e^{-i\tilde{p}\cdot x} (\mathcal{P}^\mu + i\partial^\mu) \phi_{n,p}(x) \\ &= \sum_{\tilde{p}} e^{-ix\cdot\mathcal{P}} (\mathcal{P}^\mu + i\partial^\mu) \phi_{n,p}(x) \end{aligned} \quad (2.28)$$

where the ordinary derivative on the left-hand side in Eq. (2.28) gives only residual momenta, $\mathcal{O}(\lambda^2 Q)$.

We can now express the covariant derivatives in Eq. (2.25) as

$$\begin{aligned} i\bar{n}\cdot D^c &= \bar{\mathcal{P}} + g\,\bar{n}\cdot A_{n,q} \\ iD^c_\perp &= \mathcal{P}_\perp + g\,\bar{n}\cdot A^\perp_{n,q} \\ in\cdot D &= in\cdot\partial + g\,n\cdot A_{n,q} + g\,n\cdot A_s \end{aligned} \quad (2.29)$$

where the superscript c denotes that we have dropped subleading terms in λ. This gives us the leading order SCET quark Lagrangian

$$\mathcal{L}_{SCET} = \sum_{\tilde{p}_i} e^{-ix\cdot\mathcal{P}} \bar{\xi}_{n,p'}(x) \left[(in\cdot D) + i\not{D}^c_\perp \frac{1}{i\bar{n}\cdot D^c} i\not{D}^c_\perp \right] \frac{\not{\bar{n}}}{2} \xi_{n,p}(x). \tag{2.30}$$

There are several interesting features of this Lagrangian. Unlike in HQET where the label v is conserved in interactions with gluons, in SCET the interaction of a collinear quark with a collinear gluon changes its label momenta. The large overall phase and sum over labels in Eq. (2.30) enforces label momentum conservation. Soft gluons appear only in the $n\cdot D$ term and it is only this component of the residual momentum that is conserved at vertices.

The non-local $1/\bar{n}\cdot D$ term in the Lagrangian is $\mathcal{O}(Q)$ and gives rise to the coupling of n-collinear quarks to the $\bar{n}\cdot A_n$ component of arbitrary numbers of collinear gluons, which are not suppressed in the effective theory. These interactions can be expressed in terms of a collinear Wilson line

$$\begin{aligned} W &= \sum_{m=0}^{\infty} \sum_{\text{perms}} \frac{(-g)^m}{m!} \frac{\bar{n}\cdot A^{a_1}_{n,q_1} \cdots \bar{n}\cdot A^{a_m}_{n,q_m}}{\bar{n}\cdot q_1\, \bar{n}\cdot(q_1+q_2)\cdots \bar{n}\cdot(\sum_{i=1}^m q_i)} T^{a_m}\cdots T^{a_1} \\ &= \left[\sum_{\text{perms}} \exp\left(-g \frac{1}{\bar{\mathcal{P}}}\, \bar{n}\cdot A_{n,q} \right) \right], \end{aligned} \tag{2.31}$$

which in position space is

$$W_n(x) = P \exp\left[i\, g \int_{-\infty}^{x} \mathrm{d}s\, \bar{n}\cdot A_n(s\bar{n}) \right] \tag{2.32}$$

where P denotes path ordering. The Wilson line arises from integrating out the off-shell propagators in the interaction of n-collinear gluons with $\bar{n}$-collinear quark fields, see Fig. 2.3. In fact collinear gauge invariance can be used to show, for a function, f,

$$f\left(i\bar{n}\cdot D\right) = f\left(\bar{\mathcal{P}} + g\,\bar{n}\cdot A_{n,q}\right) = W_n f(\bar{\mathcal{P}}) W_n^\dagger \tag{2.33}$$

and so all gauge invariant combinations of $\bar{n}\cdot A$ appear only in n-collinear Wilson lines [13]. The SCET quark Lagrangian, Eq. (2.30), then becomes

$$\mathcal{L}_{SCET} = \sum_{\tilde{p}_i} e^{-ix\cdot\mathcal{P}} \bar{\xi}_{n,p'}(x) \left[(in\cdot D) + i\not{D}^c_\perp W_n \frac{1}{\bar{\mathcal{P}}} W_n^\dagger i\not{D}^c_\perp \right] \frac{\not{\bar{n}}}{2} \xi_{n,p}(x). \tag{2.34}$$

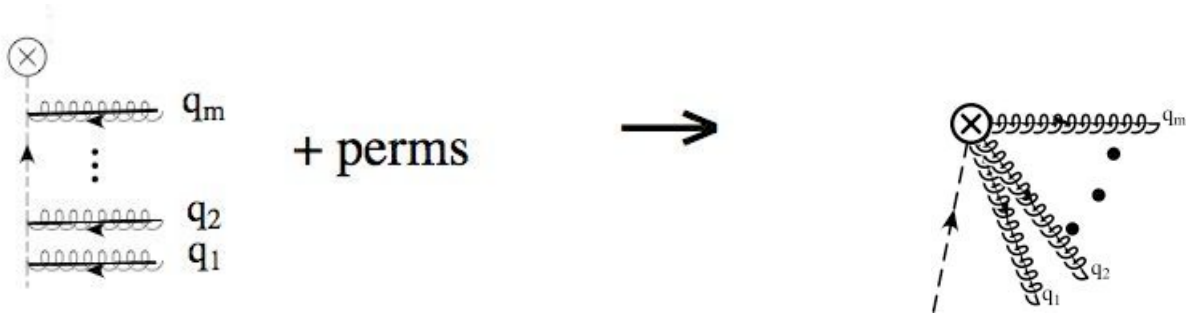

Figure 2.3: Integrating out the off-shell propagators from the interaction of n-collinear gluons with $\bar{n}$-collinear quark fields gives rise to a collinear wilson line.

A similar approach can be followed to obtain the leading $\mathcal{O}(\lambda^0)$ collinear gluon Lagrangian. Interactions coupling collinear modes and soft quarks are power suppressed and occur in the $\mathcal{O}(\lambda)$ correction to the Lagrangian [39].

The simplifications of working in the SCET framework are made manifest by the field re-definition [15]

$$\begin{aligned} &\xi_{n,p} = Y_n \xi^0_{n,p}\,, \quad A_{n,p} = Y_n A^0_{n,p} Y_n^\dagger \\ &\text{where } \; Y_n = P \exp\left[i\, g \int_{-\infty}^{x} \mathrm{d}s\, n \cdot A_s(sn) \right] \end{aligned} \tag{2.35}$$

which removes the $n \cdot A_s$ term in Eq. (2.34) and completely decouples the soft and collinear sectors at leading order in the Lagrangian. Instead, the soft gluon interactions appear as Wilson lines in the external currents, where simplifications due to the unitarity of Y_n are made clear.

There is a subtlety in the formulation of SCET outlined above which naively leads to a double counting of the contribution between soft and collinear modes. When the label momentum, $\tilde{p}$, of n-collinear quark or gluon fields is zero it has the same scaling as the soft and therefore there is an overlap between these modes. The sum over label momenta for collinear fields should in fact be restricted to be non-zero. For example Eq. (2.26)

should be

$$A^c = \sum_{\tilde{q}\neq 0} e^{-i\tilde{q}\cdot x} A^c_{n,q}(x). \tag{2.36}$$

Calculating loop graphs using the effective theory Lagrangian involves summing over label momenta and integrating over residual momenta, see Fig. 2.4. This is equivalent to integrating over all momentum space up to the restriction $\tilde{p} \neq 0$. Zero-bin subtraction

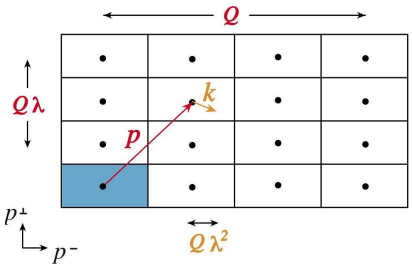

Figure 2.4: Momentum space is dived in to label momenta denoted by p, which specify a box and small residual momenta k which defines a point within the box [40].

[40] removes the $\tilde{p} = 0$ contribution in the following way

$$\sum_{\tilde{p}\neq 0} \int \mathrm{d}^4k\, \mathrm{I}_n(\tilde{p}, k) = \int \mathrm{d}^4p \left(\mathrm{I}_n(p) - \lim_{\tilde{p}\to 0} \mathrm{I}_n(p) \right) \tag{2.37}$$

where I_n is the integrand of a SCET Feynman diagram.

Virtual graphs in SCET are scaleless and vanish in dimensional regularization. Therefore it had not been noticed, until the work of Manohar and Stewart [40], that in order for the effective theory to be consistent and to properly reproduce the infrared of QCD, zero-bin subtraction is necessary. Manohar and Stewart examined virtual diagrams in SCET with different regulators to show that this was the case. They also applied the zero-bin approach to phase space integrals, but as we shall see in Chapter 4, their procedure is not consistent with cutoffs in the effective theory.

In Chapter 4 we develop an approach to to deal with phase space constraints in the effective theory which consistently applies zero-bin subtraction when integrating over

restricted regions of phase space. This provides amongst the first non-trivial examples of zero-bin subtraction and confirms the critical role the zero-bin plays in reproducing the infrared of the full theory correctly.

Chapter 3

High order perturbative corrections to the determination of $|V_{ub}|$

The contents of this chapter were published originally in "Higher order peturbative corrections to the determination of $|V_{ub}|$ from the P_+ spectrum in $B \to X_u \ell \nu_\ell$", [28].

3.1 Introduction

The total rate for the decay $B \to X_u \ell \bar{\nu}$ provides a theoretically clean determination of the magnitude of the CKM matrix element $|V_{ub}|$ as a double expansion in powers of $\alpha_s(m_b)$ and $\Lambda_{\rm QCD}/m_b$ [41]. However, to eliminate the background from $B \to X_c$ decays, strong cuts on the final state phase space are required, which can complicate the theoretical analysis. The kinematic regions in which cuts on the charged lepton energy E_ℓ, hadronic invariant mass m_X [42] and hadronic light-cone momentum $P_+ = E_X - |\vec{P}_X|$ (where E_X and $\vec{P}_X$ are the energy and three-momentum of the final state hadrons) [34] are strong enough to eliminate the charm background all correspond to the so-called shape function regime, in which the local OPE for the partial rate breaks down [43, 36]. However, in this region an expansion of the partial rate in powers of $\Lambda_{\rm QCD}/m_b$ in terms of non-local operators is still possible, and the matrix element of the leading nonlocal operator can

be measured in $B \to X_s\gamma$ decay. At leading order in $\Lambda_{\rm QCD}/m_b$, we can write

$$d\Gamma_i = \int C_i(\omega) f(\omega) + O\left(\frac{\Lambda_{\rm QCD}}{m_b}\right) \tag{3.1}$$

where i labels the decay, $C_i(\omega)$ is perturbatively calculable, and the shape function $f(\omega)$ is nonperturbative, but universal in inclusive B decays.[1] It is convenient to eliminate the shape function altogether, and express integrated rates directly in terms of one another [36, 37, 38]. For example, we can write

$$\int_0^\Delta dP_+ \frac{d\Gamma_u}{dP_+} \propto \int_0^\Delta dP_\gamma W(\Delta, P_\gamma) \frac{d\Gamma_s}{dP_\gamma} + O\left(\frac{\Lambda_{\rm QCD}}{m_b}\right) \tag{3.2}$$

where $P_\gamma \equiv m_B - 2E_\gamma$, E_γ is the photon energy and $\Delta \sim O(\Lambda_{\rm QCD})$. This defines the weight function $W(\Delta, P_\gamma)$, which can be calculated in perturbation theory. The $O(\Lambda_{\rm QCD}/m_b)$ power corrections have been extensively discussed in the literature [44, 45, 46, 47, 48, 49], and have typically been estimated to be below the 10% level for $|V_{ub}|$ [46, 47, 48], although it has been argued that subleading four-quark operators may introduce significant uncertainties [47].

The weight function $W(\Delta, P_\gamma)$ has been calculated in fixed-order perturbation theory to $O(\alpha_s^2\beta_0)$ [38]. It is also known to next-to-leading-log order, $O(\alpha_s^n \log^{n-1} m_b/\mu_i)$, where $\mu_i \sim \sqrt{\Lambda_{\rm QCD} m_b}$ is the typical invariant mass of the final state [46], generalized in [50]. It was shown in [38] that the $O(\alpha_s^2\beta_0)$ corrections to $W(\Delta, P_\gamma)$ are substantial, and the same order as the $O(\alpha_s)$ corrections. Given the size of these corrections, it is important to study the convergence of the perturbative expansion.

In this chapter we examine the behaviour of $W(\Delta, P_\gamma)$ at higher fixed orders in perturbation theory. We work in the framework of the "large-β_0" expansion, in which we calculate all terms of order $\alpha_s^n \beta_0^{n-1}$ [51, 52]. While there is no limit of QCD in which these terms formally dominate, this class of terms allows us to examine the asymptotic nature of perturbation theory, as well as giving an estimate for the size of perturbative

[1] $C(\omega)$ can be further factorized into "hard" and "jet" functions; however, for our purposes we will not make this decomposition.

corrections. We discuss the significance of these terms for the extraction of $|V_{ub}|$.

3.2 Borel Transformed Spectra and the Weight Function

Since QCD has an asymptotic perturbative expansion, it is convenient to study the Borel transformed series $B[\widetilde{R}](u)$ of a quantity $\widetilde{R}$, where

$$\widetilde{R} = R - R_{\rm tree} = \sum_{n=0}^{\infty} r_n \alpha_s^{n+1} \tag{3.3}$$

and

$$B[\widetilde{R}](u) = \sum_{n=0}^{\infty} \frac{r_n}{n!} u^n. \tag{3.4}$$

The expansion for $B[\widetilde{R}](u)$ has better convergence properties than the original expansion. $B[\widetilde{R}](u)$ can in turn be used as a generating function for the coefficients r_n

$$r_n = \frac{d^n}{du^n} B[\widetilde{R}](u)|_{u=0} \tag{3.5}$$

while the original expression R can be recovered from the Borel transform $B[\widetilde{R}](u)$ by the inverse Borel transform

$$R = R_{\rm tree} + \int_0^{\infty} du\ e^{-u/\alpha_s}\ B[\widetilde{R}](u). \tag{3.6}$$

Singularities in $B[\widetilde{R}](u)$ along the positive real u axis make the inverse Borel transform ill-defined. These are referred to as infrared renormalons [53], factorially growing contributions to the coefficients of the perturbative series, which lead to ambiguities of order $(\Lambda_{\rm QCD}/m_b)^n$. In physical quantities these ambiguities are compensated by corresponding ambiguities in the definition of higher-dimensional nonperturbative matrix elements in the operator product expansion of order $\Lambda_{\rm QCD}^n$, which render the physical quantity unambigious.[2]

[2] Although the renormalon cancellation has only been explicitly shown in some cases in the large-β_0 limit, it is assumed to hold away from this limit.

The Borel transform Eq. (3.4), in the large-β_0 limit, may be determined from the order α_s term, r_0, with finite gluon mass following [52]:

$$\begin{aligned} B[\widetilde{R}](u) &= -\frac{\sin\pi u}{\pi u} e^{5u/3} \int_0^\infty \left(\frac{\lambda^2}{m_b^2}\right)^{-u} \left(\frac{dr_0}{d\lambda^2} - \frac{r_\infty}{\lambda^2}\Theta(\lambda^2 - m_b^2 e^{5u/3})\right) d\lambda^2 \\ &\quad + \frac{1}{u}\left(\widehat{G}_0(u) - \frac{\sin\pi u}{\pi u} r_\infty\right). \end{aligned} \tag{3.7}$$

Here λ is the gluon mass and r_∞ is a constant. We have used the $\overline{\rm MS}$ scheme with the renormalization scale μ set to the pole mass, m_b. The terms $\widehat{G}_0(u)/u$ and r_∞ arise from the renormalization of the graphs involved.

The weight function $W(\Delta, P_\gamma)$ is defined through the relation between the integrated $B \to X_s\gamma$ photon energy spectrum and $B \to X_u \ell\bar{\nu}$ charged lepton spectrum,

$$\begin{aligned} \Gamma_u(\Delta) &\equiv \int_0^\Delta dP_+ \frac{d\Gamma_u}{dP_+} = \frac{|V_{ub}|^2}{|V_{tb}V_{ts}^*|^2} \frac{\pi}{6\alpha_{em} C_7^{\rm eff}(m_b)^2} \frac{m_B^2}{\overline{m}_b(m_b)^2} \int_0^\Delta dP_\gamma W(\Delta, P_\gamma) \frac{d\Gamma_{77}}{dP_\gamma} \\ &\quad + O\left(\frac{\Lambda_{QCD}}{m_b}\right) \end{aligned} \tag{3.8}$$

where $\Delta \sim \Lambda_{QCD}$ in the shape function region, and the normalization is the same as that used in [38]. Other definitions of W are possible, such as that used in [46]. As in [38], we concentrate on the contribution to the $B \to X_s\gamma$ spectrum arising from the operator $O_7 = (e/16\pi^2) m_b \bar{s_L} \sigma^{\mu\nu} F_{\mu\nu} b_R$. While other operators also contribute to the spectrum, for the purposes of studying the convergence of the series and estimating the uncertainties from higher order terms in perturbation theory we will neglect their contribution and the mixing of these with O_7. The factor of $m_B^2/\bar{m}_b^2$ pulled out of the relation arises naturally, and improves the behaviour of perturbation theory for $W(\Delta, P_\gamma)$[38].

Defining the partonic partial rates

$$\begin{aligned} \frac{1}{\Gamma_\gamma}\frac{d\Gamma_{77}}{d\bar{x}} &= \delta(\bar{x}) + g(\bar{x}) \\ \frac{1}{\Gamma_u}\frac{d\Gamma_u}{d\hat{p}_+} &= \delta(\hat{p}_+) + h(\hat{p}_+) \end{aligned} \tag{3.9}$$

where $\Gamma_\gamma = G_F^2 |V_{tb}V_{ts}^*|^2 \alpha_{em} m_b^3 [\overline{m}_b(m_b) C_7^{\rm eff}(m_b)]^2/(32\pi^4)$ and $\Gamma_u = G_F^2 |V_{ub}|^2 m_b^5/(192\pi^3)$

are the leading order widths. The partonic variables

$$\bar{x} \equiv 1 - 2E_\gamma/m_b, \qquad \hat{p}_+ \equiv (v - q/m_b) \cdot n \tag{3.10}$$

are related to the hadronic variables by

$$P_\gamma \equiv m_B - 2E_\gamma = m_b\bar{x} + \Lambda, \qquad P_+ \equiv E_X - |\vec{P}_X| = m_b\hat{p}_+ + \Lambda \tag{3.11}$$

where $\Lambda \equiv m_B - m_b$, q is the momentum of the lepton-neutrino pair, n is a light-like four vector in the $-\vec{q}$ direction and v is the four-velocity of the B meson. Convoluting the partonic rate with the shape function to obtain the hadronic rates, we find

$$W(\Delta, P_\gamma) = 1 + \int_0^{\Delta - P_\gamma} (h(p) - g(p))\, dp - \int_0^{\Delta - P_\gamma} g(p)\, [W(\Delta, p + P_\gamma) - 1]\, dp \tag{3.12}$$

where the partonic spectra are expanded to leading order in $\bar{x}$ and $\hat{p}_+$ respectively since in the shape function region they are of $O(\Lambda_{QCD}/m_b)$.

Since $g(p)$ and $h(p)$ are $O(\alpha_s)$, Eq. (3.12) may be solved iteratively for $W(\Delta, P_\gamma)$. For the purposes of this chapter, we are only interested in terms of $O(\alpha_s^n \beta_0^{n-1})$, for which the last term in Eq. (3.12) does not contribute; therefore, we can write

$$W(\Delta, P_\gamma) = \widehat{\Gamma}_u^p(\Delta - P_\gamma) - \widehat{\Gamma}_{77}^p(\Delta - P_\gamma) + O(\alpha_s^n \beta_0^{n-2}) \tag{3.13}$$

where we have defined the integrated partonic rates calculated in perturbation theory,

$$\widehat{\Gamma}_{77}^p(\Delta) = \frac{1}{\Gamma_\gamma} \int_0^\Delta \frac{d\Gamma_{77}}{d\bar{x}} d\bar{x} \tag{3.14}$$

and

$$\widehat{\Gamma}_u^p(\Delta) = \frac{1}{\Gamma_u} \int_0^\Delta \frac{d\Gamma_u}{d\hat{p}_+} d\hat{p}_+. \tag{3.15}$$

The corresponding quantities $\widetilde{W}$, $\widetilde{\Gamma}_{77}^p$ and $\widetilde{\Gamma}_u^p$ are defined by subtracting the tree level contribution.

Calculating the parton level photon spectrum with a massive gluon is straightforward, and was done in [38]. Integrating the rate with a massive gluon over the endpoint region

and performing the integral Eq. (3.7), we find the Borel transform of the integrated partonic rate:

$$\begin{aligned} B[\widetilde{\Gamma}^p_{77}(\Delta)](u) &= e^{5u/3}\left(\frac{2(u-1)}{u^2}\left(\frac{\Delta}{m_b}\right)^{-2u} - \left(\frac{2}{u-1}-\frac{3}{u}-\frac{4}{u^2}+\frac{1}{u-2}\right)\frac{\sin\pi u}{\pi u}\left(\frac{\Delta}{m_b}\right)^{-u}\right. \\ &\quad \left. + \frac{2\sin\pi u}{\pi u^2} + \frac{(1+u)\,(3u^2-2u-2)\,\Gamma(u)^2}{(u-2)(u-1)u\Gamma(2u)\cos\pi u}\right) \\ &\quad + \frac{1}{u}\left(\widehat{G}_0(u) - \frac{2e^{5u/3}\sin\pi u}{\pi u}\right). \end{aligned} \tag{3.16}$$

Since the operator O_7 requires renormalization, the last line arises from the $\overline{\rm MS}$ counterterm. $\widehat{G}_0(u)$ is given by

$$\widehat{G}_0(u) = \sum_{n=0}^{\infty}\frac{g_n}{n!}u^n \tag{3.17}$$

and g_n are the coefficients of the expansion of $G_0(u)$ [52]

$$G_0(u) = \sum_{m=0}^{\infty} g_m u^m = \frac{2(2u+1)\Gamma(4+2u)}{3(u+2)(u+1)\Gamma(2+u)^2}\frac{\sin\pi u}{\pi u}. \tag{3.18}$$

The Borel transform of the differential photon spectrum away from the $\bar{x}=0$ endpoint was calculated in [54]. Integrating this result from $\bar{x}=0$ to $\bar{x}=\Delta$ reproduces the Δ dependent terms of our result, Eq. (3.16). (The Δ-independent terms depend on the virtual contribution and cannot be directly compared against [54]).

The calculation of the Borel transform of the semileptonic partial rate $\widehat{\Gamma}^p_u(\Delta)$ is significantly more involved than for $B\to X_s\gamma$. The Borel transform of the triple-differential $B\to X_u\ell\bar{\nu}$ spectrum was calculated in [55]. Rather than integrate this result over the appropriate phase space, we instead calculated the integrated rate $\Gamma_u(\Delta)$ for a massive gluon, and then performed the integral (3.7). The result has the comparatively simple

form

$$\begin{aligned} B[\widetilde{\Gamma}^p_u(\Delta)](u) &= e^{5u/3}\left(\frac{2(u-1)}{u^2}\left(\frac{\Delta}{m_b}\right)^{-2u}\right. \\ &+\left(\frac{5}{3(u-3)}-\frac{2}{u-2}-\frac{5}{3(u-1)}+\frac{7}{3u}+\frac{2}{u^2}-\frac{1}{3(u-4)}\right)\frac{2\sin\pi u}{\pi u}\left(\frac{\Delta}{m_b}\right)^{-u} \\ &+\frac{\Gamma(u)^2}{(u-4)(u-2)(u-1)u\Gamma(2u)\cos\pi u}\left(\frac{1}{3}(9u^4-103u^3-62u^2+38u+24)\right. \\ &\left.\left.-16u(1+u)(2u-1)\left(\frac{\pi}{\sin 2\pi u}+\psi(u)-\psi(2u)\right)\right)\right) \end{aligned} \tag{3.19}$$

where $\psi(u)=\Gamma'(u)/\Gamma(u)$ is the digamma function.

The Borel transformed weight function is given by the difference between Eq. (3.19) and Eq. (3.16). Note that the terms proportional to $(\Delta/m_b)^{-2u}/u^2$ and $(\Delta/m_b)^{-u}\sin\pi u/u^3$, which generate the $\alpha_s^n\ln^{n+1}(\Delta/m_b)$ logs, cancel in the difference. This reflects the universality of the leading Sudakov logs. We can resum this contribution by evaluating the inverse Borel transform, Eq. (3.6). However the result does not exponentiate because higher powers of logs, up to $\alpha_s^n\ln^{2n}$ double logs, are not included since they are suppressed in β_0. The resummed $\alpha_s^n\ln^{n+1}(\Delta/m_b)$ logs from Eq. (3.32) and Eq. (3.33) are given by

$$\begin{aligned} &\frac{C_F}{\beta_0}\int_0^\infty du\; e^{-\frac{4\pi u}{\alpha_s\beta_0}}\frac{2}{u^2}\left(-\left(\frac{\Delta}{m_b}\right)^{-2u}+2\left(\frac{\Delta}{m_b}\right)^{-u}-1\right) \\ &\qquad=\frac{C_F}{\beta_0}\left(4\ln\frac{\Delta}{m_b}\ln\frac{1+a}{1+2a}+\frac{8\pi}{\alpha_s\beta_0}\ln\frac{(1+a)^2}{1+2a}\right) \end{aligned} \tag{3.20}$$

where $a\equiv\frac{\alpha_s(m_b)\beta_0}{4\pi}\ln\frac{\Delta}{m_b}$.

The final result for the Borel transformed weight function is

$$\begin{aligned} B[\widetilde{W}(\Delta,P_\gamma)](u) &= e^{5u/3}\left(\frac{2\sin\pi u}{\pi u^2}\left(\frac{(u-5)(3u-4)}{(u-4)(u-3)(u-2)(u-1)}\left(\frac{\Delta-P_\gamma}{m_b}\right)^{-u}-1\right)\right. \\ &-\frac{\Gamma(u)^2}{\Gamma(2u)(u-4)(u-2)(u-1)\cos\pi u}\left(16(u+1)(2u-1)\left(\frac{\pi}{\sin 2\pi u}+\psi(u)-\psi(2u)\right)\right. \\ &\left.\left.+\frac{2}{3}(5u+2)(7u+1)\right)\right)-\frac{1}{u}\left(\widehat{G}_0(u)-\frac{2e^{5u/3}\sin\pi u}{\pi u}\right) \end{aligned} \tag{3.21}$$

where $\widehat{G}_0(u)$ is obtained from Eq. (3.17) and Eq. (3.18).Eq. (3.21) is the main result of this chapter.

The Borel transforms can be used to generate the $O(\alpha_s^n \beta_0^{n-1})$ terms in the perturbative expansion via the relation Eq. (3.5). Writing

$$\begin{aligned}
\widehat{\Gamma}^p_{77}(\Delta) &= 1 + \sum_{i=1}^{\infty} C_n^s(\Delta) \frac{\alpha_s(m_b)^n \beta_0^{n-1} C_F}{(4\pi)^n} \\
\widehat{\Gamma}^p_{u}(\Delta) &= 1 + \sum_{i=1}^{\infty} C_n^u(\Delta) \frac{\alpha_s(m_b)^n \beta_0^{n-1} C_F}{(4\pi)^n} \\
W(\Delta, P_\gamma) &= 1 + \sum_{i=1}^{\infty} W_n(\Delta, P_\gamma) \frac{\alpha_s(m_b)^n \beta_0^{n-1} C_F}{(4\pi)^n}
\end{aligned} \tag{3.22}$$

we can easily find the coefficients $C_n^s(\Delta)$, $C_n^u(\Delta)$ and $W_n(\Delta, P_\gamma)$ to any order. The coefficients are given up to $n = 5$ in Appendix 4.A.

The leading log (LL) and next-to-leading log (NLL) terms in Eq. (3.34) are contained within the renormalization group resummed NLL result in soft-collinear effective theory (SCET), $W(\Delta, P_\gamma)^{\rm NLL}_{\rm SCET}$, obtained from [34, 56, 57, 46]. The SCET result sums logs of μ_i^2/m_b^2, where $\mu_i^2 \sim O(\Lambda_{QCD} m_b)$. In the Appendix 3.B we verify that the leading β_0 terms agree with Eq. (3.36) by expanding in $\alpha_s(m_b)$ and then expanding logs of μ_i^2/m_b^2 and $\mu_i^2/(m_b(\Delta - P_\gamma))$. Our results also agree with those in [38, 58, 59].

3.3 Results and Discussion

3.3.1 Renormalons and Borel Resummation

The leading renormalon ambiguity in both the photon and semileptonic spectra is $O(\Lambda_{QCD}/m_b)$ due to the pole at $u = 1/2$ in $B[\widetilde{\Gamma}^p_u(\Delta)](u)$ and $B[\widetilde{\Gamma}^p_{77}(\Delta)](u)$. The divergence does not cancel between the spectra and gives rise to a pole at $u = 1/2$ in the Borel transformed weight function. This is consistent with the presence of nonperturbative corrections to $W(\Delta, P_\gamma)$ at $O(\Lambda_{QCD}/m_b)$ due to subleading shape functions [44].

The Borel transform of the weight function can be written in terms of $\Delta - P_\gamma$ independent and dependent pieces, $B[\widetilde{W}_0](u)$ and $B[\widetilde{W}_1](u)$ respectively,

$$\begin{aligned} B[\widetilde{W}_0](u) &= e^{5u/3}\left(\frac{2\sin\pi u}{\pi u^2}\left(\frac{(u-5)(3u-4)}{(u-4)(u-3)(u-2)(u-1)}-1\right)\right. \\ &\quad -\frac{\Gamma(u)^2}{\Gamma(2u)(u-4)(u-2)(u-1)\cos\pi u}\left(16(u+1)(2u-1)\left(\frac{\pi}{\sin 2\pi u}+\psi(u)-\psi(2u)\right)\right. \\ &\quad \left.\left.+\frac{2}{3}(5u+2)(7u+1)\right)\right)-\frac{1}{u}\left(\widehat{G}_0(u)-\frac{2e^{5u/3}\sin\pi u}{\pi u}\right) \end{aligned} \tag{3.23}$$

$$B[\widetilde{W}_1(\Delta,P_\gamma)](u)=\frac{2\sin\pi u}{\pi u^2}\frac{e^{5u/3}(u-5)(3u-4)}{(u-4)(u-3)(u-2)(u-1)}\left(\left(\frac{\Delta-P_\gamma}{m_b}\right)^{-u}-1\right) \tag{3.24}$$

where we have defined $B[\widetilde{W}_0](u)$ and $B[\widetilde{W}_1](u)$ such that they are finite as $u\to 0$. Note that $B[\widetilde{W}_1](u)$ has no singularities for positive u. Therefore the inverse Borel transform of Eq. (3.24), $\widetilde{W}_1$, is well defined and unambiguously resums logarithms of $(\Delta-P_\gamma)/m_b$. This tells us that the poor behavior in the perturbative expansion of the weight function is entirely due to the constant terms, $\widetilde{W}_0$, which are generated by $B[\widetilde{W}_0](u)$.

The relevant quantity in determining $|V_{ub}|$ is the weight function convolved with the $B\to X_s\gamma$ photon spectrum, as in Eq. (3.8). It is interesting to note that the integrated quantity can have a renormalon ambiguity that is not present in the weight function. In order to illustrate this we calculate the Borel transform of $\widetilde{W}_1$, which is renormalon free, convolved with a simple model of the normalized $B\to X_s\gamma$ spectrum,

$$\frac{1}{\Gamma_\gamma}\frac{d\Gamma_s}{dP_\gamma}=\frac{b^b}{\Gamma(b)\Lambda^b}P_\gamma^{b-1}e^{-\frac{bP_\gamma}{\Lambda}} \tag{3.25}$$

where $b=2.5$ and $\Lambda=0.77$ GeV [46]. This is straightforward to obtain from Eq. (3.24):

$$\begin{aligned} B\left[\int_0^\Delta dP_\gamma\widetilde{W}_1\frac{1}{\Gamma_\gamma}\frac{d\Gamma_s}{dP_\gamma}\right](u) &= e^{5u/3}\frac{2\sin\pi u}{\pi u^2}\frac{(u-5)(3u-4)}{(u-4)(u-3)(u-2)(u-1)}\left(\frac{\Gamma\left(b,\frac{b\Delta}{\Lambda}\right)}{\Gamma(b)}\right. \\ &\quad \left.+\left(-1+\left(\frac{b\Delta}{\Lambda}\right)^b\left(\frac{\Delta}{m_b}\right)^{-u}\frac{\Gamma(1-u)}{\Gamma(1-u+b)}{}_1F_1\left[b;1-u+b;\frac{-b\Delta}{\Lambda}\right]\right)\right) \end{aligned} \tag{3.26}$$

where $\Gamma(a,z)=\int_z^\infty t^{a-1}e^{-t}dt$ is the incomplete Gamma function. The $\Gamma(1-u)$ term in Eq. (3.26) gives rise to a pole at $u=1$, which corresponds to an order $O((\Lambda_{QCD}/m_b)^2)$

ambiguity in the integrated quantity. This arises because higher order terms in the perturbative expansion of $\widetilde{W}_1$ have more powers of $\ln(\Delta - P_\gamma)/m_b$ and therefore are more singular near the end point. However since the renormalon in $B[\widetilde{W}_0](u)$ is at $u = 1/2$, the factorial growth in the integrated quantity is dominated by the constant terms in the weight function rather than the logarithms.

It is amusing to notice that if the $\alpha_s^n \ln(\Delta/m_b)^{n+1}$ Sudakov logs did not cancel between $\widehat{\Gamma}_u^p(\Delta)$ and $\widehat{\Gamma}_{77}^p(\Delta)$ these would give rise to a $((\Delta - P_\gamma)/m_b)^{-2u}$ term in the Borel transform of the weight function. When integrated over P_γ with Eq. (3.25) this would lead to a pole at $u = 1/2$, the same order as the renormalon in $B[\widetilde{W}_0](u)$.

Since $B[\widetilde{W}_1](u)$ has no poles in u, the inverse Borel transform of Eq. (3.24) is well-defined. We may therefore use Eq. (3.24) to sum all terms containing powers of $\ln((\Delta - P_\gamma)/m_b)$ (terms of order $\alpha_s^n \beta_0^{n-1} \log^{n-m}(\Delta - P_\gamma)/m_b$, for $n = 1$ to infinity and $m = 0$ to $n - 1$). While we were unable to obtain a closed-form result for this quantity, by expanding Eq. (3.24) in powers of u it is straightforward to sum all terms of order $\alpha_s^n \beta_0^{n-1} \log^{n-m}(\Delta - P_\gamma)/m_b$, for $n = m + 1$ to infinity and for fixed $m \geq 0$, by evaluating the inverse Borel transform

$$\begin{aligned} W(\Delta, P_\gamma)_{\rm resummed} &= \frac{C_F}{\beta_0} \int_0^\infty du\; e^{-\frac{4\pi u}{\alpha_s \beta_0}} C_{m-1} u^{m-1} \left(\left(\frac{\Delta - P_\gamma}{m_b} \right)^{-u} - 1 \right) \qquad (3.27) \\ &= \frac{C_F C_{m-1}}{\beta_0} \Gamma(m) \left(\frac{\alpha_s \beta_0}{4\pi} \right)^m \left(\left(1 + \frac{\alpha_s \beta_0}{4\pi} \ln \frac{\Delta - P_\gamma}{m_b} \right)^{-m} - 1 \right) \end{aligned}$$

where C_{m-1} is the coefficient of the $u^{m-1} \left(\frac{\Delta - P_\gamma}{m_b} \right)^{-u}$ term in Eq. (3.24), and the second line follows for $m > 0$. The constant non-logarithmic terms in the weight function are not included in Eq. (3.27), as they arise from $\widetilde{W}_0$, but may be obtained from the expansion Eq. (3.34) to give the full resummed logarithmic result. At leading-log (LL), $m = 0$, we find

$$W(\Delta, P_\gamma)_{\beta_0}^{LL} = 1 - \tfrac{5 C_F}{3 \beta_0} \ln \left(\tfrac{\alpha_s(m_b)\beta_0}{4\pi} \ln \tfrac{\Delta - P_\gamma}{m_b} + 1 \right). \qquad (3.28)$$

We explicitly show the NLL, the next-to-next-to-leading logarithmic (NNLL) $\alpha_s^n \beta_0^{n-1} \ln^{n-2}$ and next-to-next-to-next-to-leading logarithmic (NNNLL) $\alpha_s^n \beta_0^{n-1} \ln^{n-3}$ terms below:

$$\begin{aligned}
W(\Delta, P_\gamma)^{NLL}_{\beta_0} &= \frac{\alpha_s(m_b) C_F}{4\pi} \left[\frac{14}{3} \left(\frac{1}{1+b} - 1 \right) + \left(\frac{167}{36} - \frac{2\pi^2}{3} \right) \right] \\
W(\Delta, P_\gamma)^{NNLL}_{\beta_0} &= \frac{\alpha_s(m_b)^2 \beta_0 C_F}{(4\pi)^2} \left[\left(\frac{1559}{216} - \frac{5\pi^2}{18} \right) \left(\frac{1}{(1+b)^2} - 1 \right) \right. \\
&\quad \left. + \left(\frac{3857}{144} - \frac{16\pi^2}{9} - 12\zeta(3) \right) \right] \\
W(\Delta, P_\gamma)^{NNNLL}_{\beta_0} &= \frac{\alpha_s(m_b)^3 \beta_0^2 C_F}{(4\pi)^3} \left[\left(\frac{65545}{3888} - \frac{14\pi^2}{9} \right) \left(\frac{1}{(1+b)^3} - 1 \right) \right. \\
&\quad \left. + \left(\frac{90043}{864} - \frac{13\pi^2}{108} - \frac{16\pi^4}{15} - \frac{166\zeta(3)}{3} \right) \right] . \qquad (3.29)
\end{aligned}$$

where $b \equiv \frac{\alpha_s(m_b)\beta_0}{4\pi} \ln \frac{\Delta - P_\gamma}{m_b}$. These results provide a useful check of our calculation, as they may be compared with the corresponding resummed expressions in SCET, obtained from [34, 56, 57, 46]. Setting $\mu_i = \sqrt{m_b(\Delta - P_\gamma)}$, we verify that the resummed LL and NLL contributions in the large β_0 limit, Eq. (3.28) and Eq. (3.29), are contained within the RG resummed NLL SCET result.

Finally, the renormalon in the weight function suggests that the dominant contribution to its perturbative expansion is from non-logarithmic terms. We can investigate this numerically by considering the leading logarithmic expansion away from the $P_\gamma \to \Delta$ end point. Following [38], we combine all known terms from Eq. (3.34) and Eq. (3.36), and take the ratio of the various logarithmic terms. While this misses the contributions of terms beyond NLL and subleading in β_0, we can hope that the values below are still indicative of the relative contributions of the various terms. Taking $m_b = 4.8$ GeV, $\alpha_s(m_b) = 0.22$ and $\mu_i^2/m_b^2 \sim (\Delta - P_\gamma)/m_b = 1/9$ as in [38] we find the following ratios of

the logarithmic terms at each order in α_s:

$$\begin{aligned}
\alpha_s^3: &\quad O(\log^3) : O(\log^2) : O(\log^1) : O(\log^0) = 1 : 2.1 : 1.8 : -6.0 \\
\alpha_s^4: &\quad O(\log^4) : O(\log^3) : O(\log^2) : O(\log^1) : O(\log^0) = 1 : 3.5 : 2.9 : 0.4 : -26 \\
\alpha_s^5: &\quad O(\log^5) : O(\log^4) : O(\log^3) : O(\log^2) : O(\log^1) : O(\log^0) = \\
&\qquad\qquad 1 : 4.9 : 4.2 : 1.0 : -2.3 : -119. \qquad (3.30)
\end{aligned}$$

From these results, we can make two observations. First, the renormalon ambiguity in the weight function is reflected in the rapid growth of the non-logarithmic terms, which dominate the perturbative expansion. However, this bad behaviour of perturbation theory is unphysical: in a consistent approach to $O(1/m_b)$, the renormalon in the weight function will cancel with a corresponding ambiguity in the definitions of the subleading shape functions. This cancellation would be manifest if the subleading shape functions were consistently extracted from physical observables, but since they are currently modelled, no such cancellation is manifest. We will see in the next section that the estimated uncertainty in $|V_{ub}|$ from the factorially growing terms is small compared to other sources of error, so we will not attempt in this chapter to absorb the renormalon ambiguity into subleading shape functions. These results do, however, underscore the fact that separating the bad behaviour of perturbation theory from the $O(1/m_b)$ corrections is not a well-defined procedure.

Second, assuming the pattern in Eq. (3.30) continued to hold beyond the large-β_0 and NLL terms included here, it indicates that terms which are enhanced by more powers of $\log \mu_i^2/m_b^2 \sim \log(1/9) \sim -2$ do not dominate over terms with fewer powers of logarithms. Since the logarithmic terms do not suffer from renormalon ambiguities, and, therefore, no cancellation against the subleading operators is expected for these terms, this pattern should not change once subleading operators are consistently included. Thus, these results support the conclusion of [38] that fixed-order perturbation theory is more appropriate than a leading-log resummation for the extraction of $|V_{ub}|$ (see also [60, 61]).

3.3.2 Determination of $|V_{ub}|$

From a phenomenological perspective, our results are most useful as an estimate of the size of higher-order perturbative corrections to the extraction of $|V_{ub}|$ via Eq. (3.8). The perturbative results in Eq. (3.34) for $W(\Delta, P_\gamma)$ are plotted in Fig. 3.1 at different orders in the $\alpha_s^n \beta_0^{n-1}$ expansion. Throughout this section, we will use the values $m_b = 4.8$ GeV and $\alpha_s(m_b) = 0.22$ for numerical evaluations, and take $\Delta = m_D^2/m_B = 0.66$ GeV, corresponding to the kinematic cut which removes the $B \to X_c$ background. At tree level, the weight function is 1 (the dotted line in Fig. 3.1 and Fig. 3.2). Curve (a) in Fig. 3.1 shows the weight function up to $O(\alpha_s^2\beta_0)$, calculated previously in [38], while curves (b), (c) and (d) show the results to $O(\alpha_s^3\beta_0^2)$, $O(\alpha_s^4\beta_0^3)$ and $O(\alpha_s^5\beta_0^4)$.

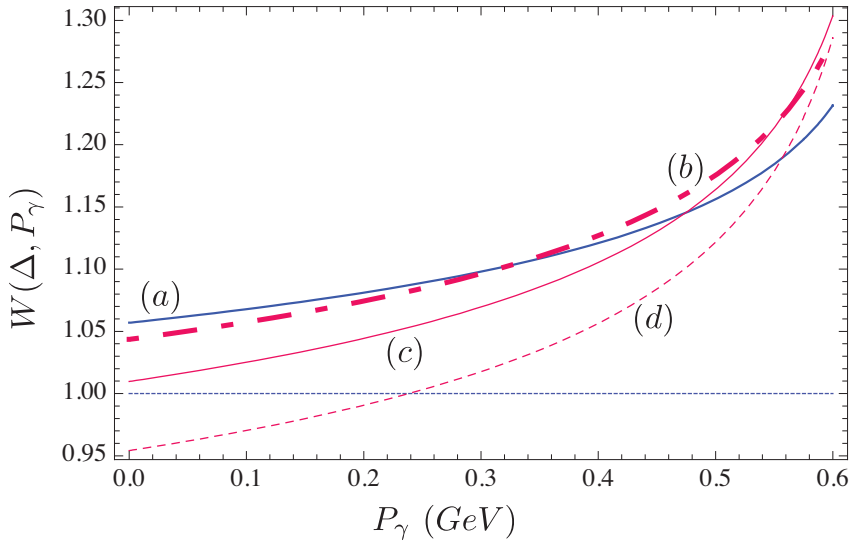

Figure 3.1: $W(\Delta, P_\gamma)$ from Eq. (3.34) is shown including terms up to the following order: (a) $O(\alpha_s^2\beta_0)$, (b) $O(\alpha_s^3\beta_0^2)$, (c) $O(\alpha_s^4\beta_0^3)$ and (d) $O(\alpha_s^5\beta_0^4)$.

It is clear from the plots that the perturbative series for $W(\Delta, P_\gamma)$ is not converging well, as was discussed in the previous section, due largely to the factorial growth of the constant terms in $W(\Delta, P_\gamma)$. As we will discuss shortly, the results suggest that the optimal perturbative estimate is obtained by truncating the series at $O(\alpha_s^3)$, and using the $O(\alpha_s^4)$ result as an estimate of the corresponding perturbative uncertainty. In Fig.

3.2 we therefore compare the fixed-order $\alpha_s^3\beta_0^2$ result to other perturbative estimates of the weight function. Curve (a) shows all known terms up to $O(\alpha_s^3)$: the complete NLL terms from Eq. (3.36), combined with the additional large β_0 terms in Eq. (3.34) that are higher order in the leading log expansion. The gray band around the curve gives the perturbative error estimate given by the $O(\alpha_s^4\beta_0^3)$ term. The result is very close to the large-β_0 calculation up to $O(\alpha_s^3\beta_0^2)$, shown in Curve (b). Curve (c) shows the complete NLL resummed result.

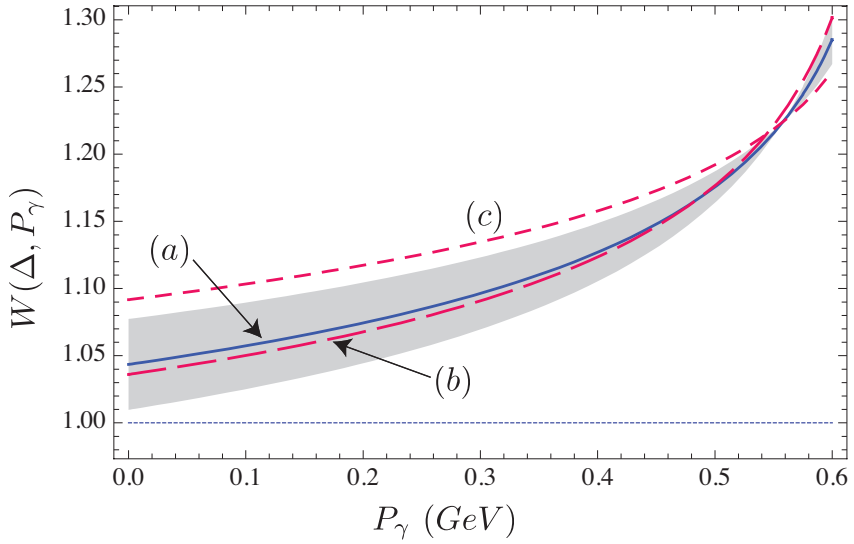

Figure 3.2: (a) $W(\Delta, P_\gamma)$ with all terms to $O(\alpha_s^3)$ from Eq. (3.34) and Eq. (3.36). The grey region is the error estimate obtained from the $\alpha_s^4\beta_0^3$ term. (b) $W(\Delta, P_\gamma)$ up to $O(\alpha_s^3\beta_0^2)$ from Eq. (3.34). (c) The resummed NLL SCET result, $W(\Delta, P_\gamma)^{\rm NLL}_{\rm SCET}$.

Tree	$O(\alpha_s)$	$O(\alpha_s^2\beta_0)$	$O(\alpha_s^3\beta_0^2)$	$O(\alpha_s^4\beta_0^3)$	$O(\alpha_s^5\beta_0^4)$	$O(\alpha_s^6\beta_0^5)$	$O(\alpha_s^7\beta_0^6)$
1	1.08	1.15	1.17	1.16	1.12	1.04	0.88

Table 3.1: $\widehat{\Gamma}_u(\Delta)$ for different orders in the "large-β_0" expansion of $W(\Delta, P_\gamma)$, Eq. (3.34).

As discussed in the previous section, the integral in Eq. (3.8) has a worse perturbative expansion than the weight function itself, since at higher orders in perturbation theory $W(\Delta, P_\gamma)$ is more singular at the endpoint of integration. Hence, to determine the

Tree	SCET LL	SCET NLL	All known terms to $O(\alpha_s^3)$
1	1.10	1.18	1.17

Table 3.2: $\widehat{\Gamma}_u(\Delta)$ for the resummed LL and NLL weight function in SCET, and all terms up to $O(\alpha_s^3)$ from Eq. (3.34) and Eq. (3.36).

effects of perturbative corrections on the determination of $|V_{ub}|$, we must look at the perturbative expansion of Eq. (3.8) rather than that of $W(\Delta, P_\gamma)$. For the purposes of estimating the size of higher order terms, we adopt the simple model of the normalized $B \to X_s\gamma$ spectrum, Eq. (3.25). We obtain $\widehat{\Gamma}_u(\Delta)$, the integrated $B \to X_u\ell\bar{\nu}_l$ decay rate normalized to the tree level value,

$$\widehat{\Gamma}_u(\Delta) = \frac{1}{\Gamma_u}\int_0^\Delta dP_+ \frac{d\Gamma_u}{dP_+} \tag{3.31}$$

shown in Table 5.3.1. We include several more terms than are explicitly shown in Eq. (3.34) to demonstrate that the series appears to converge up to $O(\alpha_s^4\beta_0^3)$ and then begins to diverge. This suggests that the optimal perturbative result is given by including all terms up to $O(\alpha_s^3)$ and using the $O(\alpha_s^4)$ contribution to estimate the perturbative uncertainty. At this stage, our best estimate of this result is obtained by including all known terms up to $O(\alpha_s^3)$ from Eq. (3.34) and Eq. (3.36), and estimating the uncertainty from the $O(\alpha_s^4\beta_0^3)$ term. Table 3.2 gives $\widehat{\Gamma}_u(\Delta)$ obtained from the renormalization group resummed LL and NLL weight function in SCET, as well as all terms up to $O(\alpha_s^3)$ from Eq. (3.34) and Eq. (3.36). We see that the NLL result is in agreement with the optimal perturbative value, within the error. The perturbative uncertainty in $|V_{ub}|$, estimated from the $O(\alpha_s^4\beta_0^3)$ terms is approximately 0.5%, which is far smaller than the order 5% theoretical uncertainty in $|V_{ub}|$ from subleading shape functions, error in the b quark mass and other sources [46].

3.4 Conclusions

We have calculated the Borel transform of the $B \to X_u \ell \bar{\nu}_\ell \; P_+$ spectrum and $B \to X_s \gamma \; P_\gamma$ spectrum to leading order in Λ_{QCD}/m_b, from which we determine the Borel transform of the weight function. The leading renormalon in $W(\Delta, P_\gamma)$ is confirmed to be at $u = 1/2$, corresponding to nonperturbative corrections at $O(\Lambda_{QCD}/m_b)$. The $\alpha_s^n \beta_0^{n-1}$ terms are easily obtained from the Borel transform of the weight function and are given analytically to $n = 5$. We are able to resum logarithms of $(\Delta - P_\gamma)/m_b$ in the large β_0 limit of the weight function since the relevant terms in $B[W(\Delta, P_\gamma)](u)$ are renormalon free. However we show that integrating these terms over P_γ introduces a renormalon. Comparing all known terms in the perturbative expansion of the weight function, we find no numerical enhancement of leading logarithms, suggesting that fixed-order perturbation theory is more appropriate than a leading-log resummation.

From our results we estimate the size of higher-order perturbative corrections on the extraction of $|V_{ub}|$ using a model for the $B \to X_s \gamma$ photon spectrum. We have shown that $\widehat{\Gamma}_u(\Delta)$ begins to diverge beyond $O(\alpha_s^4 \beta_0^3)$ in the β_0 expansion of the weight function. This suggests that the best perturbative estimate is given by including terms up to $O(\alpha_s^3)$ with the theoretical uncertainty given by the $\alpha_s^4 \beta_0^3$ term. We show that this result is in good agreement with the resummed NLL SCET result.

3.A Expanding out the functions

$$
\begin{aligned}
C_1^s(\Delta) &= -2\ln^2\frac{\Delta}{m_b} - 7\ln\frac{\Delta}{m_b} - \frac{4\pi^2}{3} - 5 \\
C_2^s(\Delta) &= 2\ln^3\frac{\Delta}{m_b} + \frac{13}{6}\ln^2\frac{\Delta}{m_b} + \left(-\frac{85}{6} + \frac{2\pi^2}{3}\right)\ln\frac{\Delta}{m_b} - 4\zeta(3) - \frac{91\pi^2}{18} - \frac{631}{36} \\
C_3^s(\Delta) &= -\frac{7}{3}\ln^4\frac{\Delta}{m_b} + \frac{1}{3}\ln^3\frac{\Delta}{m_b} + \left(\frac{275}{18} - \frac{2\pi^2}{3}\right)\ln^2\frac{\Delta}{m_b} + \frac{1}{18}\left(-581 + 58\pi^2\right)\ln\frac{\Delta}{m_b} \\
&\quad + \frac{1}{324}\left(-12727 - 6366\pi^2 - 108\pi^4 - 13824\zeta(3)\right) \\
C_4^s(\Delta) &= 3\ln^5\frac{\Delta}{m_b} - \frac{35}{12}\ln^4\frac{\Delta}{m_b} + \left(-\frac{35}{2} + \frac{2\pi^2}{3}\right)\ln^3\frac{\Delta}{m_b} + \left(\frac{6029}{108} - \frac{29\pi^2}{6}\right)\ln^2\frac{\Delta}{m_b} \\
&\quad + \left(-\frac{9557}{108} + \frac{235\pi^2}{18} - \frac{\pi^4}{5}\right)\ln\frac{\Delta}{m_b} - 72\zeta(5) - \frac{555}{2}\zeta(3) + \pi^2\left(-\frac{24959}{324} - 8\zeta(3)\right) \\
&\quad - \frac{57\pi^4}{10} - \frac{283555}{2592} \\
C_5^s(\Delta) &= -\frac{62}{15}\ln^6\frac{\Delta}{m_b} + \frac{33}{5}\ln^5\frac{\Delta}{m_b} + \left(\frac{395}{18} - \frac{2\pi^2}{3}\right)\ln^4\frac{\Delta}{m_b} + \left(-\frac{2543}{27} + \frac{58\pi^2}{9}\right)\ln^3\frac{\Delta}{m_b} \\
&\quad + \left(\frac{32171}{162} - \frac{235\pi^2}{9} + \frac{2\pi^4}{5}\right)\ln^2\frac{\Delta}{m_b} + \left(-\frac{50189}{162} + \frac{4429\pi^2}{81} - \frac{29\pi^4}{15}\right)\ln\frac{\Delta}{m_b} \\
&\quad - \frac{7392583}{19440} - \frac{154997\pi^2}{486} - \frac{3932\pi^4}{75} - \frac{494\pi^6}{315} - \frac{7452}{5}\zeta(5) \\
&\quad - \left(\frac{205219}{135} + \frac{496\pi^2}{3} + 96\zeta(3)\right)\zeta(3). \qquad (3.32)
\end{aligned}
$$

$$
\begin{aligned}
C_1^u(\Delta) &= -2\ln^2\frac{\Delta}{m_b} - \frac{26}{3}\ln\frac{\Delta}{m_b} - 2\pi^2 - \frac{13}{36} \\
C_2^u(\Delta) &= 2\ln^3\frac{\Delta}{m_b} + 3\ln^2\frac{\Delta}{m_b} + \left(-\frac{113}{6} + \frac{2\pi^2}{3}\right)\ln\frac{\Delta}{m_b} - 16\zeta(3) - \frac{41\pi^2}{6} + \frac{1333}{144} \\
C_3^u(\Delta) &= -\frac{7}{3}\ln^4\frac{\Delta}{m_b} - \frac{2}{9}\ln^3\frac{\Delta}{m_b} + \left(\frac{359}{18} - \frac{2\pi^2}{3}\right)\ln^2\frac{\Delta}{m_b} + \left(-\frac{5045}{108} + \frac{34\pi^2}{9}\right)\ln\frac{\Delta}{m_b} \\
&\quad + \frac{168313}{2592} - \frac{2135\pi^2}{108} - \frac{7\pi^4}{5} - 98\zeta(3) \\
C_4^u(\Delta) &= 3\ln^5\frac{\Delta}{m_b} - \frac{5}{2}\ln^4\frac{\Delta}{m_b} + \frac{1}{6}\left(-133 + 4\pi^2\right)\ln^3\frac{\Delta}{m_b} + \left(\frac{16735}{216} - \frac{17\pi^2}{3}\right)\ln^2\frac{\Delta}{m_b} \\
&\quad + \left(-\frac{180229}{1296} + \frac{319\pi^2}{18} - \frac{\pi^4}{5}\right)\ln\frac{\Delta}{m_b} - 432\zeta(5) - \left(\frac{1807}{6} + 40\pi^2\right)\zeta(3) - \frac{13129\pi^2}{432} \\
&\quad - \frac{79\pi^4}{6} + \frac{11428313}{31104} \\
C_5^u(\Delta) &= -\frac{62}{15}\ln^6\frac{\Delta}{m_b} + \frac{94}{15}\ln^5\frac{\Delta}{m_b} + \left(\frac{479}{18} - \frac{2\pi^2}{3}\right)\ln^4\frac{\Delta}{m_b} + \left(-\frac{2215}{18} + \frac{68\pi^2}{9}\right)\ln^3\frac{\Delta}{m_b} \\
&\quad + \left(\frac{21581}{72} - \frac{319\pi^2}{9} + \frac{2\pi^4}{5}\right)\ln^2\frac{\Delta}{m_b} + \left(-\frac{668117}{1296} + \frac{13535\pi^2}{162} - \frac{34\pi^4}{15}\right)\ln\frac{\Delta}{m_b} - 4920\zeta(5) \\
&\quad + \left(\frac{29741}{54} - \frac{1408\pi^2}{3} - 672\zeta(3)\right)\zeta(3) + \frac{8231\pi^2}{48} - \frac{2774\pi^6}{315} - \frac{1649\pi^4}{30} + \frac{64526377}{31104}. \qquad (3.33)
\end{aligned}
$$

$$
\begin{aligned}
W_1(\Delta,P_\gamma) &= -\frac{5}{3}\ln\frac{\Delta-P_\gamma}{m_b}-\frac{2\pi^2}{3}+\frac{167}{36}\\
W_2(\Delta,P_\gamma) &= \frac{5}{6}\ln^2\frac{\Delta-P_\gamma}{m_b}-\frac{14}{3}\ln\frac{\Delta-P_\gamma}{m_b}+\frac{3857}{144}-\frac{16\pi^2}{9}-12\zeta(3)\\
W_3(\Delta,P_\gamma) &= -\frac{5}{9}\ln^3\frac{\Delta-P_\gamma}{m_b}+\frac{14}{3}\ln^2\frac{\Delta-P_\gamma}{m_b}+\left(\frac{5\pi^2}{9}-\frac{1559}{108}\right)\ln\frac{\Delta-P_\gamma}{m_b}+\frac{90043}{864}\\
&\quad -\frac{13\pi^2}{108}-\frac{16\pi^4}{15}-\frac{166}{3}\zeta(3)\\
W_4(\Delta,P_\gamma) &= \frac{5}{12}\ln^4\frac{\Delta-P_\gamma}{m_b}-\frac{14}{3}\ln^3\frac{\Delta-P_\gamma}{m_b}+\left(\frac{1559}{72}-\frac{5\pi^2}{6}\right)\ln^2\frac{\Delta-P_\gamma}{m_b}\\
&\quad +\left(\frac{14\pi^2}{3}-\frac{65545}{1296}\right)\ln\frac{\Delta-P_\gamma}{m_b}-360\zeta(5)-\left(\frac{71}{3}+32\pi^2\right)\zeta(3)\\
&\quad -\frac{112\pi^4}{15}+\frac{60449\pi^2}{1296}+\frac{14830973}{31104}\\
W_5(\Delta,P_\gamma) &= -\frac{1}{3}\ln^5\frac{\Delta-P_\gamma}{m_b}+\frac{14}{3}\ln^4\frac{\Delta-P_\gamma}{m_b}+\left(-\frac{1559}{54}+\frac{10\pi^2}{9}\right)\ln^3\frac{\Delta-P_\gamma}{m_b}\\
&\quad +\left(\frac{65545}{648}-\frac{28\pi^2}{3}\right)\ln^2\frac{\Delta-P_\gamma}{m_b}+\left(-\frac{266605}{1296}+\frac{1559\pi^2}{54}-\frac{\pi^4}{3}\right)\ln\frac{\Delta-P_\gamma}{m_b}\\
&\quad -\frac{17148}{5}\zeta(5)+\left(-576\zeta(3)+\frac{20709}{10}-304\pi^2\right)\zeta(3)-\frac{152\pi^6}{21}-\frac{127\pi^4}{50}\\
&\quad +\frac{1906687\pi^2}{3888}+\frac{381772549}{155520}. \qquad (3.34)
\end{aligned}
$$

3.B The Weight Function to NLL Order

The renormalization group resummed NLL weight function has been calculated in SCET, [34, 56, 57, 46]. By expanding $W(\Delta,P_\gamma)^{\rm NLL}_{\rm SCET}$ in $\alpha_s(m_b)$ and re-expanding the logarithms of μ_i^2/m_b^2 and $\mu_i^2/(m_b(\Delta-P_\gamma))$ we find

$$
W(\Delta,P_\gamma)^{\rm NLL}_{\rm SCET}=1+\sum_{i=1}^{\infty}W_n(\Delta,P_\gamma)^{\rm NLL}_{\rm SCET}\frac{\alpha_s(m_b)^nC_F}{(4\pi)^n} \qquad (3.35)
$$

and the first coefficients are given by:

$$
\begin{aligned}
W_1(\Delta,P_\gamma)^{\rm NLL}_{\rm SCET} &= -\frac{5}{3}\ln\frac{\Delta-P_\gamma}{m_b}-\frac{2\pi^2}{3}+\frac{167}{36}\\
W_2(\Delta,P_\gamma)^{\rm NLL}_{\rm SCET} &= \left(\frac{5\beta_0}{6}+\frac{92}{27}\right)\ln^2\frac{\Delta-P_\gamma}{m_b}+\left(-\frac{14\beta_0}{3}+\frac{128}{3}\zeta(3)+\frac{85\pi^2}{27}-\frac{5122}{81}\right)\ln\frac{\Delta-P_\gamma}{m_b}\\
W_3(\Delta,P_\gamma)^{\rm NLL}_{\rm SCET} &= \left(-\frac{5\beta_0^2}{9}-\frac{92\beta_0}{27}-\frac{1616}{243}\right)\ln^3\frac{\Delta-P_\gamma}{m_b}+\left(\frac{14\beta_0^2}{3}+\left(-\frac{64}{3}\zeta(3)-\frac{65\pi^2}{27}\right.\right.\\
&\quad\left.\left.+\frac{11501}{162}\right)\beta_0-\frac{2560}{27}\zeta(3)-\frac{512\pi^4}{135}-\frac{2392\pi^2}{243}+\frac{68155}{162}\right)\ln^2\frac{\Delta-P_\gamma}{m_b}\\
W_4(\Delta,P_\gamma)^{\rm NLL}_{\rm SCET} &= \left(\frac{5\beta_0^3}{12}+\frac{253\beta_0^2}{81}+\frac{808\beta_0}{81}+\frac{27584}{2187}\right)\ln^4\frac{\Delta-P_\gamma}{m_b}+\left(-\frac{14\beta_0^3}{3}+\left(\frac{128}{9}\zeta(3)\right.\right.\\
&\quad\left.+\frac{175\pi^2}{81}-\frac{19981}{243}\right)\beta_0^2+\left(\frac{2560}{27}\zeta(3)+\frac{512\pi^4}{135}+\frac{3220\pi^2}{243}-\frac{243991}{486}\right)\beta_0\\
&\quad+\frac{65536}{27}\zeta(5)+\frac{47104}{243}\zeta(3)+\frac{2048\pi^4}{243}+\frac{56560\pi^2}{2187}-\frac{21384356}{6561}\Bigg)\ln^3\frac{\Delta-P_\gamma}{m_b}\\
W_5(\Delta,P_\gamma)^{\rm NLL}_{\rm SCET} &= \left(-\frac{\beta_0^4}{3}-\frac{230\beta_0^3}{81}-\frac{2828\beta_0^2}{243}-\frac{55168\beta_0}{2187}-\frac{462080}{19683}\right)\ln^5\frac{\Delta-P_\gamma}{m_b}\\
&\quad+\left(\frac{14\beta_0^4}{3}+\left(-\frac{32}{3}\zeta(3)-\frac{55\pi^2}{27}+\frac{89585}{972}\right)\beta_0^3+\left(-\frac{7040}{81}\zeta(3)-\frac{1408\pi^4}{405}\right.\right.\\
&\quad\left.-\frac{11132\pi^2}{729}+\frac{548459}{972}\right)\beta_0^2+\left(-\frac{32768}{9}\zeta(5)-\frac{23552}{81}\zeta(3)-\frac{1024\pi^4}{81}\right.\\
&\quad\left.-\frac{35552\pi^2}{729}+\frac{3675094}{729}\right)\beta_0-\frac{1310720}{243}\zeta(5)-\frac{827392}{2187}\zeta(3)-\frac{262144\pi^6}{15309}\\
&\quad\left.-\frac{188416\pi^4}{10935}-\frac{1213696\pi^2}{19683}+\frac{1371073480}{59049}\right)\ln^4\frac{\Delta-P_\gamma}{m_b}. \qquad (3.36)
\end{aligned}
$$

We verify that the leading β_0 terms agree with Eq. (3.34).

Chapter 4

Phase Space and Jet Definitions in SCET

The material in this chapter appeared originally in the publication, "Phase Space and Jet definitions in SCET", [29].

4.1 Introduction

The study of jets provides an important tool to investigate strong interactions and tests QCD over a wide range of scales, from partonic hard scattering to the evolution of hadronic final states that make up the jets. Hadronic jets also play an integral role in searches for physics beyond the Standard Model. Soft-collinear effective theory (SCET) [6, 13, 14, 15, 16] provides a useful framework to study jets, reproducing results from QCD obtained from traditional factorization techniques (see, for example, [7, 8]) while systematically including power corrections and organizing perturbative resummation.

The effective theory separates the scales of the underlying hard interaction from the scales associated with the collinear particles in the jets and the long-distance soft physics. Unlike QCD, particles in SCET whose momenta have parametrically different scaling are

described by separate fields - in this case, either (ultra-)soft or collinear[1]. Their light-cone components, $p = (n \cdot p, \bar{n} \cdot p, p_\perp) = (p^+, p^-, p^\perp)$ scale as :

$$p_s \sim Q(\lambda^2, \lambda^2, \lambda^2), \; p_c \sim Q(1, \lambda^2, \lambda) \tag{4.1}$$

where n and $\bar{n}$ are light-cone vectors in the $\pm\vec{n}$ direction and λ is a small dimensionless parameter which is determined by the dynamics. At leading order in λ the soft and collinear modes decouple in the SCET Lagrangian. These properties of the effective theory have been utilized to prove factorization, resum large logarithms and parameterize nonperturbative corrections for event shapes in the two jet limit [62, 63, 64, 11] and for massive top quark jets [65], for example. The factorization of generic fully differential jet cross sections has also been shown independent of jet observables for e^+e^- and pp collisions [66]. For an n-jet cross section with a given jet definition to fully factorize, however, the phase space constraints should also factorize appropriately in the effective field theory (EFT). Such factorization of phase space constraints has not yet been shown in any scheme other than the hemisphere scheme [66] (in which all events are dijet).

In this chapter we study the two-jet cross section for e^+e^- collisions in SCET, using three jet algorithms: a cone algorithm, Sterman-Weinberg (SW) [18], which defines a jet based on an angularity cut and was considered in the context of SCET in [62, 63, 67], as well as two clustering algorithms, JADE [68] and $k_\perp$ [9], which iteratively combine partons into jets based on kinematic conditions. This is a first step towards the broader goal of determining the appropriate factorization theorem and resumming logarithms using SCET. While we do not consider here the more general problem of factorization theorems for jets, we point out some implications of our results for factorization theorems, in particular showing that the form of the factorization in SCET depends on the ultraviolet regulator. The main point of this chapter is instead to demonstrate the relationship between the cutoffs in the effective field theory and phase space limits, and to consider

[1] In situations with multiple collinear directions, there are collinear modes for each direction.

their implications for dijet rates in SCET. Since SCET has no hard cutoff separating soft from collinear regions of phase space, some care is required to perform phase space integrals consistently. The NLO dijet rate in SCET also demonstrates the interplay of divergences between the soft and collinear sectors, and provides nontrivial examples of the zero-bin subtraction [40].

4.2 Phase Space in QCD and SCET

At each order in perturbation theory, a jet algorithm corresponds to a scheme to partition the available phase space into regions with different numbers of jets. At $O(\alpha_s)$, the phase space for $e^+e^- \to$ hadrons or hadronic Z decay was discussed in SCET in [40] using the variables $x_i = \frac{2p_i \cdot q}{q^2}$, where $q = p_1 + p_2 + p_3$ is the total momentum of the process and $p_{1,2,3}$ are the momenta of the quark, antiquark and gluon, respectively. In our discussion we will find it more convenient to choose the independent variables to be the light-cone components of the gluon momentum, $p_3^+ \equiv n \cdot p_3$ and $p_3^- \equiv \bar{n} \cdot p_3$, and fix the coordinates by choosing the antiquark to be moving purely in the $\bar{n}$ direction (i.e. $p_2^- = p_2^\perp = 0$). The resulting phase space is illustrated schematically in Fig. 4.1. Note that because our choice of coordinates is not symmetric in the n and $\bar{n}$ directions, the phase space is not symmetric under exchange of the p_3^+ and p_3^- axes. (For example, in the upper left the antiquark is constrained to be soft, while in the lower right the quark and antiquark recoil against the gluon, and so either the quark or the antiquark may be soft, or both may be $\bar{n}$-collinear.)

In the shaded regions, two of the partons recoil approximately back-to-back and the third is either soft or recoils roughly parallel with one of the other two, while in the central unshaded region all three partons recoil in different directions. Thus, the shaded region roughly corresponds to two-jet events, while the central region corresponds to three-jet events. The precise details of this correspondence are determined by the particular jet

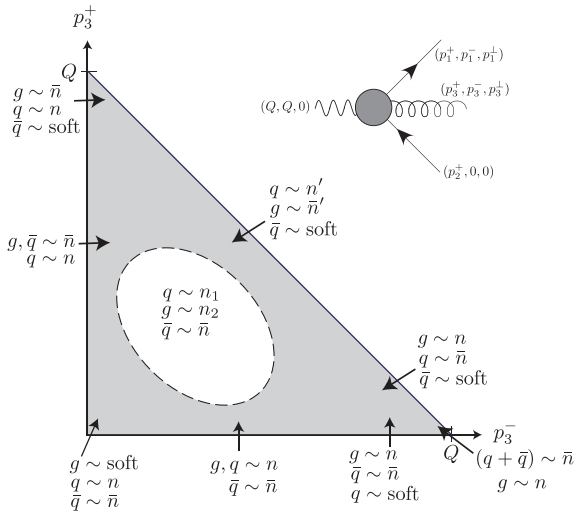

Figure 4.1: Three-body phase space in p_3^+, p_3^- variables. The shaded area indicates regions which may be described with two collinear directions in SCET; the white region in the centre requires three directions.

algorithm being used.

Within the effective field theory there are natural degrees of freedom associated with each region of the two jet phase space, as indicated in Fig. 4.1. The complete dijet rate, however, requires integrating over all these regions, and since SCET has no hard cutoff separating soft and collinear degrees of freedom, it would seem that each mode should be integrated over the full QCD phase space (this is the approach followed in [40]). However, this is inconsistent with the effective theory, since, for example, integrating a soft gluon in the collinear region would require it to have momentum well above the cutoff for soft modes in SCET.

Instead, a phase space integral which extends above the cutoff for the relevant mode should be replaced by an ultraviolet divergence, which would then be regulated and renormalized in the usual way. This occurs naturally in SCET because of the multipole expansion for momenta at the vertices. The kinematics for soft and collinear gluon emission is shown in Fig. 4.2, where $p^\pm$ scale as Q, $p^\perp$ scale as λQ and the k's scale as $\lambda^2 Q$. Because of the multipole expansion, a given component of momentum is not

conserved at vertices involving particles whose typical momenta scale differently with λ. As a consequence, the phase space for each mode in SCET differs from that in full QCD, and it is misleading to use the kinematics in Fig. 4.1 in the effective theory. For example, in the soft emission graph in Fig. 4.2, conservation of momentum requires $p_1^- = Q$, $p_2^+ = Q$, while the k's are unconstrained. It is integrals over these unconstrained momenta which will give rise to ultraviolet divergent phase space integrals in the EFT. This is the approach followed in [11], where ultraviolet divergent phase space integrals are obtained for the soft and jet functions at NLO for angularity distributions in SCET. This is also what happens in SCET in loop graphs, where both soft and collinear degrees of freedom propagate, integrated over the appropriate kinematic variables. Since phase space integrals are just loop graphs with internal propagators placed on shell, the same rules apply.

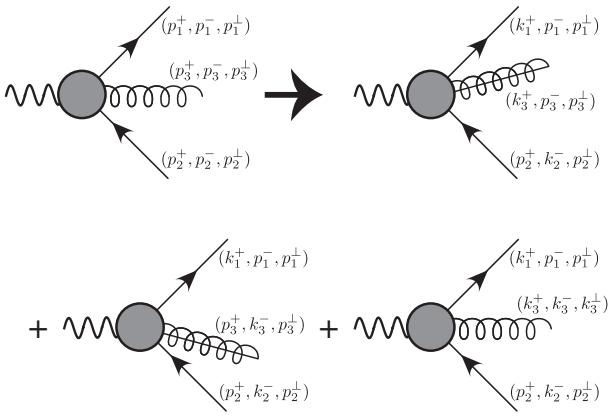

Figure 4.2: Kinematics in SCET. In the first SCET diagram the gluon is n-collinear, in the second it is $\bar{n}$-collinear, and in the third it is soft. Additional diagrams with soft quarks arise at higher order in λ.

It is straightforward to illustrate this for various jet definitions. In the SW definition, a two-jet event is defined as one in which all but a fraction β of the total energy of the event is deposited in two back-to-back cones with half angle δ [18]. The JADE algorithm

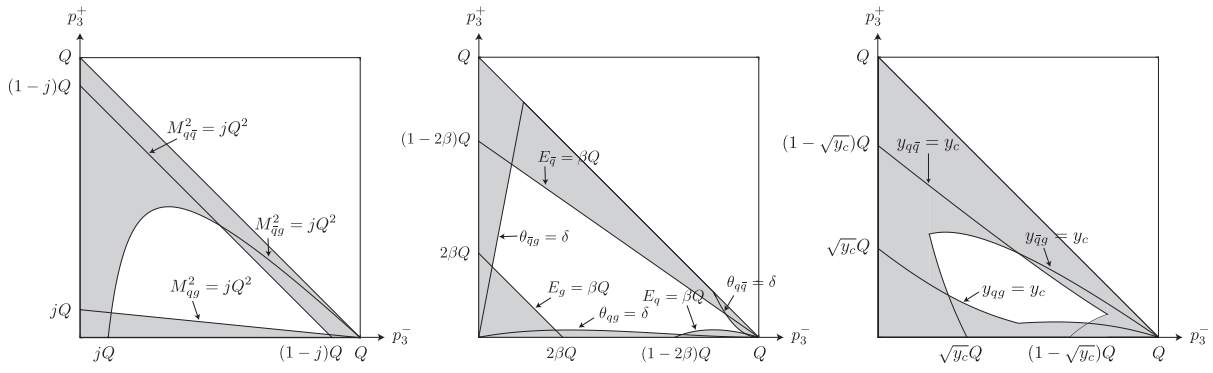

(a) JADE *(b)* SW *(c)* $k_\perp$

Figure 4.3: Three-body phase space for different jet definitions in QCD. The shaded region corresponds to the two jet region; the unshaded region in the centre is the three-jet region.

requires that the invariant mass M_{ik}^2 of every pair of final-state partons i and k be calculated. If any are less than a fraction, j, of the total center of mass energy squared, Q^2, then the momenta of the pair with the smallest invariant mass are combined into a single jet according to a recombination scheme which is part of the jet definition, the details of which are not relevant at $O(\alpha_s)$. This process is repeated until no pair has an invariant mass less than jQ^2. The $k_\perp$ algorithm is a modified version of the JADE algorithm which clusters partons based on their relative transverse momentum rather than their invariant mass. The corresponding kinematic variable is

$$y_{ij} = \frac{2}{Q^2}(1-\cos\theta_{ij})\min\left(E_i^2, E_j^2\right). \tag{4.2}$$

For massless particles this is equal to

$$y_{ij} = \frac{M_{ij}^2}{Q^2}\min\left(\frac{E_i}{E_j}, \frac{E_j}{E_i}\right). \tag{4.3}$$

The final states with the smallest y_{ij}, given that it is less than a resolution parameter y_c, are combined according to a combination prescription. This process is repeated until all pairs have $y_{ij} > y_c$. In Fig. 4.3 we illustrate the two-jet regions in QCD as defined by the JADE, SW and $k_\perp$ algorithms. The SCET regime for the two-jet cross section

corresponds to choosing the parameters δ, β, j or y_c to be much less than one in the respective jet definition.

For the two jet JADE cross section, for example, integrating k_3^+ in the soft sector all the way up to Q, as in Fig. 4.3(a), corresponds to integrating the gluon momentum far above the cutoff. In the EFT, the upper limit of integration should therefore be replaced by an ultraviolet cutoff. Indeed, while the regions of integration for the various jet definitions are quite complicated, as far as the soft gluon is concerned they should have no structure above the soft scale. A similar situation holds for collinear gluons, where the effective cutoffs in the perpendicular and anti-collinear directions are parametrically smaller than Q.

At $O(\alpha_s)$, the JADE algorithm corresponds to a cut on the invariant masses M_{ij} of each pair of partons: if $M_{ij}^2 < jQ^2$, the partons are considered to lie in the same jet, and the event is a two-jet event. The constraints in full QCD shown in Fig. 4.3(a) are

$$\frac{M_{qg}^2}{Q^2} = \frac{p_3^+}{Q - p_3^-} < j, \quad \frac{M_{\bar{q}g}^2}{Q^2} = \frac{p_3^-}{Q} - \frac{p_3^+ p_3^-}{Q(Q - p_3^-)} < j, \frac{M_{q\bar{q}}^2}{Q^2} = \frac{Q - p_3^- - p_3^+}{Q} < j. \quad (4.4)$$

Expanding these constraints in the n-collinear sector, we find

$$\frac{M_{qg}^2}{Q^2} = \frac{k_3^+}{Q - p_3^-} < j, \quad \frac{M_{\bar{q}g}^2}{Q^2} = \frac{p_3^-}{Q} < j, \frac{M_{q\bar{q}}^2}{Q^2} = \frac{Q - p_3^-}{Q} < j \quad (4.5)$$

while in the soft sector we obtain

$$\frac{M_{qg}^2}{Q^2} = \frac{k_3^+}{Q} < j, \quad \frac{M_{\bar{q}g}^2}{Q^2} = \frac{k_3^-}{Q} < j \quad (4.6)$$

(while the constraint $M_{q\bar{q}}^2 < jQ^2$ is never satisfied). Finally, in order to avoid double-counting of the soft sector, the zero-bin of the collinear region must be subtracted [40]. Taking the soft limit of the n-collinear region in Eq. (4.5) gives the same region as the soft sector, Eq. (4.6). The corresponding regions of phase-space are shown in Fig. 4.4(a, b).

We note that, as required, the phase space contains no explicit reference to any scales above the cutoff of the theory and has no structure above this scale.

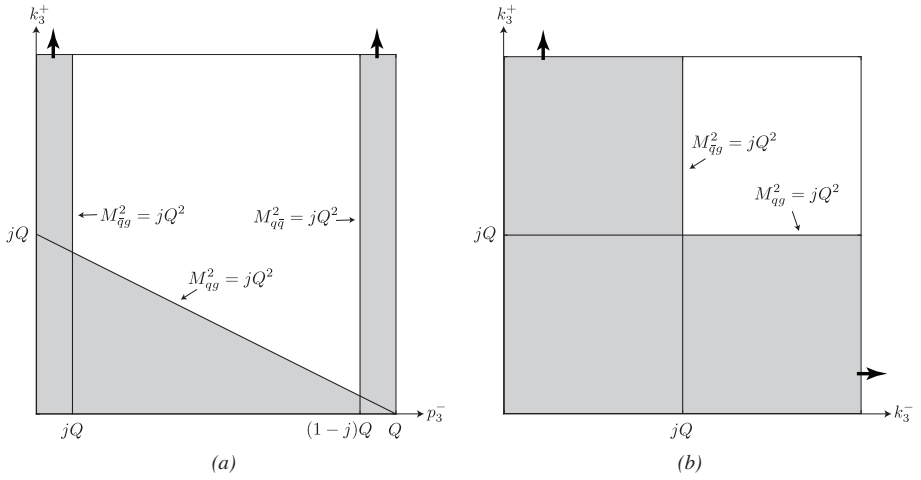

Figure 4.4: Phase space corresponding to two-jet events using the JADE algorithm in (a) the n-collinear gluon sector, and (b) the soft gluon and zero-bin sectors. The thick arrows indicate integrations to infinity.

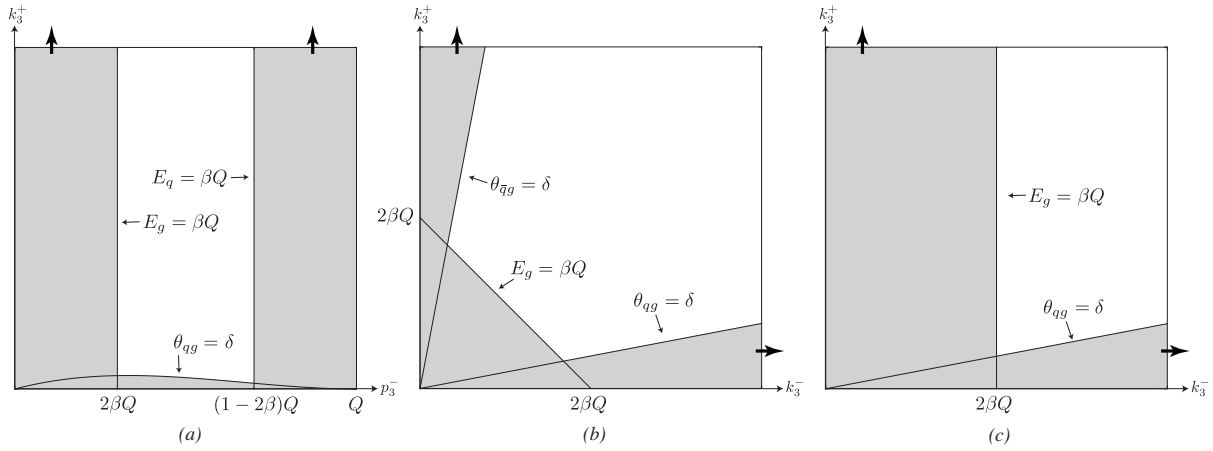

Figure 4.5: Phase space corresponding to two-jet events using the SW algorithm in (a) the n-collinear gluon sector, (b) the soft gluon sector, and (c) the zero-bin sector. As before, the thick arrows indicate integrations to infinity.

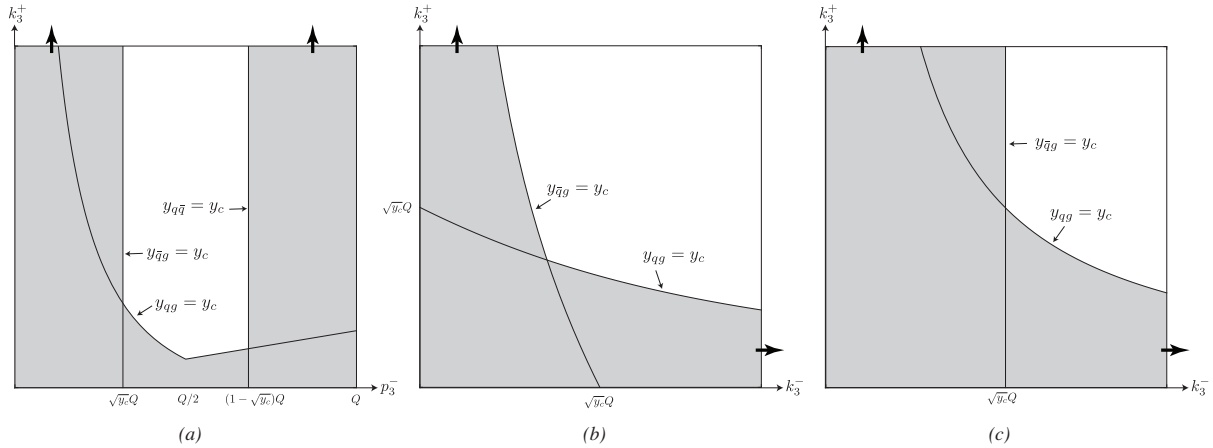

Figure 4.6: As Fig. 4.5, but using the $k_\perp$ algorithm.

Jet Definition	n-collinear regions	soft regions	zero-bin regions
JADE	$k_3^+ < j(Q - p_3^-)$	$k_3^+ < jQ$	$k_3^+ < jQ$
	$p_3^- < jQ$	$k_3^- < jQ$	$k_3^- < jQ$
	$p_3^- > Q(1-j)$		
SW	$k_3^+ < p_3^- \frac{(Q-p_3^-)^2}{Q^2}\delta^2$	$\frac{k_3^+}{k_3^+ + k_3^-} < \delta^2$	$k_3^+ < \delta^2 p_3^-$
	$p_3^- < 2\beta Q$	$\frac{k_3^-}{k_3^+ + k_3^-} < \delta^2$	$p_3^- < 2\beta Q$
	$p_3^- > (1-2\beta)Q$	$k_3^+ + k_3^- < 2\beta Q$	
$k_\perp$	$\min\left(\frac{k_3^+}{p_3^-}, \frac{k_3^+ p_3^-}{(Q-p_3^-)^2}\right) < y_c$	$\left(k_3^+ + k_3^-\right) k_3^+ < y_c Q^2$	$k_3^+ p_3^- < y_c Q^2$
	$(p_3^-)^2 < y_c Q^2$	$\left(k_3^+ + k_3^-\right) k_3^- < y_c Q^2$	$(p_3^-)^2 < y_c Q^2$
	$(Q - p_3^-)^2 < y_c Q^2$		

Table 4.1: Two-jet regions of three-body phase space for JADE, Sterman-Weinberg (SW) and $k_\perp$ jet algorithms.

Similar constraints in the soft, collinear and zero-bin sectors are easily obtained for the SW and $k_\perp$ definitions, and are summarized in Table 4.1. Note that in both SW and $k_\perp$, the zero-bin region is not the same as the soft region, since taking the soft limit of the n-collinear phase space is not the same as taking the soft limit of the full QCD phase space. The corresponding regions are illustrated in Figs. 4.5 and 4.6.

Note that we have not had to specify the SCET expansion parameter λ in order to expand the phase space in the soft and collinear sectors; we have only assumed that $\lambda \ll 1$ so that the multipole expansion is valid. Similarly, we have not assumed any relative scaling between β and δ in the SW jet definition.

4.3 Dijet Rates to $O(\alpha_s)$

In this section we calculate the NLO dijet rate (denoted f_2) in the JADE, SW and $k_\perp$ schemes in SCET, which is straightforward to do given the phase space regions of the previous section. We show that in each case SCET reproduces full QCD, as it must, up to power corrections. We examine the scales that appear in the soft and collinear cross sections, where the power counting parameter λ is determined by the dynamics in each algorithm. It is instructive to note the cancellation of ultraviolet divergences between the soft and collinear real emission contributions. We also consider the infrared safety of the soft and collinear rates separately.

At $O(\alpha_s)$ the only contribution to the dijet rate comes from the two-jet SCET operator $O_2 = \bar{\xi}_n W_n \gamma^\mu W_{\bar{n}}^\dagger \xi_{\bar{n}}$. The matching calculation from the full QCD current $\bar{\psi}\gamma^\mu\psi$ onto O_2 has been performed many times in the literature [69, 67, 12], with the Wilson coefficient

$$C_2 = 1 + \frac{\alpha_s C_F}{2\pi}\left(-\frac{1}{2}\ln^2\frac{\mu^2}{-Q^2} - \frac{3}{2}\ln\frac{\mu^2}{-Q^2} - 4 + \frac{\pi^2}{12}\right) \tag{4.7}$$

and the $\overline{\text{MS}}$ counterterm

$$Z_2 = 1 + \frac{\alpha_s C_F}{2\pi}\left(\frac{1}{\epsilon^2} + \frac{3}{2\epsilon} + \frac{1}{\epsilon}\ln\frac{\mu^2}{-Q^2}\right) \tag{4.8}$$

where we are working in $d = 4 - 2\epsilon$ dimensions. The SCET differential cross section for soft gluon emission is given by

$$\frac{1}{\sigma_0} d\sigma^s = \frac{\alpha_s C_F}{2\pi} \frac{\mu^{2\epsilon} e^{\epsilon\gamma_E}}{\Gamma(1-\epsilon)} dk_3^+ dk_3^- \frac{2\,\theta(k_3^+ k_3^-)}{(k_3^+)^{1+\epsilon}(k_3^-)^{1+\epsilon}} \tag{4.9}$$

while for n-collinear gluon emission it is

$$\frac{1}{\sigma_0} d\sigma^n = \frac{\alpha_s C_F}{2\pi} \frac{\mu^{2\epsilon} e^{\epsilon\gamma_E}}{\Gamma(1-\epsilon)} dk_3^+ dp_3^- \frac{(p_3^- k_3^+)^{-\epsilon}}{Q k_3^+} \left(\frac{p_3^-}{Q}(1-\epsilon) + 2\frac{Q - p_3^-}{p_3^-} \right) \tag{4.10}$$

where $\sigma_0 = (4\pi\alpha^2/Q^2) \sum_f e_f^2$ is the leading order Born cross section with a sum over the (anti-)quark charges e_f. The dependence on $\vec{k}_3^\perp$ and $\vec{p}_3^\perp$ has been eliminated via the gluon on-shell condition, and the integral over the $2 - 2\epsilon$ perpendicular components of the gluon momentum has been performed in each case.

Finally, the differential rate in the gluon zero-bin region, $d\sigma^{n0}$, is obtained by taking the soft limit of Eq. (4.10), which is the same as the soft rate,

$$d\sigma^{n0} = d\sigma^s. \tag{4.11}$$

(There are also zero-bin regions corresponding to the quark and antiquarks becoming soft, but they are higher order in λ and we will not consider them here.) For the n-collinear region there are two zero-bins: $p_3^- \to 0$ and $p_1^- \to 0$, but the contribution to the cross section from the latter is of higher order in λ and so we will not consider them here.

4.3.1 JADE

Integrating the soft rate over the soft dijet region (4.6) in the JADE definition gives

$$\frac{1}{\sigma_0} \sigma^s_{\text{JADE}} = \frac{\alpha_s C_F}{2\pi} \left(-\frac{2}{\epsilon^2} - \frac{2}{\epsilon} \ln \frac{\mu^2}{j^2 Q^2} - \ln^2 \frac{\mu^2}{j^2 Q^2} + \frac{\pi^2}{6} \right)$$

where we have taken $j \ll 1$ and kept only the leading terms in j. Integrating the n-collinear rate over the region (4.5), we find

$$\frac{1}{\sigma_0} \tilde{\sigma}^n_{\text{JADE}} = \frac{\alpha_s C_F}{2\pi} \left(\frac{3}{2\epsilon} + \frac{2}{\epsilon} \ln j + \frac{3}{2} \ln \frac{\mu^2}{j Q^2} + 2 \ln \frac{\mu^2}{Q^2} \ln j - 3 \ln^2 j - \frac{\pi^2}{3} + \frac{7}{2} \right) \tag{4.12}$$

where the tilde denotes that the zero-bin has not been subtracted. The rate in the zero-bin region is identical to that in the soft region, and so the zero-bin subtracted result for the emission of an n-collinear gluon is

$$\begin{aligned}\frac{1}{\sigma_0}\sigma^n_{\rm JADE} &= \frac{1}{\sigma_0}(\tilde\sigma^n_{\rm JADE}-\sigma^{n0}_{\rm JADE}) = \frac{1}{\sigma_0}(\tilde\sigma^n_{\rm JADE}-\sigma^s_{\rm JADE})\\ &= \frac{\alpha_s C_F}{2\pi}\left(\frac{2}{\epsilon^2}+\frac{3}{2\epsilon}+\frac{2}{\epsilon}\ln\frac{\mu^2}{jQ^2}+\frac{3}{2}\ln\frac{\mu^2}{jQ^2}\right.\\ &\quad \left.+\ln^2\frac{\mu^2}{jQ^2}-\frac{\pi^2}{2}+\frac{7}{2}\right). \end{aligned} \tag{4.13}$$

The emission of a collinear gluon in the $\bar n$ direction, i.e. from the anti-quark, can be calculated in a similar way, and it gives the same contribution.

In pure dimensional regularization, all the virtual vertex corrections and the wave-function renormalizations involve scaleless integrals and thus vanish. Hence we only need to add up the real emission contributions:

$$\begin{aligned}\frac{1}{\sigma_0}\sigma^R_{\rm JADE} &= \frac{1}{\sigma_0}\left((\tilde\sigma^n_{\rm JADE}-\sigma^{n0}_{\rm JADE})+(\tilde\sigma^{\bar n}_{\rm JADE}-\sigma^{\bar n 0}_{\rm JADE})+\sigma^s_{\rm JADE}\right)\\ &= \frac{1}{\sigma_0}(\tilde\sigma^n_{\rm JADE}+\tilde\sigma^{\bar n}_{\rm JADE}-\sigma^s_{\rm JADE})\\ &= \frac{\alpha_s C_F}{2\pi}\left(\frac{2}{\epsilon^2}+\frac{3}{\epsilon}+\frac{2}{\epsilon}\ln\frac{\mu^2}{Q^2}-2\ln^2 j+\ln^2\frac{\mu^2}{Q^2}\right.\\ &\quad \left.+3\ln\frac{\mu^2}{jQ^2}-\frac{5\pi^2}{6}+7\right). \end{aligned} \tag{4.14}$$

Note that the soft contribution enters into the final expression with a minus sign. This is a consequence of zero-bin subtraction and the fact that zero-bins are identical to the soft contribution. Similar observations have been pointed out in [70, 71, 72]. The divergent terms in Eq. (4.14) are cancelled by the counter term $|Z_2|^2$, and including the Wilson coefficient, $|C_2|^2$, gives the two-jet fraction

$$\begin{aligned} f_2^{\rm JADE} &= \frac{|C_2|^2}{|Z_2|^2}\left(1+\frac{1}{\sigma_0}\left(\sigma^n_{\rm JADE}+\sigma^{\bar n}_{\rm JADE}+\sigma^s_{\rm JADE}\right)\right)\\ &= 1+\frac{\alpha_s C_F}{2\pi}\left(-2\ln^2 j-3\ln j+\frac{\pi^2}{3}-1\right). \end{aligned}$$

This result agrees with the full QCD calculation given in [73, 74].

It is instructive to comment on a few details of the SCET result. First of all, since dimensional regularization regulates both the infrared and ultraviolet divergences, the cancellation of ultraviolet divergences between the soft and collinear emissions is not explicit. To show how this works, we can repeat the calculation with the quark and anti-quark offshell, $p_1^2, p_2^2 \sim \lambda^2 \neq 0$, so that all $1/\epsilon$ divergences in the calculation are ultraviolet. The calculation is given in Appendix 4.A. The resulting rate for soft gluon emission over the JADE phase space is

$$\begin{aligned}\frac{1}{\sigma_0}\sigma^s_{\rm JADE} &= \frac{\alpha_s C_F}{2\pi}\left(-\frac{2}{\epsilon}\left(\ln\frac{p_1^2}{jQ^2}+\ln\frac{p_2^2}{jQ^2}\right)+\left(\ln\frac{p_1^2}{Q^2}+\ln\frac{p_2^2}{Q^2}\right)^2\right.\\ &\quad\left.-2\left(\ln\frac{p_1^2}{Q^2}+\ln\frac{p_2^2}{Q^2}\right)\ln\frac{\mu^2}{Q^2}\right)+\cdots\end{aligned}$$

where the ellipses denote finite constant terms which are not relevant for the discussion. The unsubtracted n-collinear cross section is

$$\begin{aligned}\frac{1}{\sigma_0}\tilde{\sigma}^n_{\rm JADE} &= \frac{\alpha_s C_F}{2\pi}\left(-\frac{2}{\epsilon^2}+\frac{2}{\epsilon}\left(\ln\frac{p_1^2}{jQ^2}-\ln\frac{\mu^2}{j^2Q^2}\right)\right.\\ &\quad\left.-\ln^2\frac{p_1^2}{Q^2}+2\ln\frac{\mu^2}{Q^2}\ln\frac{p_1^2}{Q^2}+\frac{3}{2}\ln\frac{p_1^2}{Q^2}\right)+\ldots\end{aligned} \tag{4.15}$$

while the zero-bin region gives

$$\frac{1}{\sigma_0}\sigma^{n0}_{\rm JADE} = \frac{\alpha_s C_F}{2\pi}\left(-\frac{2}{\epsilon^2}-\frac{2}{\epsilon}\ln\frac{\mu^2}{j^2Q^2}\right)+\ldots\ . \tag{4.16}$$

Thus, the zero-bin subtracted n-collinear cross section is

$$\frac{1}{\sigma_0}\sigma^n_{\rm JADE} = \frac{\alpha_s C_F}{2\pi}\left(\frac{2}{\epsilon}\ln\frac{p_1^2}{jQ^2}-\ln^2\frac{p_1^2}{Q^2}+2\ln\frac{\mu^2}{Q^2}\ln\frac{p_1^2}{Q^2}+\frac{3}{2}\ln\frac{p_1^2}{Q^2}\right)+\ldots\ .$$

The result for $\bar{n}$-collinear gluon emission will be the same as that for n-collinear gluon emission with the replacement $p_1^2 \to p_2^2$. Note that the $1/\epsilon^2$ divergence from collinear emission is removed by the zero-bin. Combining the real emission contributions to the JADE cross section, Eq. (4.17), we see that while the phase-space integrals for soft and collinear gluon emission are individually ultraviolet divergent, with mixed ultraviolet infrared divergent terms, the ultraviolet divergences cancel in the sum:

$$\frac{1}{\sigma_0}\sigma^R_{\rm JADE} = \frac{\alpha_s C_F}{2\pi}\left(2\ln\frac{p_1^2}{Q^2}\ln\frac{p_2^2}{Q^2}+\frac{3}{2}\ln\frac{p_1^2}{Q^2}+\frac{3}{2}\ln\frac{p_2^2}{Q^2}\right)+\ldots\ .$$

This is the same cancellation which occurs at the one-loop level in SCET [6], in which separately ultraviolet and infrared divergent terms cancel in the sum of the soft and collinear graphs.

The soft and collinear sectors are also individually infrared finite for the JADE algorithm. The soft virtual vertex correction is given by [12], and contributes equally to the two-jet rate in all definitions

$$\frac{1}{\sigma_0}\sigma_V^s = \frac{\alpha_s C_F}{2\pi}\left(-\frac{2}{\epsilon^2} - \frac{2}{\epsilon}\ln\left(-\frac{\mu^2 Q^2}{p_1^2 p_2^2}\right) - \ln^2\left(-\frac{\mu^2 Q^2}{p_1^2 p_2^2}\right)\right) + \dots \ . \tag{4.17}$$

The soft wavefunction renormalization graphs are zero and so the cross section in the soft sector is given by

$$\frac{1}{\sigma_0}\left(\sigma_{\rm JADE}^s + \sigma_V^s\right) = \frac{\alpha_s C_F}{2\pi}\left(-\frac{2}{\epsilon^2} - \frac{4}{\epsilon}\ln\frac{\mu}{jQ}\right) + \dots \ . \tag{4.18}$$

The result is purely ultraviolet divergent and agrees with the pure dimensional regularization calculation in Eq. (4.12). The collinear contribution is similarly free of infrared divergences.

Second, we note that the scale at which the logarithms in the NLO n-collinear rate are minimized, $\mu = \sqrt{j}Q$, determines the collinear or jet scale in SCET, λQ, and that without the zero-bin subtraction there is no value of μ at which the logarithms in Eq. (4.12) are minimized. The logarithms in the soft rate (4.12) are minimized at $\mu = jQ$, the expected soft scale in SCET, $\lambda^2 Q$. From Fig. 4.4 we see that jQ is the relevant soft scale that emerges from the multipole expansion of the JADE phase space constraints. However, as we shall see from the SW two-jet soft rate, this is not universally the case. The true soft scale depends on the details of the soft theory, which is not addressed here. Furthermore the calculation of the leading logarithmic contribution in full QCD [75, 74] shows that the resummed result is not simply given by the exponentiation of the NLO term. It has been demonstrated that the emission of two soft gluons with large angular separation can be combined to constitute a third jet in the JADE clustering algorithm. These types of configurations change the leading-logarithmic two jet fraction and spoil

naive exponentiation, as the emission of subsequent soft gluons qualitatively changes the phase space constraints. These configurations also involve the parametrically lower scale j^2Q [75], which complicates the summing of logarithms of j. However, this effect does not arise until $O(\alpha_s^2)$, which is beyond the order to which we are working.

Finally, it is instructive to look more closely at the zero-bin subtractions in different regions of phase space. In particular, while the n-collinear region of integration naturally describes the region where the n-collinear quark and gluon form a jet (see Fig. 4.4(a)), it also includes regions where the antiquark and the gluon, as well as the quark and the antiquark, form jets. In order for an n-collinear gluon to form a jet with an $\bar{n}$-collinear antiquark, the gluon must be soft, and as a result one would expect the entire contribution from this region of phase space to be cancelled by the zero-bin subtraction. Similarly, the region where the n-collinear quark and $\bar{n}$-collinear antiquark form a jet should be cancelled by the corresponding quark and antiquark zero-bins; however, these are subleading in j. We show below that this is indeed the case at $O(\alpha_s)$.[2]

The region where the n-collinear gluon and $\bar{n}$-collinear quark form a jet in the JADE algorithm is defined by the region

$$k_3^+ > p_3^- \frac{(Q - p_3^-)}{Q}, \qquad 0 < p_3^- < jQ \tag{4.19}$$

and integrating the differential rate (4.10) over this region gives

$$\frac{\alpha_s C_F}{2\pi} \left(-\frac{1}{\epsilon^2} - \frac{2}{\epsilon} \ln \frac{\mu}{jQ} + \frac{\pi^2}{12} - 2 \ln^2 \frac{\mu}{jQ} \right) \tag{4.20}$$

where, as usual, we have dropped terms subleading in j. The zero-bin constraints for the same jet are

$$k_3^+ > k_3^-, \qquad 0 < k_3^- < jQ \tag{4.21}$$

and integrating the differential rate (4.11) over this region and expanding in j gives the same result as (4.20). Hence this region is entirely zero-bin and is absent from the n-collinear rate, thereby reducing the combinations of partons that need to be considered.

[2] We thank S. Freedman for this observation.

Similarly, the region where the quark and antiquark form a jet is

$$k_3^+ > \frac{(Q-p_3^-)^2}{Q}, \qquad Q(1-j) < p_3^- < Q \tag{4.22}$$

and integrating Eq. (4.11) over this region gives a result of order j, and so the rate vanishes to the order we are working. We expect that such cancellations will continue beyond leading order, simplifying the combinatorics of clustering multi-gluon states.

4.3.2 Sterman-Weinberg and $k_\perp$ Jet Definitions

It is straightforward to repeat the calculations of the previous section for the SW and $k_\perp$ jet definitions. However, each of these algorithms introduces additional features not present in the JADE calculation: the relevant scales are different and in both cases the zero-bin contribution is distinct from the soft contribution. Furthermore, in the $k_\perp$ definition the soft and collinear rates are not individually infrared safe using dimensional regularization to regulate the ultraviolet, indicating that the rate does not factorize into well-defined soft and collinear contributions in this scheme in SCET.

SW

Jets in the SW definition were studied in SCET in [62, 63, 67]. In these papers it was argued that because the kinematic cuts on the soft phase space were much larger than the typical soft scale, the soft phase space integral should be unrestricted. In [62, 63] this is because the scaling $\beta \sim \delta$ is chosen, while in [67] β is taken to be of order δ^2, but the soft scale is taken to be $\Lambda_{\rm QCD}$. Our results differ, as we have not assumed any relative scaling between βQ, δQ and $\Lambda_{\rm QCD}$, and we argue that SCET power counting uniquely requires the restricted soft phase space in Fig. 4.5(b). (We expect, however, that if $\beta \sim \delta$, SCET should be matched at a lower scale onto a new effective theory with unrestricted soft phase space.)

Integrating the differential cross section in Eq. (4.9) over the phase space generated

by the corresponding constraints, we find

$$\frac{1}{\sigma_0}\sigma^s_{\rm SW} = \frac{\alpha_s C_F}{2\pi}\left(\frac{4}{\epsilon}\ln\delta - 4\ln^2\delta + 8\ln\delta\ln\frac{\mu}{2\beta Q} - \frac{\pi^2}{3}\right).$$

By introducing quark and anti-quark off-shellnesses as we did for the JADE algorithm, it can be shown that the total soft contribution, $\left(\sigma^s_{\rm SW} + \sigma^s_V\right)/\sigma_0$, is infrared finite, and the $1/\epsilon$ terms are ultraviolet divergences. The logarithms in Eq. (4.23) cannot be minimized for any choice of μ since there is a large $\ln\delta$ in the $1/\epsilon$ term. (See, however, [76] in which factorization and resummation in the SW two-jet rate were studied in perturbative QCD.)

Integrating Eq. (4.10) over the phase space given by the collinear SW constraints, we find the naïve n-collinear contribution to be

$$\frac{1}{\sigma_0}\tilde{\sigma}^n_{\rm SW} = \frac{\alpha_s C_F}{2\pi}\left(\frac{1}{\epsilon}\left(\frac{3}{2} + 2\ln 2\beta\right) + 3\ln\frac{\mu}{\delta Q} + 2\ln 2\beta\ln\frac{\mu^2}{2\beta\delta^2 Q^2} + \frac{13}{2} - \frac{2\pi^2}{3}\right).$$

Note that there is no reasonable scale μ at which all the logarithms are minimized. We now need to subtract the $p_3^- \to 0$ zero-bin of the SW n-collinear contribution. Integrating over the relevant phase space gives us

$$\frac{1}{\sigma_0}\sigma^{n0}_{\rm SW} = \frac{\alpha_s C_F}{2\pi}\left(-\frac{1}{\epsilon^2} - \frac{2}{\epsilon}\ln\frac{\mu}{2\beta\delta Q} - 2\ln^2\frac{\mu}{2\beta\delta Q} + \frac{\pi^2}{12}\right). \tag{4.23}$$

The zero-bin gives a nontrivial contribution that is not equal to the soft contribution, because the region of integration generated by taking the collinear and then soft limit is not the same as taking the soft limit of the QCD SW phase space. It is interesting to note that the scale in the n-collinear zero-bin, $\beta\delta Q$, corresponds to the $p_\perp$ of a parton at the edge of the cone with the maximum energy allowed outside the cone, βQ. This corresponds to the intersection point of Fig. 4.5(c), generated by a consistent expansion of phase space constraints in the effective theory.

The zero-bin subtracted result for the n-collinear sector is

$$\frac{1}{\sigma_0}(\tilde{\sigma}^n_{\rm SW} - \sigma^{n0}_{\rm SW}) = \frac{\alpha_s C_F}{2\pi}\left(\frac{1}{\epsilon^2} + \frac{3}{2\epsilon} + \frac{2}{\epsilon}\ln\frac{\mu}{\delta Q} + 3\ln\frac{\mu}{\delta Q} + 2\ln^2\frac{\mu}{\delta Q} - \frac{3\pi^2}{4} + \frac{13}{2}\right)$$

where the logarithms are now minimized at $\mu = \delta Q$, unlike in Eq. (4.23). The collinear scale, δQ, corresponds to the $p_\perp$ of a parton at the edge of the cone with typical collinear

energy $O(Q)$. The emission of a collinear gluon in the $\bar{n}$ direction, i.e. from the anti-quark, gives the same result.

The n-collinear rate is independent of the jet parameter β, because the phase space region in Fig. 4.5(b) with a collinear gluon outside the cone with energy less than βQ, where $\beta \ll 1$, corresponds to the zero-bin. This contribution is entirely removed by the zero-bin subtraction and Eq. (4.24) is given only by the region where the n-collinear quark and gluon lie in the cone. This underscores the consistency of the phase space expansion in Section 4.2 and the zero-bin prescription. The soft sector resolves the cone in addition to the scale βQ and gives rise to the double logarithm cross term in the SW result below.

Combining these results gives

$$\begin{aligned} f_2^{\rm SW} &= \frac{|C_2|^2}{|Z_2|^2}\left(1+\frac{2}{\sigma_0}(\tilde{\sigma}^n_{\rm SW}-\sigma^{n0}_{\rm SW})+\frac{1}{\sigma_0}\sigma^s_{\rm SW}\right) \\ &= 1+\frac{\alpha_s C_F}{\pi}\left(-4\ln 2\beta\ln\delta-3\ln\delta-\frac{\pi^2}{3}+\frac{5}{2}\right) \end{aligned}$$

in agreement with the full QCD calculation [18].

$k_\perp$

The $k_\perp$ two-jet rate in SCET reveals a more subtle cancellation of divergences than the previous two algorithms and highlights again the importance of zero-bin subtractions. Integrating the differential cross section for the emission of a soft gluon over the soft phase space in Fig. 4.6(b), we find that $\sigma^s_{k_\perp}$ is not regulated in dimensional regularization. Performing the k_3^+ integral first over the $\bar{q}g$ jet region of phase space, we obtain a term proportional to

$$\frac{d\sigma^s_{k_\perp}}{dk_3^-} \propto \frac{\left(Q^2 y_c-(k_3^-)^2\right)^{-\epsilon}}{\epsilon\; k_3^-}+\cdots, \tag{4.24}$$

where the ellipses denote terms which are finite in $d=4-2\epsilon$ dimensions. This term causes the k_3^- integration to diverge at zero. A similar problem arises when integrating over the soft region generated by the qg jet constraint. Despite this divergence, the total

two-jet cross section is finite in QCD and so must be finite in SCET. The region that gives rise to this divergence is also integrated over in the zero-bin calculations and since the soft and zero-bin integrands are the same the divergence cancels in the difference. Integrating the soft differential rate over the combined soft and zero-bin regions gives a finite result in d dimensions:

$$\frac{1}{\sigma_0}(\sigma^s_{k_\perp} - \sigma^{n0}_{k_\perp} - \sigma^{\bar{n}0}_{k_\perp}) = \frac{\alpha_s C_F}{2\pi}\left(\frac{2}{\epsilon^2} + \frac{2}{\epsilon}\ln\frac{\mu^2}{y_c Q^2} + \ln^2\frac{\mu^2}{y_c Q^2} - \frac{\pi^2}{3}\right)$$

where we see the soft scale $\sqrt{y_c}Q$ appear as in Fig. 4.6. We combine this with the rate to produce an n-collinear gluon,

$$\frac{1}{\sigma_0}\tilde{\sigma}^n_{k_\perp} = \frac{\alpha_s C_F}{2\pi}\left(\frac{1}{\epsilon}\left(\frac{3}{2} + \ln y_c\right) + \ln\frac{\mu^2}{y_c Q^2}\left(\frac{3}{2} + \ln y_c\right) - 3\ln 2 - \frac{\pi^2}{3} + \frac{7}{2}\right) \tag{4.25}$$

to obtain the total two-jet rate for emission of a real gluon

$$\begin{aligned}&\frac{1}{\sigma_0}(\tilde{\sigma}^n_{k_\perp} + \tilde{\sigma}^{\bar{n}}_{k_\perp} + \sigma^s_{k_\perp} - \sigma^{n0}_{k_\perp} - \sigma^{\bar{n}0}_{k_\perp}) \\ = \;& \frac{\alpha_s C_F}{2\pi}\left(\frac{2}{\epsilon^2} + \frac{1}{\epsilon}\left(2\ln\frac{\mu^2}{Q^2} + 3\right) + \ln^2\frac{\mu^2}{Q^2} + 3\ln\frac{\mu^2}{Q^2} - \ln^2 y_c - 3\ln y_c - 6\ln 2 - \pi^2 + 7\right)\end{aligned}$$

where again n and $\bar{n}$ collinear gluon emission give the same contribution and the virtual piece vanishes. Including the counter-term Z_2 and the Wilson coefficient C_2, we reproduce the known NLO $k_\perp$ result [74]

$$f_2^{k_\perp} = 1 + \frac{\alpha_s C_F}{2\pi}\left(-\ln^2 y_c - 3\ln y_c - 6\ln 2 + \frac{\pi^2}{6} - 1\right).$$

This calculation re-emphasizes the importance of zero-bin subtraction: without it, the evaluation of a finite $f_2^{k_\perp}$ would not be possible. Since the soft and collinear cross sections are not regulated in dimensional regularization, it is useful to regulate the infrared and ultraviolet divergences separately by taking the outgoing quark and antiquark off-shell. The resulting rate for soft gluon emission then becomes

$$\frac{1}{\sigma_0}\sigma^s_{k_\perp} = \frac{\alpha_s C_F}{2\pi}\ln^2\frac{p_1^2 p_2^2}{Q^4\, y_c} + \dots\ . \tag{4.26}$$

Note that unlike the previous algorithms, the soft real emission result is not ultraviolet divergent. Combining this with the contribution from the soft virtual vertex correction (4.17) gives

$$\frac{1}{\sigma_0}\left(\sigma^s_{k_\perp}+\sigma^s_V\right)=\frac{\alpha_s C_F}{2\pi}\left(-\frac{2}{\epsilon^2}-\frac{2}{\epsilon}\ln\frac{\mu^2Q^2}{p_1^2p_2^2}+2\ln\frac{p_1^2p_2^2}{Q^4}\ln\frac{\mu^2}{y_cQ^2}\right)+\dots. \tag{4.27}$$

This shows explicitly that the rate in the soft sector is not infrared safe.

The rate for n-collinear gluon emission and the zero-bin are, respectively,

$$\begin{aligned}\frac{1}{\sigma_0}\tilde{\sigma}^n_{k_\perp}&=\frac{\alpha_s C_F}{2\pi}\left(-\frac{2}{\epsilon^2}-\frac{2}{\epsilon}\ln\frac{\mu^2}{p_1^2\sqrt{y_c}}-\ln^2\frac{\mu^2}{p_1^2}+\frac{3}{2}\ln\frac{p_1^2}{Q^2y_c}\right)+\dots\\ \frac{1}{\sigma_0}\sigma^{n0}_{k_\perp}&=\frac{\alpha_s C_F}{2\pi}\left(-\frac{2}{\epsilon^2}-\frac{2}{\epsilon}\ln\frac{\mu^2}{p_1^2\sqrt{y_c}}+\ln^2\frac{p_1^2}{y_cQ^2}-\ln^2\frac{\mu^2}{p_1^2}\right)+\dots\ .\end{aligned} \tag{4.28}$$

and their difference gives us the zero-bin subtracted result

$$\frac{1}{\sigma_0}\sigma^n_{k_\perp}=\frac{\alpha_s C_F}{2\pi}\left(-\ln^2\frac{p_1^2}{y_c\,Q^2}+\frac{3}{2}\ln\frac{p_1^2}{y_c\,Q^2}\right)+\dots\ . \tag{4.29}$$

As with the soft sector, the phase-space integration for the n-collinear real emission is ultraviolet finite but infrared divergent. Combining the real emission contributions to the $k_\perp$ two-jet cross section, we find

$$\begin{aligned}\frac{1}{\sigma_0}\sigma^R_{k_\perp}&=\frac{1}{\sigma_0}(\sigma^n_{k_\perp}+\sigma^{\bar{n}}_{k_\perp}+\sigma^s_{k_\perp})\\ &=\frac{\alpha_s C_F}{2\pi}\left(\frac{3}{2}\left(\ln\frac{p_1^2}{Q^2}+\ln\frac{p_2^2}{Q^2}\right)+2\ln\frac{p_1^2}{Q^2}\ln\frac{p_2^2}{Q^2}\right)+\dots\ .\end{aligned} \tag{4.30}$$

The infrared divergences in Eq. (4.30) are completely cancelled by the total virtual contribution σ_V given in Eq. (4.40). As expected, the virtual graphs convert the infrared divergences in the real emission diagrams into ultraviolet ones. While SCET reproduces the known NLO $k_\perp$ result, the soft and collinear rates are not independently infrared safe, indicating for the $k_\perp$ phase space the soft and collinear modes do not factorize in SCET using dimensional regularization to regulate the ultraviolet.

4.4 Factorization and Scheme-Dependence

It is useful to examine the failure of SCET to factorize the $k_\perp$ rate into separately infrared safe soft and collinear pieces, particularly given the fact that the regions of integration for the soft gluons are quite similar in the infrared between $k_\perp$ and JADE. Instead, the bad behaviour in Eq. (4.24) comes from the region of large k^+ and small k^- and vice-versa - a region which is infrared divergent, but sensitive to the ultraviolet regulator. Since, as we have shown, the ultraviolet divergences in the phase space integrals cancel between the soft and collinear degrees of freedom, this is an unphysical region, and so cancels from the total rate. The same cancellation occurs at the one-loop level, in which terms of order $1/\epsilon_{\rm UV} \ln p_i^2$ cancel between soft and collinear graphs [6]. However, this unphysical region can also be eliminated by defining the soft function with a cutoff Λ_f. In particular, we show in this section that while the $k_\perp$ algorithm in dimensional regularization does not factorize in SCET into separate infrared safe contributions, regulating the ultraviolet with a cutoff on the light-cone components of the gluon momentum,

$$|k^+| < \Lambda_f, \quad |k^-| < \Lambda_f \tag{4.31}$$

results in an infrared safe soft function.

Integrating the soft rate over the relevant region for $k_\perp$, including the cutoff (4.31), and continuing to work in d dimensions to regulate the infrared, we find for real soft gluon emission

$$\frac{1}{\sigma_0}\sigma^s_{k_\perp} = \frac{\alpha_s C_F}{2\pi}\left(\frac{2}{\epsilon^2} + \frac{2}{\epsilon}\ln\frac{\mu^2}{\Lambda_f^2} - \ln^2\frac{y_c Q^2}{\Lambda_f^2} + \ln^2\frac{\mu^2}{\Lambda_f^2} - \frac{\pi^2}{3}\right)$$

Similarly, the same regulator for soft real gluon emission in the JADE algorithm gives

$$\frac{1}{\sigma_0}\sigma^s_{\rm JADE} = \frac{\alpha_s C_F}{2\pi}\left(\frac{2}{\epsilon^2} + \frac{2}{\epsilon}\ln\frac{\mu^2}{\Lambda_f^2} - \frac{1}{2}\ln^2\frac{j^2 Q^2}{\Lambda_f^2} + \ln^2\frac{\mu^2}{\Lambda_f^2} - \frac{\pi^2}{6}\right)$$

Note that with a cutoff, the $1/\epsilon^2$ and Sudakov double logs $\ln^2 j$ and $\ln^2 y_c$ are entirely contained within the soft function, as opposed to pure dimensional regularization, in

which the collinear graphs also contain double logs. This is in agreement with [75, 74], where the Sudakov logs are calculated entirely from the soft graphs.

The soft virtual vertex correction with a cutoff of Λ_f in $|k^+|$ and $|k^-|$ gives a modified vertex correction

$$\sigma_V^s = \frac{\alpha_s C_F}{2\pi}\left(-\frac{2}{\epsilon^2} - \frac{2}{\epsilon}\ln\frac{\mu^2}{\Lambda_f^2} - \ln^2\frac{\mu^2}{\Lambda_f^2} + \frac{\pi^2}{6}\right) \tag{4.32}$$

giving the finite results

$$\begin{aligned}\frac{1}{\sigma_0}\left(\sigma^s_{k_\perp} + \sigma_V^s\right) &= -\frac{\alpha_s C_F}{2\pi}\left(\ln^2\frac{y_c Q^2}{\Lambda_f^2} + \frac{\pi^2}{6}\right). \\ \frac{1}{\sigma_0}\left(\sigma^s_{\rm JADE} + \sigma_V^s\right) &= -\frac{\alpha_s C_F}{4\pi}\ln^2\frac{j^2 Q^2}{\Lambda_f^2}.\end{aligned} \tag{4.33}$$

Note that the infrared divergences cancel between the real and virtual graphs, and that there are no large logs in the soft function for Λ_f of order the relevant soft scale, jQ or $\sqrt{y_c}Q$.

These results demonstrate the fact that factorization of rates in SCET into soft and collinear components is scheme-dependent. Such dependence on infrared regulators was also noted in a different context in [11] and [77]. Using the method introduced in [11] to test infrared safety at one loop, one would conclude that the soft contribution to the $k_\perp$ rate is infrared divergent. This differs from our results, because, as we have shown, the infrared safety of the soft function is ultraviolet regulator dependent. Introducing a cutoff removes the unphysical region of $k^\pm \to 0$ and $k^\mp \to \infty$ and results in an infrared safe soft contribution to the two-jet $k_\perp$ rate.[3] The bad behaviour of $k_\perp$ in dimensional regularization in SCET is therefore a feature of dimensional regularization, not of SCET. The factorization for jet rates depends on the ultraviolet regulator of the theory as well as the infrared.

[3]Similarly, the NLO soft function for angularities, τ_a, for $1 < a < 2$ integrated over τ_a between 0 and 1 can be shown to be infrared finite if defined with an ultraviolet cutoff.

4.5 Conclusion

We have presented a consistent treatment of phase-space integrals over soft and collinear degrees of freedom in SCET, illustrating this with the explicit example of the NLO dijet rate for three different jet algorithms. In this approach the phase space for different modes in the effective theory are insensitive to details above their cutoff, giving real emission contributions with ultraviolet divergences which cancel between the collinear and soft sectors. Although the leading order SCET Lagrangian separates soft and collinear modes and the differential cross section has been shown to factorize, we demonstrated that using dimensional regularization the $k_\perp$ algorithm does not factorize into infrared safe soft and collinear rates. We showed that this is related to a divergence in an unphysical region which cancels between the soft and collinear sectors, and is sensitive to the ultraviolet regulator.

Zero-bin subtraction is necessary to consistently integrate over the phase space configurations that need to be considered in a given jet algorithm. The zero-bin subtraction was shown to entirely remove regions of the naïve collinear rate where n and $\bar{n}$ collinear degrees of freedom form a jet at NLO in the JADE algorithm and for collinear partons outside the cone in SW. The $k_\perp$ and SW dijet rates provide nontrivial examples of zero-bin subtraction, which are different from the soft contribution.

We have not attempted to sum logarithms of the small jet parameters at this stage. While the running of C_2 makes summing some of the logarithms straightforward, the soft physics in these theories is more complicated. For example, the JADE algorithm is known not to exponentiate: there are three-jet configurations which contribute at $O(\alpha_s^2 \ln^4 j)$ in which two gluons, which would naïvely be unresolved from the quarks, are combined to form a third jet [75]. Such configurations have no simple relation to the one-gluon phase space and are not obtained by exponentiating the one-loop result. From an effective field theory viewpoint, these configurations also involve the scale $j^2 Q$, which is parametrically smaller than the soft scale jQ. The soft function for the SW algorithm, in contrast,

naïvely has an anomalous dimension of order $\ln\delta$, and so large logarithms of δ cannot be resummed in this formulation of the low-energy theory.

4.A Offshell calculations

The SCET differential cross section for soft gluon emission and offshell quarks, $p_1^2, p_2^2 \neq 0$, is

$$\frac{1}{\sigma_0} d\sigma^s = \frac{\alpha_s C_F}{2\pi} \frac{\mu^{2\epsilon} e^{\epsilon\gamma_E}}{\Gamma(1-\epsilon)}\, \theta(k_3^+ k_3^-)\, dk_3^+ dk_3^- \frac{2\,Q^2\,(k_3^+ k_3^-)^{-\epsilon}}{(Qk_3^+ + p_1^2)(Qk_3^- + p_2^2)}, \tag{4.34}$$

where $p_1^2 = Qk_1^+$, $p_2^2 = Qk_2^-$ and $p_3^2 = 0$. The JADE two-jet constraints become

$$\frac{M_{13}^2}{Q^2} = \frac{Qk_3^+ + p_1^2}{Q^2} < j, \quad \frac{M_{23}^2}{Q^2} = \frac{Qk_3^- + p_2^2}{Q^2} < j, \quad \frac{M_{12}^2}{Q^2} = 1 \tag{4.35}$$

and integrating over the soft phase space gives

$$\begin{aligned} \frac{1}{\sigma_0}\sigma^s_{\text{JADE}} &= \frac{\alpha_s C_F}{2\pi} \left(\frac{1}{\epsilon} \left(4\ln j - 2\ln\frac{p_1^2}{Q^2} - 2\ln\frac{p_2^2}{Q^2} \right) + \left(\ln\frac{p_1^2}{Q^2} + \ln\frac{p_2^2}{Q^2} \right)^2 \right. \\ &\quad \left. - 2\left(\ln\frac{p_1^2}{Q^2} + \ln\frac{p_2^2}{Q^2} \right) \ln\frac{\mu^2}{Q^2} \right) + \cdots \end{aligned} \tag{4.36}$$

where the ellipses denote finite constant terms.

Similarly, the SCET differential cross section for n-collinear gluon emission with offshellness is

$$\frac{1}{\sigma_0} d\sigma^n = \frac{\alpha_s C_F}{2\pi} \frac{\mu^{2\epsilon} e^{\epsilon\gamma_E}}{\Gamma(1-\epsilon)} dk_3^+ dp_3^- (p_3^- k_3^+)^{-\epsilon} \left(\frac{(1-\epsilon)\, p_3^- k_3^+}{(p_1^2 + Qk_3^+)^2} + \frac{2(Q - p_3^-)}{p_3^-(p_1^2 + Qk_3^+)} \right)$$

and the corresponding JADE two-jet constraints are

$$\begin{aligned} \frac{M_{13}^2}{Q^2} &= \frac{Qk_3^+ + p_1^2}{Q(Q - p_3^-)} < j, \quad \frac{M_{23}^2}{Q^2} = \frac{Qp_3^- + p_2^2}{Q^2} < j, \\ \frac{M_{12}^2}{Q^2} &= \frac{Q(Q - p_3^-) + p_1^2 + p_2^2}{Q^2} < j. \end{aligned} \tag{4.37}$$

Note that the off-shellnesses in M_{23}^2 and M_{12}^2 are suppressed with respect to the label momenta and thus can be dropped. Integrating Eq. (4.37) over the phase space given by

these constraints, we find

$$\begin{aligned}\frac{1}{\sigma_0}\tilde{\sigma}^n_{\rm JADE} &= \frac{\alpha_s C_F}{2\pi}\left(-\frac{2}{\epsilon^2}+\frac{1}{\epsilon}\left(2\ln j+2\ln\frac{p_1^2}{Q^2}-2\ln\frac{\mu^2}{Q^2}\right)\right.\\ &\quad\left.-\ln^2\frac{p_1^2}{Q^2}+2\ln\frac{\mu^2}{Q^2}\ln\frac{p_1^2}{Q^2}+\frac{3}{2}\ln\frac{p_1^2}{Q^2}\right)+\dots\ .\end{aligned}$$

The $p_3^- \to 0$ zero-bin for the n-collinear differential cross section is obtained from Eq. (4.37) by taking the soft limit:

$$\frac{1}{\sigma_0}d\sigma^{n0} = \frac{\alpha_s C_F}{2\pi}\frac{\mu^{2\epsilon}e^{\epsilon\gamma_E}}{\Gamma(1-\epsilon)}dk_3^+dp_3^-(p_3^-k_3^+)^{-\epsilon}\frac{2\,Q}{p_3^-(p_1^2+Qk_3^+)}. \tag{4.38}$$

The JADE constraints for this zero-bin are the same as the soft ones in Eq. (4.35). Performing the phase space integration gives

$$\frac{1}{\sigma_0}\sigma^{n0}_{\rm JADE} = \frac{\alpha_s C_F}{2\pi}\left(-\frac{2}{\epsilon^2}-\frac{2}{\epsilon}\ln\frac{\mu^2}{j^2Q^2}\right)+\dots\ . \tag{4.39}$$

The zero-bin subtracted result, which is the difference betweem Eq. (4.38) and Eq. (4.39), is not particularly illuminating. It should be noted, however, that this zero-bin subtraction gets rid of the $1/\epsilon^2$ term, which is also absent in the contribution from soft gluon emission in Eq. (4.36). Thus the total contribution from real gluon emission is free of such terms. The result for $\bar{n}$-collinear gluon emission will be the same as that for n-collinear gluon emission with $p_1^2 \to p_2^2$. Combining the real emission contributions to the JADE cross section gives

$$\begin{aligned}\frac{1}{\sigma_0}\sigma^R_{\rm JADE} &= \frac{1}{\sigma_0}\left((\tilde{\sigma}^n_{\rm JADE}-\sigma^{n0}_{\rm JADE})+(\tilde{\sigma}^{\bar{n}}_{\rm JADE}-\sigma^{\bar{n}0}_{\rm JADE})+\sigma^s_{\rm JADE}\right)\\ &= \frac{\alpha_s C_F}{2\pi}\left(2\ln\frac{p_1^2}{Q^2}\ln\frac{p_2^2}{Q^2}+\frac{3}{2}\ln\frac{p_1^2}{Q^2}+\frac{3}{2}\ln\frac{p_2^2}{Q^2}\right)+\dots\ .\end{aligned}$$

Notice that this result is free of ultraviolet divergences, and off-shellness is regulating all of its infrared divergences. The collinear and the soft sectors are individually ultraviolet divergent, but these ultraviolet divergences arising from the phase space cancel completely with one another in the sum.

With off-shellness, the virtual diagrams are no longer zero, and they have been previously calculated with off-shellness, for example in [69] for deep inelastic scattering and

in [12] for e^+e^- annihilation. The zero-bin subtractions of the collinear virtual graphs also vanish with this regulator [40, 72]. At the amplitude level, we sum up all the virtual vertex corrections and subtract half the wavefunction renormalization for each external (anti-)quark:

$$\begin{aligned} I_V &= \frac{\alpha_s C_F}{4\pi}\left(\frac{2}{\epsilon^2}+\frac{3}{\epsilon}-\frac{2}{\epsilon}\ln\frac{-Q^2}{\mu^2}-2\ln\frac{p_1^2}{Q^2}\ln\frac{p_2^2}{Q^2}\right. \\ &\quad \left.-\frac{3}{2}\ln\frac{p_1^2}{Q^2}-\frac{3}{2}\ln\frac{p_2^2}{Q^2}\right)+\dots\ . \end{aligned} \tag{4.40}$$

The virtual graphs' contribution to the two-jet rate is $\sigma_V = 2Re(I_V)$. We can then see that the IR divergences from real gluon emission in Eq. (4.40) will be completely cancelled by the virtual contributions, and the UV divergent terms in σ_V will be cancelled by the counter term $|Z_2|^2$.

We can also focus on the soft sector to investigate its IR safety. The soft virtual vertex correction is given by [12]:

$$I_V^s = \frac{\alpha_s C_F}{4\pi}\left(-\frac{2}{\epsilon^2}-\frac{2}{\epsilon}\ln\left(-\frac{\mu^2Q^2}{p_1^2p_2^2}\right)-\ln^2\left(-\frac{\mu^2Q^2}{p_1^2p_2^2}\right)\right)+\dots\ . \tag{4.41}$$

The soft wavefunction renormalisation graphs are zero, so in the soft sector, the soft virtual vertex correction and the soft gluon bremstrahhlung are the only two diagrams we need to add:

$$\frac{1}{\sigma_0}\left(\sigma^s_{\rm JADE}+\sigma^s_V\right)=\frac{\alpha_s C_F}{2\pi}\left(-\frac{2}{\epsilon^2}-\frac{4}{\epsilon}\ln\frac{\mu}{jQ}\right)+\dots\ . \tag{4.42}$$

This agrees with our pure dimensional regularization calculation in Eq. (4.12). This also shows that the rate in the soft sector is infrared finite. The collinear contribution is also IR safe because the sum of all sectors is free of infrared divergences.

$k_\perp$: The $k_\perp$ phase space regions shown in Table 4.1 are not affected by the introduction of the off-shellnesses, with the only exception that the constraint

$$\min\left(\frac{k_3^+}{p_3^-},\frac{k_3^+p_3^-}{(Q-p_3^-)^2}\right)<y_c \tag{4.43}$$

is slightly modified to

$$\min\left(\frac{Q-p_3^-}{p_3^-},\frac{p_3^-}{Q-p_3^-}\right)\frac{Q^2k_3^+ + p_3^- p_1^2}{Q^2(Q-p_3^-)} < y_c. \tag{4.44}$$

The calculation is otherwise straightforward.

Chapter 5

Light Octet Scalars, a Heavy Higgs and Minimal Flavour Violation

This chapter was originally published in "Light Octet Scalars, a Heavy Higgs and Minimal Flavour Violation", [30].

5.1 Introduction

Most physicists believe that new physics beyond the Standard Model (SM) awaits discovery at the LHC, and experiments at the Large Hadron Collider (LHC) will soon probe the weak scale and (hopefully) reveal the nature of whatever new physics lies beyond the Standard Model. Since the Higgs sector is among the least understood in the SM, new scalar physics could well be what is found.

However, to be found at the Tevatron or the LHC, any such new scalar physics should be associated with a comparatively low scale, $\Lambda \sim$ TeV. And because the scale is low, it must be checked that the new physics cannot contribute to processes that are well-measured and agree well with the SM, such as electroweak precision data (EWPD) and flavour-changing neutral currents (FCNCs). This suggests taking most seriously those kinds of new physics that suppress such contributions in a natural way. This can be

elegantly accomplished if the effective field theory (EFT) appropriate to low energies obeys approximate symmetries, such as a custodial symmetry $SU(2)_C$ [78, 79, 80] for EWPD and the principle of minimal flavor violation (MFV) [20, 21, 22, 23, 24, 25], which suppresses FCNCs when formulated appropriately [81, 82, 83].

Recently, it was discovered [27] that there are comparatively few kinds of exotic scalars that are flavour singlets and can have Yukawa couplings with SM fermions in a way that is consistent with MFV. The only two possible scalar representations allowed are those of the SM Higgs or octet scalars, respectively transforming under the gauge group $SU(3) \times SU(2) \times U(1)$ as $(\mathbf{1}, \mathbf{2})_{\mathbf{1/2}}$ or $(\mathbf{8}, \mathbf{2})_{\mathbf{1/2}}$.

In this chapter we examine what constraints EWPD[1], flavour physics, and direct production constraints place on the general scalar sector consistent with MFV. To this end we consider the Manohar-Wise model, for which only one $(\mathbf{1}, \mathbf{2})_{\mathbf{1/2}}$ scalar and one $(\mathbf{8}, \mathbf{2})_{\mathbf{1/2}}$ scalar are present.

Since it is the quality of SM fits to electroweak precision data that at present provide our only direct evidence for the existence of the SM Higgs, it is perhaps not surprising that the existence of a scalar octet can alter the Higgs properties to which such fits point. In particular, the best-fit value of the Higgs mass obtained from SM fits to EWPD is now $96^{+29}_{-24}\,\mathrm{GeV}$ [84]. We find that for the Manohar-Wise model, EWPD fits both change the implications for the Higgs mass, and limit the allowed mass range of the extended scalar sector.

We find that when the masses of the Higgs and octet scalars are approximately degenerate, the electroweak fits allow both the Higgs and the octet to be light, with masses $\sim 100\,\mathrm{GeV}$ (or even lighter for some components). Alternatively, agreement with EWPD also allows the octet and the Higgs doublets to be both heavy, with masses $\sim 1\,\mathrm{TeV}$. The Higgs doublet can be heavy and remain consistent with precision fits because its

[1]We thank J. Erler for private communication on the recent update to the EWPD fit results related to [84].

contribution to the relevant observables is partially cancelled by the contribution of the octet doublet. Having such a heavy Higgs without ruining electroweak fits is attractive, as a resolution of the so-called 'LEP Paradox' [19]. We find that the precision electroweak fits generically prefer to limit the splittings among some of the octet components, but by an amount that does not require fine tuning of parameters in the potential. (The overall masses of the two multiplets are subject to the usual issues associated with the electroweak hierarchy.)

The plan of this chapter is as follows, in Section 5.2 we review the Manohar-Wise model, and describe its motivation as a general scalar sector that can both allow an approximate custodial symmetry and satisfy MFV. In Section 5.3 we present our results for the phenomenology of the model. In particular, we describe its implications for an EWPD fit, and explore the parameter space that allows both doublets to be either light or heavy. Since the fits prefer a scalar spectrum that is approximately custodially symmetric, we also study loop-induced $\mathrm{SU}(2)_C$ breaking, and demonstrate that the allowed parameter space is not fine tuned. This section also describes direct-production constraints on the Higgs and octet scalar, coming from both LEP2 and the Tevatron, and reexamines how previously studied flavour constraints change if the new octets are comparatively light. We find that the octets can pass all these tests, for parameters with scalars that are either light or heavy. Some conclusions are briefly summarized in Section 5.4.

5.2 Theory

In this section we recap the main features of the the model, obtained by supplementing the SM with an colour-octet, $SU_L(2)$-doublet scalar. Particular attention is spent on its approximate symmetries, since these underly the motivation to naturally satisfy FCNC and EWPD constraints.

Motivation for $(\mathbf{8},\mathbf{2})_{1/2}$ scalars.

Minimal Flavour Violation (MFV) is a framework for having flavour-dependent masses without introducing unwanted flavour changing neutral currents (FCNCs). It assumes all breaking of the underlying approximate $\mathrm{SU}(3)_U \times \mathrm{SU}(3)_D \times \mathrm{SU}(3)_Q$ flavour symmetry of the SM is proportional to the up- or down-quark Yukawa matrices. The fact that only scalars transforming as $(\mathbf{8},\mathbf{2})_{1/2}$, or as the SM Higgs [27], can Yukawa couple to SM fermions consistent with MFV is the motivation of the phenomenological study we present here.

However, we also note that octet scalars appear in many specific new-physics scenarios, including various SUSY constructions [85, 86], topcolour models [87], and models with extra dimensions [88, 89]. Various approaches to grand unification also have light colour octet scalars, including Pati-Salam unification [90] and SU(5) unification [91, 92, 93]. Colour octet doublets have also recently been used to study new mechanisms for neutrino mass generation [94]. Octet scalar doublets appear naturally in models of the Chiral-Colour [95, 96] type where QCD originates in the chiral colour group $\mathrm{SU_L}(3) \times \mathrm{SU_R}(3)$, since in this case octet doublets are expected in addition to the Higgs as $\mathbf{3}\otimes\bar{\mathbf{3}} = \mathbf{8}\oplus\mathbf{1}$. As discussed in [97] one can also consider the class of models where the SM is extended with $\mathrm{SU(N)} \times \mathrm{SU(3)_C} \times \mathrm{SU(2)_L} \times \mathrm{U(1)_Y}$ and imagine model-building composite Higgs models with a $(\mathbf{8},\mathbf{2})_{1/2}$ scalar in the low energy spectrum. We emphasize that although many BSM scenarios contain $(\mathbf{8},\mathbf{2})_{1/2}$ scalars our motivation is essentially phenomenological.

5.2.1 The Manohar-Wise model

In the Manohar Wise model [27], the scalar sector of the SM is supplemented with the $(\mathbf{8},\mathbf{2})_{\mathbf{1/2}}$ scalar denoted

$$S^A = \begin{pmatrix} S^{A+} \\ S^{A0} \end{pmatrix} \tag{5.1}$$

where A is the colour index.

The Yukawa couplings of the $(\mathbf{8},\mathbf{2})_{\mathbf{1/2}}$ scalar to quarks is determined up to overall complex constants, η_U and η_D, to be

$$L = \eta_U \, g^U_{ij} \, \bar{u}^i_R T^A (S^A)^T \, \epsilon \, Q^j_L - \eta_D \, g^D_{ij} \, \bar{d}^i_R T^A (S^A)^\dagger \, Q^j_L + h.c, \tag{5.2}$$

where g^U and g^D are the standard model Yukawa matrices, i, j are flavor indices and

$$\epsilon = \begin{pmatrix} 0 & 1 \\ -1 & 0 \end{pmatrix}. \tag{5.3}$$

The most general renormalizable potential [27] is

$$\begin{aligned} V &= \frac{\lambda}{4}\left(H^{\dagger\, i} H_i - \frac{v^2}{2}\right)^2 + 2m_S^2 \,\mathrm{Tr}\left(S^{\dagger\, i} S_i\right) + \lambda_1 H^{\dagger\, i} H_i \,\mathrm{Tr}\left(S^{\dagger\, j} S_j\right) + \lambda_2 H^{\dagger\, i} H_j \,\mathrm{Tr}\left(S^{\dagger\, j} S_i\right) \\ &+ \left[\lambda_3 H^{\dagger\, i} H^{\dagger\, j} \,\mathrm{Tr}\left(S_i S_j\right) + \lambda_4 H^{\dagger\, i} \,\mathrm{Tr}\left(S^{\dagger\, j} S_j S_i\right) + \lambda_5 H^{\dagger\, i} \,\mathrm{Tr}\left(S^{\dagger\, j} S_i S_j\right) + h.c.\right] \\ &+ \lambda_6 \mathrm{Tr}\left(S^{\dagger\, i} S_i S^{\dagger\, j} S_j\right) + \lambda_7 \mathrm{Tr}\left(S^{\dagger\, i} S_j S^{\dagger\, j} S_i\right) + \lambda_8 \mathrm{Tr}\left(S^{\dagger\, i} S_i\right) \mathrm{Tr}\left(S^{\dagger\, j} S_j\right) \\ &+ \lambda_9 \mathrm{Tr}\left(S^{\dagger\, i} S_j\right) \mathrm{Tr}\left(S^{\dagger\, j} S_i\right) + \lambda_{10} \mathrm{Tr}\left(S_i S_j\right) \mathrm{Tr}\left(S^{\dagger\, i} S^{\dagger\, j}\right) + \lambda_{11} \mathrm{Tr}\left(S_i S_j \, S^{\dagger\, j} S^{\dagger\, i}\right), \end{aligned} \tag{5.4}$$

where i and j are SU(2) indices and $S = S^A T^A$. Since a field redefinition can be used to make λ_3 real, this represents 14 real parameters in the potential beyond those of the SM, which reduce to 9 in the custodial SU(2) symmetric case — see eqs. (5.9) through (5.12), below. No new parameters enter in the couplings of the $(\mathbf{8},\mathbf{2})_{\mathbf{1/2}}$ scalar to the electroweak gauge bosons since it has the same electroweak quantum numbers as the Higgs. We use this fact to bound the masses of the octets in Section 5.3.1. The $\lambda_{1,2,3}$ terms in Eq.(5.4) lift the mass degeneracy of the octet states when the Higgs acquires a vacuum expectation value. Expanding the neutral scalar octet as

$$S^{A\,0} = \frac{S_R^{A\,0} + i S_I^{A\,0}}{\sqrt{2}} \tag{5.5}$$

the tree level masses become [27]

$$\begin{aligned} M_\pm^2 &= M_S^2 + \lambda_1 \frac{v^2}{4} \\ M_R^2 &= M_S^2 + (\lambda_1 + \lambda_2 + 2\lambda_3)\frac{v^2}{4} \\ M_I^2 &= M_S^2 + (\lambda_1 + \lambda_2 - 2\lambda_3)\frac{v^2}{4}. \end{aligned} \tag{5.6}$$

Custodial symmetry

We find below that EWPD fits prefer the masses of some of the scalars in these models to be approximately degenerate in mass. In particular, fits prefer a mass pattern that can be naturally understood as being due to an approximate custodial $\mathrm{SU(2)_C}$ symmetry, under which the SM vector bosons transform as a triplet and the Higgs transforms as a singlet and a triplet. This symmetry is broken in the SM both by hypercharge gauge interactions, and by the mass splittings within fermion electroweak doublets.

For these reasons we next explore the implications of the custodial-invariant limit, for which $\mathrm{SU(2)_C}$ is an exact symmetry of the underlying new physics beyond the SM. In this scenario, it is interesting to examine the case that $\mathrm{SU(2)_C}$ is preserved in the Manohar-Wise model potential at a high scale $\sim 1\,\mathrm{TeV}$, up to the breaking that must be induced by the SM. Imposing exact $\mathrm{SU(2)_C}$ on the octet Higgs potential we find that the potential can be rewritten in terms of bi-doublets

$$\Phi = (\epsilon\,\phi^\star, \phi)\,, \qquad \mathcal{S}_A = (\epsilon\, S_A^\star, S_A), \tag{5.7}$$

where ϵ is given in Eqn. (5.3) and the most general gauge- and custodial-invariant potential becomes

$$\begin{aligned} V = \frac{\lambda}{16}\left[\mathrm{Tr}\,\left(\Phi^\dagger\,\Phi\right) - v^2\right]^2 + \frac{m_S^2}{2}\,\mathrm{Tr}\,\left(\mathcal{S}_A{}^\dagger \mathcal{S}_A\right) + \frac{\lambda_1}{8}\,\mathrm{Tr}\,\left(\Phi^\dagger\,\Phi\right)\,\mathrm{Tr}\,\left(\mathcal{S}_A{}^\dagger \mathcal{S}_A\right), \\ + a_1\,\mathrm{Tr}\,\left(\mathcal{S}^\dagger\,\Phi\right)\mathrm{Tr}\left(\mathcal{S}^\dagger\,\Phi\right) + \left(b_1\,\mathrm{Tr}[\mathrm{T^A\,T^B\,T^C}]\mathrm{Tr}\,\left(\Phi^\dagger\,\mathcal{S}_A\,\mathcal{S}_B^\dagger\,\mathcal{S}_C\right) + h.c.\right) \\ + c_1\,\mathrm{Tr}[\mathrm{T^A\,T^B\,T^C}]\mathrm{Tr}\,\left(\mathcal{S}_A^\dagger\,\mathcal{S}_C\right)\,\mathrm{Tr}\left(\mathcal{S}_B^\dagger\,\Phi\right), \\ + d_1\,\mathrm{Tr}[\mathrm{T^A\,T^B\,T^C\,T^D}]\mathrm{Tr}\,\left(\mathcal{S}_A^\dagger\,\mathcal{S}_B\right)\,\mathrm{Tr}\left(\mathcal{S}_C^\dagger\,\mathcal{S}_D\right), \\ + e_1\,\mathrm{Tr}[\mathrm{T^A\,T^B}]\,\mathrm{Tr}[\mathrm{T^C\,T^D}]\mathrm{Tr}\,\left(\mathcal{S}_A^\dagger\,\mathcal{S}_B\right)\,\mathrm{Tr}\left(\mathcal{S}_C^\dagger\,\mathcal{S}_D\right), \\ + f_1\,\mathrm{Tr}[\mathrm{T^A\,T^B}]\,\mathrm{Tr}[\mathrm{T^C\,T^D}]\mathrm{Tr}\,\left(\mathcal{S}_A^\dagger\,\mathcal{S}_C\right)\,\mathrm{Tr}\left(\mathcal{S}_B^\dagger\,\mathcal{S}_D\right), \end{aligned} \tag{5.8}$$

where $\mathrm{T_A}$ is used as a basis in colour space with 9 independent terms when the potential is $\mathrm{SU(2)_C}$ invariant.[2] Expanding out the potential and comparing to the general result

[2] An alternative way to obtain this count is to regard $\mathrm{SU(2)}_L \times \mathrm{SU(2)}_C$ as $SO(4)$, with both $\vec{H}$ and

of eq. (5.4), we confirm the result of [27] that $\mathrm{SU}(2)_\mathrm{C}$ implies

$$2\,\lambda_3 = \lambda_2, \tag{5.9}$$

$$2\,\lambda_6 = 2\,\lambda_7 = \lambda_{11}, \tag{5.10}$$

$$\lambda_9 = \lambda_{10}\,, \tag{5.11}$$

but we also find the additional constraint[3]

$$\lambda_4 = \lambda_5^\star. \tag{5.12}$$

Note that this constraint can effect the production mechanism of the octets at Tevatron and LHC. We see in particular that because $\mathrm{SU}(2)_\mathrm{C}$ symmetry implies $\lambda_2 = 2\lambda_3$, in this limit $M_\pm$ and M_I become degenerate.

5.2.2 Naturalness issues

In general, even if the scalar potential is required to be custodial invariant at a particular scale, it does not remain so under renormalization due to the presence of custodial-breaking interactions within the SM itself. In this section we compute these one-loop symmetry breaking effects, allowing us to quantify the extent to which the custodial-invariant potential is fine-tuned. To do so we calculate in Feynman gauge and note that ghost fields do not couple to the components of the S doublet. We also neglect goldstone boson contributions to the mass splitting as they come from the $\mathrm{SU}(2)_\mathrm{C}$ symmetric potential and so therefore cancel out in the mass splittings; not leading to mixing between the S_R and S_I states.

$\vec{S}^A$ transforming as real fields in the 4-dimensional representation. In this case the invariants of the potential can be written $m_S^2(\vec{S}^A\cdot\vec{S}^A)$, $d_{ABC}(\vec{H}\cdot\vec{S}^A)(\vec{S}^B\cdot\vec{S}^C)$, $f_{ABC}(\vec{H}_i\cdot\vec{S}^A_j\vec{S}^B_k\cdot\vec{S}^C_l)\,\epsilon^{ijkl}$, $(\vec{H}\cdot\vec{H})(\vec{S}^A\cdot\vec{S}^A)$, $(\vec{H}\cdot\vec{S}^A)(\vec{H}\cdot\vec{S}^A)$, $(\vec{S}^A\cdot\vec{S}^A)^2$ and the two independent ways of colour-contracting $(\vec{S}^A\cdot\vec{S}^B)(\vec{S}^C\cdot\vec{S}^D)$.

[3] We thank A Manohar for communication on this point clearing up a subtlety.

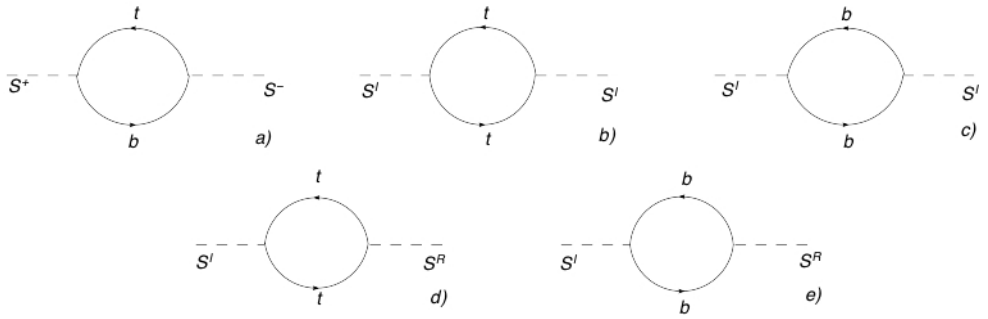

Figure 5.1: SU(2) violating contributions to $S^I, S^\pm$ masses from the yukawa sector of the theory.

$\mathrm{SU(2)_C}$ breaking due to Yukawa corrections

The breaking of $\mathrm{SU(2)_C}$ due to Yukawa couplings is straightforward, the requisite diagrams are given by Fig 5.1.

The correction to the mass $S^-\,S^+$ two point function comes from diagram (a) and is given by

$$\begin{aligned}\delta\langle T\{S^+\,S^-\}\rangle_Y &= -\delta_{ab}\,\frac{(m_b^2\,|\eta_D|^2+m_t^2\,|\eta_U|^2)[A_0(m_b^2)+A_0(m_t^2)-p^2B_0(p^2,m_b^2,m_t^2)]}{16\,\pi^2v^2} \\ &\quad -\delta_{ab}\,\frac{(m_b^4\,|\eta_D|^2+m_t^4\,|\eta_U|^2+m_b^2\,m_t^2(|\eta_D|^2+|\eta_U|^2-2\,\eta_D\,\eta_U-2\,\eta_D^\star\,\eta_U^\star))\,B_0(p^2,m_b^2,m_t^2))}{16\,\pi^2v^2}\end{aligned} \tag{5.13}$$

where we express our results in terms of Passarino-Veltman (PV) functions whose definitions are given in [111], and we set $|V_{tb}|\simeq 1$.

The contributions to the S_I^2 operator comes from the diagrams (b) and (c) and is given by

$$\begin{aligned}\delta\langle T\{S^I\,S^I\}\rangle_Y &= -\delta_{ab}\,\frac{m_t^2(2A_0(m_t^2)\,|\eta_U|^2+B_0(p^2,m_t^2,m_t^2)(4\,m_t^2\,\mathrm{Im}[\eta_U]^2-p^2\,|\eta_U|^2))}{16\,\pi^2v^2}, \\ &- \delta_{ab}\,\frac{m_b^2(2A_0(m_b^2)\,|\eta_D|^2+B_0(p^2,m_b^2,m_b^2)(4\,m_b^2\,\mathrm{Im}[\eta_D]^2-p^2\,|\eta_D|^2))}{16\,\pi^2v^2}\end{aligned} \tag{5.14}$$

We are interested in the mass splitting of M_I^2 and $M_\pm^2$, however to the accuracy we work one can also easily calculate the shifts to $\delta\langle T\{S^R\,S^R\}\rangle_Y$ and $\delta\langle T\{S^R\,S^I\}\rangle_Y$ due to the mixing induced between the real and imaginary components of S^{A0}. With these results we can then obtain the contributions to the diagonalized M_I'. The correction

to $\delta\langle T\{S^R\,S^R\}\rangle_Y$ is given by the same diagrams as $\delta\langle T\{S^I\,S^I\}\rangle_Y$ with the appropriate replacements, giving

$$\begin{aligned}\delta\langle T\{S^R\,S^R\}\rangle_Y &= -\delta_{ab}\,\frac{m_t^2(2A_0(m_t^2)\,|\eta_U|^2+B_0(p^2,m_t^2,m_t^2)(4\,m_t^2\,\mathrm{Re}[\eta_U]^2-p^2\,|\eta_U|^2))}{16\,\pi^2 v^2},\\ &\quad -\delta_{ab}\,\frac{m_b^2(2A_0(m_b^2)\,|\eta_D|^2+B_0(p^2,m_b^2,m_b^2)(4\,m_b^2\,\mathrm{Re}[\eta_D]^2-p^2\,|\eta_D|^2))}{16\,\pi^2 v^2}.\end{aligned} \tag{5.15}$$

The mixing of the S_R, S_I fields at one loop $\delta\langle T\{S^R\,S^I\}\rangle_Y$ is given by diagrams (d,e) and is given by

$$\delta\langle T\{S^R\,S^I\}\rangle_Y = -\delta_{ab}\frac{(m_b^4\,\mathrm{Re}[\eta_D]\,\mathrm{Im}[\eta_D]\,B_0(p^2,m_b^2,m_b^2)-m_t^4\,\mathrm{Re}[\eta_u]\,\mathrm{Im}[\eta_U]\,B_0(p^2,m_t^2,m_t^2))}{4\,\pi^2\,v^2}$$

which is only nonzero when at least one of the MFV proportionality constants η_D, η_U are imaginary as expected. We define the mixing angle and renormalize the theory in the Appendix.

Gauge sector $\mathrm{SU(2)_C}$ violating corrections

Calculating the required four diagrams represented by diagrams (g,i) in Fig 5.2 one finds

$$\delta\langle T\{S^I\,S^I\}\rangle_G = \frac{g_1^2}{16\pi^2}\delta^{AB}\left(\frac{dA_0[M_W^2]}{2}+\frac{dA_0[M_Z^2]}{4c_W^2}-\frac{1}{2}I_3[p^2,M_W^2,M_\pm^2]-\frac{1}{4c_W^2}I_3[p^2,M_Z^2,M_R^2]\right)$$

where $c_W \equiv cos[\theta_W]$ and the integral is given in terms of PV functions as follows

$$I_3[p^2,M_a^2,M_b^2] = (2\,p^2+2M_b^2-M_a^2)B_0[p^2,M_a^2,M_b^2]+2A_0[M_a^2]-A_0[M_b^2]. \tag{5.16}$$

The result for $\delta\langle T\{S^R\,S^R\}\rangle_G$ is identical up to the replacement $M_R \to M_I$. One can similarly calculate the other six diagrams corresponding to (f,h) that give the following contribution for $\delta\langle T\{S^+\,S^-\}\rangle_G$ in terms of PV functions[4]

$$\begin{aligned}\delta\,\langle T\{S^+\,S^-\}\rangle_G &= \frac{g_1^2}{16\pi^2}\,\delta^{AB}\left(\frac{dA_0[M_W^2]}{2}+\frac{d(1-2s_W^2)^2A_0[M_Z^2]}{4c_W^2}-\frac{1}{4}I_3[p^2,M_W^2,M_R^2]\right.\\ &\quad \left.-\frac{1}{4}I_3[p^2,M_W^2,M_I^2]-\frac{(1-2s_W^2)^2}{4c_W^2}I_3[p^2,M_Z^2,M_\pm^2]-s^2I_3[p^2,0,M_\pm^2]\right)\end{aligned} \tag{5.17}$$

[4]Note that diagram (f) with a photon loop is scaleless and vanishes in dim reg.

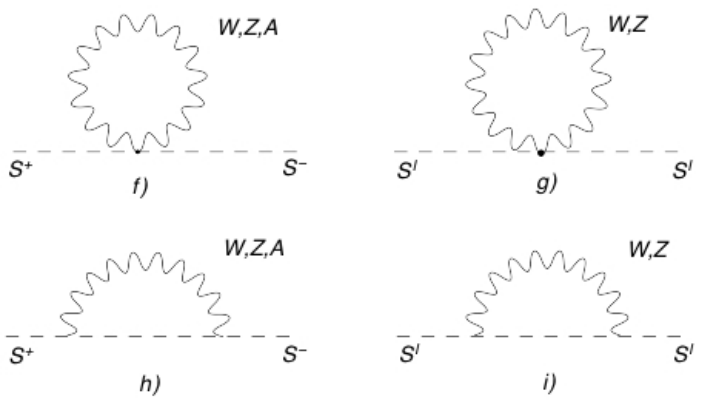

Figure 5.2: SU(2) violating contributions from the gauge sector of the theory.

Mixing between the states S^I, S^R is forbidden in the gauge sector as the couplings are real.

Given these loop-generated effects, we wish to estimate how large the custodial-symmetry-breaking interactions are once we run down to observable energies from the scale of new physics. The answer depends on how far we must run, however due to the hierarchy problem of the Higgs mass (which is only accentuated when more light scalars are added to the spectrum), it is likely that new physics must intervene at a relatively low scale for new physics of $\sim$ TeV. Such a low scale for a UV completion implies that the symmetry structure of the UV theory is consistent with EWPD and flavour constraints.

The splitting induced by SM interactions is given by the difference between the renormalized mass at Λ and the low scale, where we ignore the running for simplicity in this estimate

$$\int_{\Lambda}^{m} \left(\frac{\partial M_i^2}{\partial \mu}\right) \partial\mu = M_i^2 \left[Z_{Mi}^{\alpha}(\mu = \Lambda) - Z_{Mi}^{\alpha}(\mu = m)\right], \tag{5.18}$$

where Z_{Mi}^{α} is the leading perturbative correction of the mass counterterms, whose values are given explicitly in the appendix using a zero-momentum subtraction scheme.

As is shown in detail in the next section, the largest $M_I, M_{\pm}$ $\mathrm{SU}(2)_{\mathrm{C}}$ violating mass-splitting that is allowed by our EWPD fit is approximately $\sim 40(55)\,\mathrm{GeV}$ for the entire 68%(95%) confidence regions (see Figure 5.6). We now examine how natural such a small

splitting is assuming a typical low mass of 150 GeV.

In determining the splitting, the values of η_i employed are critical. For the lower bound on the η_i we take the one approximate loop radiatively induced value $\eta_i \sim 0.35^2/(16\,\pi^2)$. Note that we use the result of [109] that determined an upper bound on $|\eta_U|$ from the effect of the octet on $R_b = (Z \to \bar{b}\,b)/(Z \to \text{Hadrons})$. For charged scalar masses of $(75, 100, 200)$ GeV the one sigma allowed upper value for $|\eta_U|$ is $(0.27, 0.28, 0.33)$.

For $M_\pm = 150\,\text{GeV}$, we choose the couplings to give the largest induced splitting consistent with other experimental constraints ($\eta_U = 0.3, \eta_D = 0.45$), $M_I = 150\,\text{GeV}$ (its value before the perturbative correction in the high scale SU(2)_C preserving scenario) and $M_R = (190, 230)\,\text{GeV}$ which are the maximum values consistent with EWPD for the $(68\%, 95\%)$ regions. We find that the EWPD regions begin to have tuning for a high scale degenerate mass spectrum at $(90\,\text{TeV}, 8000\,\text{TeV})$. Conversely choosing the unknown $\eta_U, \eta_D \sim 0.35^2/(16\,\pi^2)$ one finds that the $(68\%, 95\%)$ regions begin to have some degree of tuning for scales of $(170\,\text{TeV}, 19000\,\text{TeV})$. For a UV completion that approximately preserves MFV and SU(2)_C, considering a SM and octet low energy scalar mass spectrum allowed by EWPD is not a fine tuned scenario.

5.3 Phenomenology

We next turn to the various observational constraints. As we shall see, the most robust constraints are those coming from the absence of direct pair-production at LEP, which require

$$M_\pm \gtrsim 100\ \text{GeV} \quad \text{and} \quad \text{M}_\text{R} + \text{M}_\text{I} \gtrsim 200\ \text{GeV}\,. \tag{5.19}$$

Since the octet scalar couples to both photons and gluons, these constraints are essentially kinematic up to the highest energies probed by LEP (more about which below).

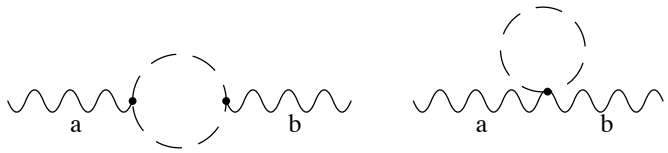

Figure 5.3: Self energies calculated for the EWPD constraints on the octets, where $(a, b) = (W^+W^-, ZZ, \gamma\gamma, Z\gamma)$. The self energies needed to determine STUVWX are given in the Appendix.

5.3.1 Fits to Electroweak Precision Data

A strong restriction on the properties of exotic scalars comes from precision electroweak measurements, whose implications we now explore in some detail. The dominant way that such scalars influence the electroweak observables is through their contributions to the gauge boson vacuum polarizations; the so-called 'oblique' corrections [100, 101, 102]. The calculation of the oblique corrections proceeds as usual with the vacuum polarizations being determined directly by evaluating the diagrams given in Figure 5.3.

When evaluating these it is important to keep in mind that the direct production constraints, eq. (5.19), can allow one of M_R or M_I to be significantly lower than 100 GeV. This is important because it precludes our using the most commonly-used three-parameter (S, T and U) parametrization of the oblique corrections [100, 101, 102], since these are based on expanding the gauge boson vacuum energies out to quadratic order: $\Pi_{ab}(q^2) \simeq A_{ab} + B_{ab}q^2$, where a and b denote one of Z, W or γ. Since the electroweak precision measurements take place at $q^2 \simeq 0$ or $q^2 \simeq M_Z^2$, using the quadratic approximation for $\Pi_{ab}(q^2)$ amounts to neglecting contributions that are of relative order M_Z^2/M^2, where M is the scale associated with the new physics of interest (in our case the new-scalar masses). This approximation becomes inadequate for M below 100 GeV, and so we must instead use the full 6-parameter description (STUVWX), such as in the formalism of ref. [98, 99]. In general, the STUVWX formalism reduces to the three-parameter STU case when all new particles become very heavy.

For ease of comparison with past results we start by quoting the results we obtain for the fit to the six parameters of the STUVWX oblique formalism, regardless of how they depend on the parameters of the Manohar-Wise model. The results are given in Table 1, which compares the results obtained by fitting 34 observables (listed in an appendix) to (*i*) all six parameters (STUVWX); (*ii*) only three parameters (STU); or just two parameters (ST). The number of degrees of freedom in these fits to $(6, 3, 2)$ parameters is $v = (28, 31, 32)$, respectively. The χ^2/v for the three fits is within one standard deviation $\sqrt{2/v} = (0.27, 0.25, 0.25)$ of the mean of 1, indicating a good quality of fit. The experimental values and theoretical predictions used are given in Table 2 in the Appendix.

Oblique	STUVWX Fit ($\chi^2/v = 0.91$)	STU Fit ($\chi^2/v = 0.99$)	ST Fit ($\chi^2/v = 0.98$)
S	0.07 ± 0.41	-0.02 ± 0.08	$-9.9 \times 10^{-3} \pm 0.08$
T	-0.40 ± 0.28	-0.02 ± 0.08	$1.1 \times 10^{-2} \pm 0.07$
U	0.65 ± 0.33	0.06 ± 0.10	-
V	0.43 ± 0.29	-	-
W	3.0 ± 2.5	-	-
X	-0.17 ± 0.15	-	-

Table 5.1: EWPD Fit Results in various schemes for the 34 observables listed in the Appendix. The STU and ST fits fix the other oblique corrections to zero as a prior input. The error listed is the square root of the diagonal element of the determined covariance matrix. The central values of the fitted oblique corrections decrease as more parameters are turned off. All three fits are consistent with past results and the PDG quoted fit results.

The correlation coefficient matrix for the three fit results are as follows,

$$M_{STUVWX} = \begin{pmatrix} 1 & 0.60 & 0.38 & -0.57 & 0 & -0.86 \\ 0.60 & 1 & -0.49 & -0.95 & 0 & -0.13 \\ 0.38 & -0.49 & 1 & 0.46 & -0.01 & -0.76 \\ -0.57 & -0.95 & 0.46 & 1 & 0 & 0.13 \\ 0 & 0 & -0.01 & 0 & 1 & 0 \\ -0.86 & -0.13 & -0.76 & 0.13 & 0 & 1 \end{pmatrix}, \tag{5.20}$$

$$M_{STU} = \begin{pmatrix} 1 & 0.84 & -0.20 \\ 0.84 & 1 & -0.49 \\ -0.20 & -0.49 & 1 \end{pmatrix}, \qquad M_{ST} = \begin{pmatrix} 1 & 0.87 \\ 0.87 & 1 \end{pmatrix}. \tag{5.21}$$

We use the results of this fit to constrain the masses allowed in the Manohar-Wise model by computing the vacuum polarizations as functions of the masses of the octet and Higgs scalars. We obtain allowed mass ranges for the scalars by demanding that the contribution of the new physics (and the difference between the floating Higgs mass and its fiducial value, which we take from the SM best fits to be 96 GeV), $\Delta\,\chi^2$ which satisfies

$$(\mathcal{C}^{-1})_{i,j}(\Delta\theta_i)\,(\Delta\theta_j) < 7.0385\,(12.592) \tag{5.22}$$

for the 68% (95%) confidence regions defined by the cumulative distribution function for the six parameter fit. Here $\mathcal{C}$ is the covariance matrix constructed from the correlation coefficient matrix given in eq. (5.20) or (5.21)

$$(\mathcal{C}^{-1})_{i,j} = \frac{1}{2}\,\frac{\partial^2\,\chi^2(\theta)}{\partial\,\theta_i\,\partial\,\theta_j}|_{\theta_i=\hat{\theta}_i} \tag{5.23}$$

and $\Delta\,\theta_i = A_i - A_i^{fit}$ is the difference in $A_i = S, T, U, V, W, X$ as a function of octet masses and the best fit value, given in Table 1.

An example of the best-fit regions for the allowed octet masses is given in Figure 5.4, which compares the quality of the constraints that are obtained using the full six-parameter (STUVWX) parametrization, as opposed to the three-parameter (STU) expression. The three panels plot the masses of the components of the octet that lie within

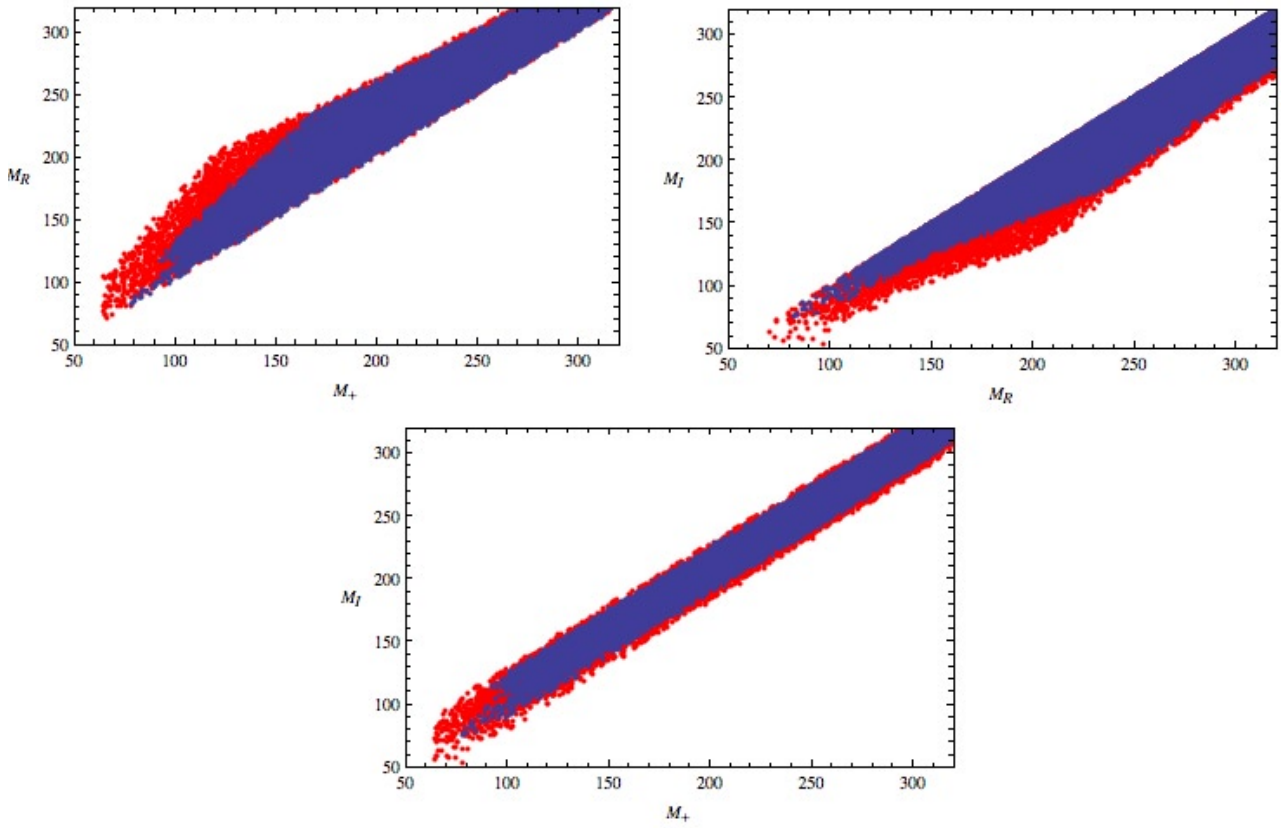

Figure 5.4: Comparison of the three and six parameter fits for low masses. (The upper two panels are not symmetric about $M_I = M_R$ and $M_R = M_+$ because we scan only through positive values for the couplings, λ_i.) The three parameter fit is red (grey) and the six parameter fit is blue (black). Contrary to naive expectations the six parameter fit is more constraining on the model despite the extra parameters; the correlations between the extra parameters (S, X and U, X and T, V) increases the constraints on the model. The masses are in GeV. EWPD constrains the mass spectrum to be approximately $\mathrm{SU}(2)_\mathrm{C}$ symmetric in either case where $M_\pm \approx M_I$.

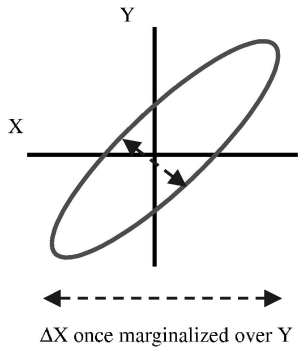

Figure 5.5: A cartoon of the best-fit confidence interval for a strongly correlated pair of variables, indicating how the best constraints can be missed once one of the variables is marginalized.

the 68% confidence ellipsoid of the best-fit value as the various scalar couplings, λ_i, are varied. The two panels of this plot show how these masses are correlated by the condition that the predictions agree with the precision electroweak measurements, and the points in the upper two panels all satisfy $M_I \leq M_R$ and $M_+ \leq M_R$ because we choose to scan only through positive values of the couplings λ_i.

The strongest correlation is between M_I and M_+, for which agreement with EWPD demands these two masses cannot be split by more than about 50 GeV. This is as might be expected given that this difference must vanish in the limit that the potential is custodial invariant. The breaking of $\mathrm{SU}(2)_\mathrm{C}$ generically leads to bad fits because custodial-breaking quantities like the parameter $\rho - 1 = \alpha T$ are measured to be very small: $\rho = 1.0004^{+0.0008}_{-0.0004}$ [108].

The comparison in Figure 5.4 also shows that the six-parameter STUVWX fit agrees with the three-parameter STU fit when all scalars are heavy, as might be expected. It also shows that the six-parameter fit is the more constraining one when the octet masses

are light. We understand that this happens because of the strong correlations amongst the oblique parameters, which implies that the best-constrained parameter direction is not aligned along any of the STUVWX axes, as shown in Figure 5.5. As a result the constraint obtained by restricting to the axes $V = W = X = 0$ can be weaker than the full result, significantly affecting the determined 68% confidence regions. For this reason our remaining results quote only the results of the full six-parameter fit.

Constraints on Octet scalars

Figure 5.6 displays the 68% and 95% confidence regions of the model for couplings that range through the values $0 < \lambda_i < 1$, while Figure 5.7 does the same for couplings that run through the larger range $0 < \lambda_i < 10$, where $i = 1, 2, 3$. As noted above, agreement with the EWPD selects an approximately $\mathrm{SU(2)_C}$ symmetric mass spectrum, where $\lambda_2 \approx 2\lambda_3$ and $|M_\pm - M_I| < 50\,\mathrm{GeV}$, but this is easily understood. Consider the case where the octets are heavy, $v^2/M_S^2 \ll 1$, which was examined in [27]. In this mass regime it is the model that constrains the mass spectrum to be degenerate, $M_\pm \approx M_R \approx M_I$, since the mass splittings scale as v^2/M_S from Eq. (5.6). The contribution of the octets to the S and T parameters,[5] is then [27]

$$S = \frac{\lambda_2\, v^2}{6\,\pi\, M_S^2}, \qquad T = \frac{v^4}{96\,\pi^2 M_S^2 s_W^2 M_W^2}(\lambda_2^2 - (2\,\lambda_3)^2), \tag{5.24}$$

where $s_W \equiv \sin(\theta_W)$. Large corrections to S and T are avoided if λ_i decreases and preserves approximate $\mathrm{SU(2)_C}$ as M_S decreases, therefore allowing smaller octet masses.

How natural are the small intra-octet splittings favoured by EWPD? If the mass splitting is induced by the potential, while $v \gg M_s$, for the octet masses to be allowed by EWPD that selects for a mass degeneracy $\Delta\, M = M_I - M_\pm$, one would have to require that the couplings the the octet-Higgs potential satisfy the scaling rule

$$\lambda_2 - 2\lambda_3 \ll 4\,\frac{\Delta\, M}{v}\,\sqrt{\lambda_1}. \tag{5.25}$$

[5] We have checked that our results in the STUVWX formalism reduce to these results when $v^2/M_S^2 \ll 1$.

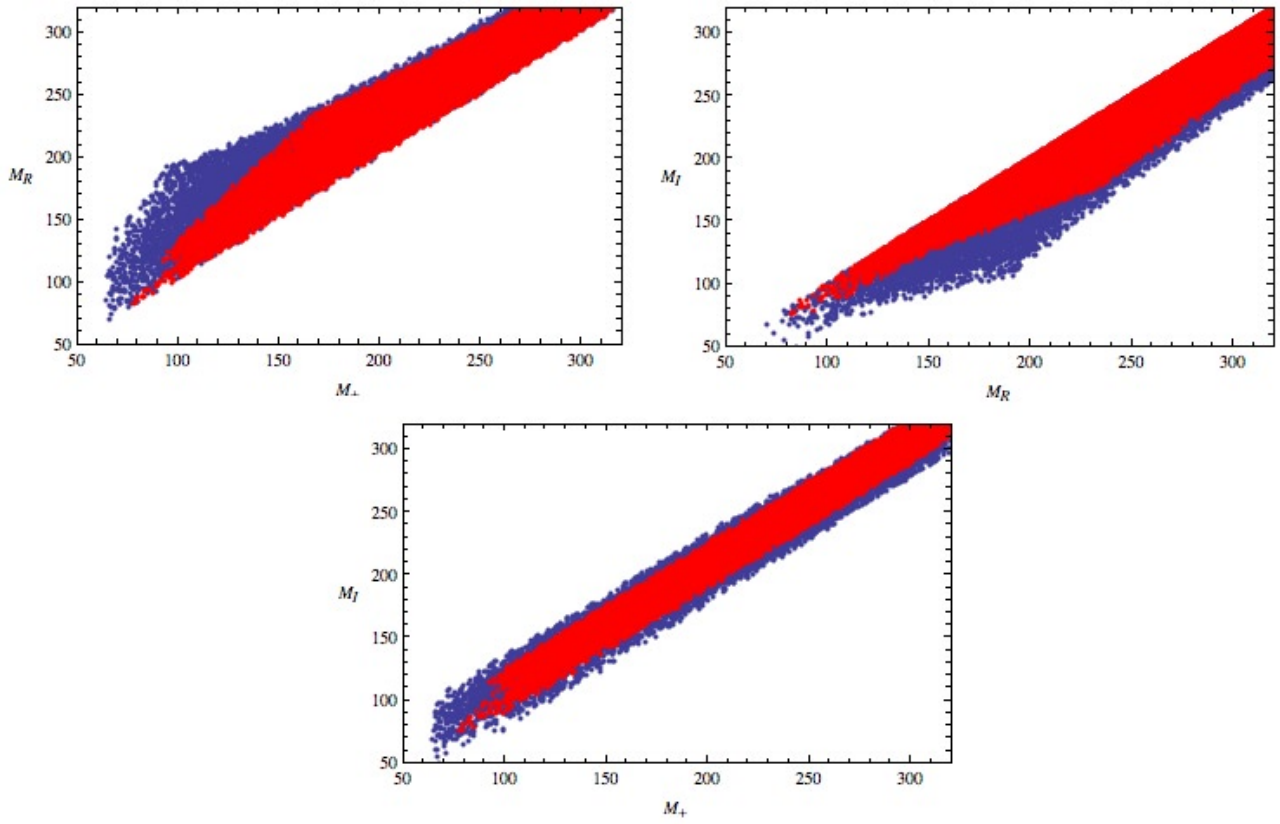

Figure 5.6: Comparison of the 68% red (grey) and 95% blue (black) confidence regions when $0 < \lambda_i < 1$. The masses are in GeV, and $M_I, M_+ \leq M_R$ because we scan only through positive values of the couplings λ_i. For low masses the 95% confidence region is significantly expanded compared to the 68% region, this is due to the spread of available masses being larger for low masses, as the mass splitting between the states scales as $\sim v^2/m_s$. We examine the naturalness of this mass spectrum in Section 2.2 and find that it is not simply a fine tuned solution for an underlying new physics sector.

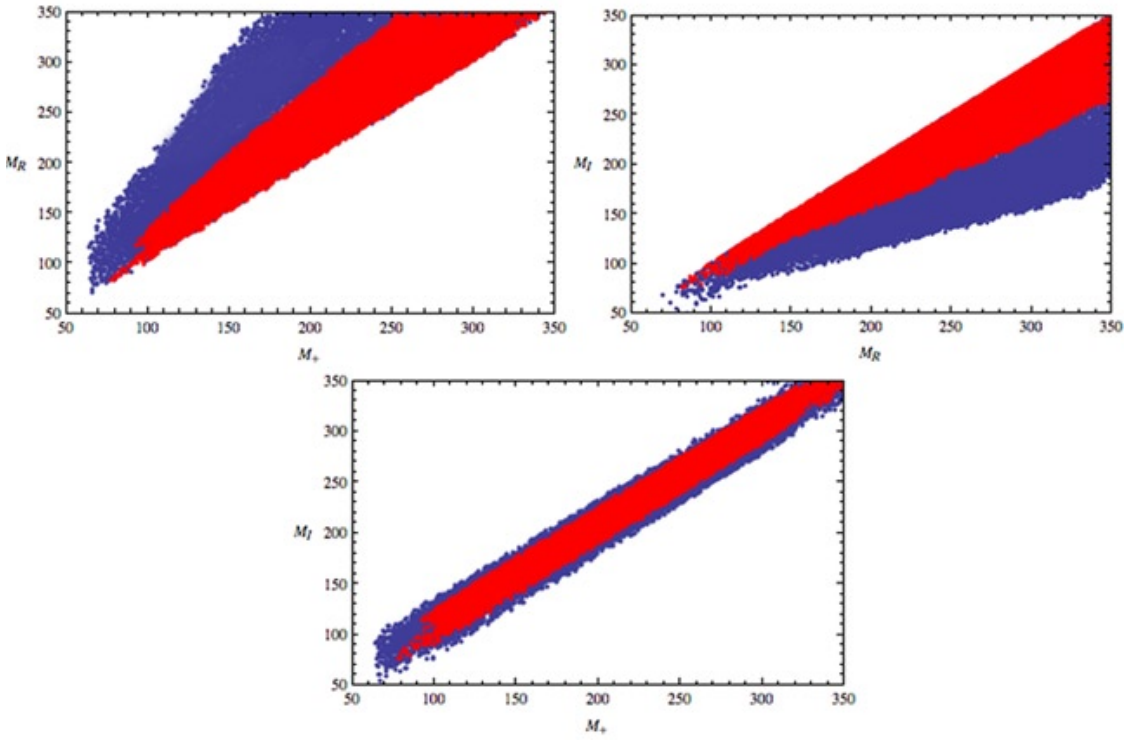

Figure 5.7: Comparison of the 68% red (grey) and 95% blue (black) confidence regions when $\lambda_i < 10$. Notice that the region selected for by EWPD for $M_I \approx M_+$ that is approximately $SU(2)_C$ symmetric is not enlarged.

As EWPD requires $\Delta M \sim 50\,\text{GeV}$ for the 95 % confidence region this is a mild hierarchy of couplings given by $\lambda_2 - 2\lambda_3 \ll 0.8\sqrt{\lambda_1}$. Conversely for the case $m_S \gg v$, one requires that the couplings the the octet-Higgs potential satisfy the scaling rule

$$\lambda_2 - 2\lambda_3 \ll 8\,\frac{(\Delta M)\, m_S}{v^2}, \tag{5.26}$$

which is easily satisfied for small λ_i (which we see below are favoured by Landau pole constraints).

The calculations presented in previous sections for the running of custodial-breaking couplings can be used to frame a criteria as to whether the above coupling pattern is natural. The scale dependence of the masses is used to estimate what the $\text{SU}(2)_\text{C}$ splitting of the masses should be in the theory below the UV scale, Λ, without tuning. One determines how high the scale Λ can be before the EWPD mass regions are excluded. This quantifies the degree of fine tuning of the masses for this scenario.[6] Since the electroweak hierarchy problem argues that the scale of new physics is likely not too much larger than the TeV regime, we find that the favoured mass splittings are natural, provided that the underlying theory approximately preserves MFV and $\text{SU}(2)_\text{C}$.

The above ranges of allowed splittings amongst scalar masses directly constrain the three couplings $\lambda_{1,2,3}$ to be small. But small λ_i, for $i \gtrsim 4$, are also favoured due to considerations of the effect of these λ_i on the running of the Higgs self coupling [97]. The mild assumption that one not encounter a Landau pole while running the Higgs self coupling up to 10 TeV, when one assumes $\lambda_{i\gtrsim 4} = 0$ and $m_h = 120\,\text{GeV}$, gives the constraints [97]

$$\lambda_1 \lesssim 1.3, \qquad \sqrt{\lambda_1^2 + \lambda_2^2} \lesssim 2.2. \tag{5.27}$$

[6] To determine the mass splitting, we technically need to diagonalize the S_I field which mixes at one loop with S^R. As the non diagonal terms in the mass matrix are one loop, the effects of this diagonalization on the mass eigenstate S_I' shifts the mass at two loop order. See the Appendix for a determination of the mixing angle. Thus to one loop order one can just take the one loop corrections to M_I and $M_\pm$ of the last two sections, properly renormalized, to determine the mass splitting through the counterterms.

However, generically $\lambda_{i \gtrsim 4} \neq 0$ and if the octets and the Higgs were part of a new sector then the cut-off scale could be lower that 10 TeV. For these reasons we only take these constraints to inspire the $\lambda_i < 1$ limit for the parameter space searches in Figure 5.6, but also examine parameter space where we relax this bound to $\lambda_i < 10$ in Figure 5.7. We emphasize that direct production bounds on the octets that rely on their fermionic decays essentially constrain the MFV proportionality factors η_i, while EWPD is complementary in that it constrains the parameters in the potential, λ_i, by constraining the mass spectrum.

Implications for the inferred Higgs mass

Adding the new octet scalar to the SM also affects the best-fit value of the Higgs mass that emerges from fits to EWPD. In particular, we now show that the presence of the octet can remove the preference of the data for a light Higgs, even if the new octet scalar is also heavy.

To determine this effect we calculate the one-loop Higgs contribution to the six oblique parameters and jointly constrain the Higgs mass and the octet masses in the fit. For example, S in this case becomes

$$S = S_{oct}(M_R, M_I, M_\pm) + S_{Higgs}(M_h) - S_{Higgs}(M_h = 96\,\mathrm{GeV}) \tag{5.28}$$

where $S_{oct(Higgs)}$ is the one-loop octet (Higgs) contribution to the S parameter. We neglect the two-loop dependence on the Higgs mass in the fit and this leads to an underestimate of the allowed parameter space, as we find the 68% (95%) confidence level values of fitting the Higgs mass alone are given by 112 (160)GeV. This gives a conservative range when comparing to the various allowed values that are strongly dependent on the priors used in the PDG .

The effect of the octets changes the preferred Higgs mass significantly, and two mechanisms are at work depending on the size of the octet mass. If the octet mass M_I is

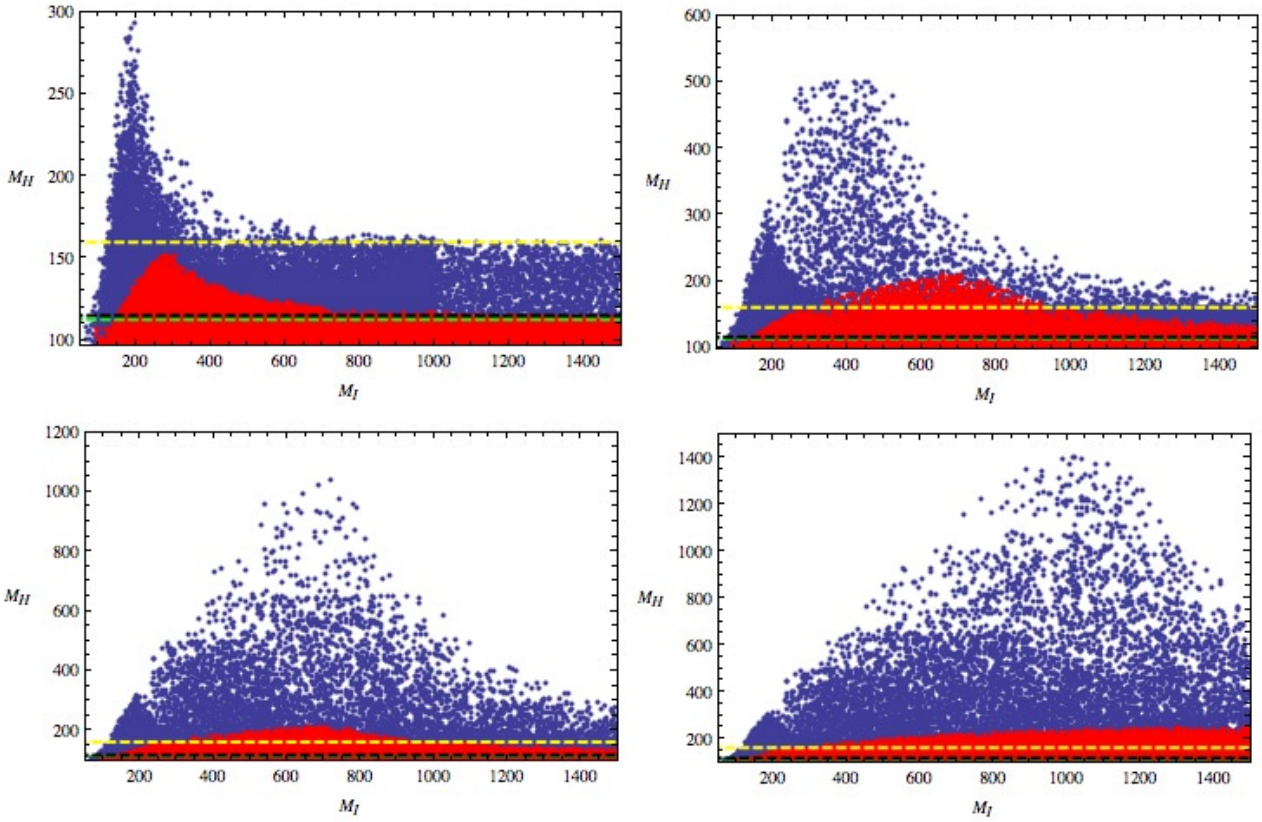

Figure 5.8: The effect of octets on the fitted value of the Higgs mass.The plots of M_h versus the other octet states are substantially the same. The green line is the 68% confidence bound where the Higgs alone is varied at one loop. The yellow line is the 95% confidence bound where the Higgs alone is varied at one loop, and the black line is the direct production bound on the Higgs mass at 95% confidence. The red (grey) region is the 68% confidence region, while the blue (black) region is the (95%) confidence region for a joint fit to the octets and the Higgs. Notice the increase in vertical scale for the diagrams as the upper limit of the λ_i is increased through 1 (upper left), 3 (upper right), 6 (lower left) and 10 (lower right). The mechanism that is allowing the Higgs mass to increase and still be in agreement with EWPD is the postitive ΔT contribution from the octets that is discussed in Section 3.1.2.

small, it can allow the Higgs mass to increase by effectively replacing it in the oblique loops, thereby giving agreement with EWPD. This is illustrated in the upper-left plot of Figure 5.8, which shows how a large Higgs mass correlates with small M_I.

The other panels of Figure 5.8 reveal another mechanism at work, however [7]. In these one sees that as the upper limit on λ_i is increased, the upper limit on the Higgs mass confidence regions becomes significantly relaxed. This is due to a cancellation between the effects of the heavy octet and the Higgs in their contributions to oblique parameters, that is made possible by a positive ΔT contribution that the octets give to χ^2. For the three-parameter fit, the χ^2 test is of the form

$$(\mathcal{C}^{-1})_{i,j}(\Delta\theta_i)\,(\Delta\theta_j) = 596\,(\Delta S)^2 - 1159\,(\Delta S)\,(\Delta T) + 751\,(\Delta T)^2 \tag{5.29}$$

where we neglect contributions that are not logarithmically sensitive to the Higgs mass at one loop, since this is all that is relevant to the argument. For the three-parameter fit, the 68% confidence region is defined by $(\mathcal{C}^{-1})_{i,j}(\Delta\theta_i)\,(\Delta\theta_j) < 3.536$ and is easily satisfied for light Higgs masses. As the Higgs mass grows, its contribution to (ΔS) and (ΔT) becomes dominated by the logarithmic dependence

$$(\Delta S) \simeq \frac{\alpha}{12\,\pi}\log\left(\frac{M_H^2}{\hat{M}_H^2}\right) \quad \text{and} \quad (\Delta T) \simeq -\frac{3\,\alpha}{16\,\pi}\log\left(\frac{M_H^2}{\hat{M}_H^2}\right), \tag{5.30}$$

where $\hat{M}_H$ is the reference value of the Higgs mass, which for our fit is 96 GeV. The crucial point is that (ΔT) is negative for $M_H > \hat{M}_H$ and for the SM this quickly excludes large Higgs masses because of the sign flip in the $(\Delta S)\,(\Delta T)$ term in χ^2.

Including the contribution of the octets in the large mass regime ($v^2/M_S^2 \ll 1$) modifies these expressions to

$$\begin{aligned}(\Delta S) &\simeq \frac{\alpha}{12\,\pi}\log\left(\frac{M_H^2}{\hat{M}_H^2}\right) + \frac{\lambda_2\,v^2}{6\,\pi\,M_S^2},\\ (\Delta T) &\simeq -\frac{3\,\alpha}{16\,\pi}\log\left(\frac{M_H^2}{\hat{M}_H^2}\right) + \frac{v^4}{96\,\pi^2 M_S^2 s_W^2 M_W^2}(\lambda_2^2 - (2\,\lambda_3)^2),\end{aligned} \tag{5.31}$$

[7] Note that we expect a careful study of the non oblique Higgs and octet mass dependence of R_b will further constrain this parameter space with all scalars heavy but not remove it.

where the factor $\lambda_2^2 - (2\,\lambda_3)^2$ comes from a factor of $(M_R^2 - M_\pm^2)(M_I^2 - M_\pm^2)$ in the octet contribution, and is a measure of the total mass splitting in the doublet. For $\lambda_i > 0$, we know $M_R^2 > M_\pm^2$ and so the octets give a positive contribution to (ΔT) so long as $M_I^2 > M_\pm^2$. The octets (or any other doublet with gauge couplings and small mass splittings) then allow (ΔT) in Eqn. 5.31 to be positive, and so allow a large degree of cancellation between the $(\Delta S)^2, (\Delta T)^2$ and $(\Delta S)(\Delta T)$ terms in Eqn. 5.29. The size of the positive (ΔT) contribution scales with the upper limit on λ_i, explaining the significant relaxation of the Higgs mass bound in Figure 5.8. We find that the Higgs and the octet scalars could both have masses $\sim 1\,\text{TeV}$ and still lie within the 95% contour mass region allowed by EWPD. We also note that we restrict our searches to positive λ_i (which must be so for at least some of the couplings to ensure the absence of runaway directions in the potential), however clearly negative λ_2 could also act to relax the EWPD bound on the Higgs mass by giving a negative contribution to (ΔS).

We emphasize the generic nature of the mechanism, wherein the contributions of TeV scale new physics can mask the contributions of a heavy Higgs to electroweak precision observables. It applies in particular when EW symmetry breaking leads to a mass splitting of an extra SU(2) doublet, since the extra doublet can give a positive contribution to (ΔT) proportional to the mass splittings of the doublet components. This has been recognized as a simple way to raise the EWPD bound on the Higgs mass by satisfying the positive (ΔT) criteria of [104]. Expressed as an effect on the ρ parameter, it also has a long history going back to observations by Veltman [103], being rediscovered for two-Higgs-doublet models in [105], and used for the construction of the Inert Two Higgs doublet (IDM) model [106].[8] In this latter model, the Higgs mass is raised, addressing the "LEP paradox", and the naturalness of the SM Higgs sector is also improved by raising the cutoff scale of the modified SM. In the IDM model a parity symmetry is imposed to avoid FCNC's.

[8]For a similar construction see [107]

We note that the example of the general scalar sector consistent with flavour constraints, the Manohar-Wise model examined in this chapter, naturally has a number of the benefits of models like the IDM while avoiding the imposition of a parity symmetry. Allowing the second doublet to couple to quarks improves its potential for detection, without introducing large FCNCs due to MFV. It is interesting that the effect of raising the Higgs mass has emerged naturally from the most general MFV scalar sector and was not a model building motivation of the MW model. Variants of the MW model, can address the naturalness of the scalar sector through raising the cut off scale and further the colour charge of the octet provided some rational for the second doublet not obtaining a *vev*, through the avoidance of the spontaneous breaking of colour. Also, for the entire parameter range, octets skew the distribution of the allowed Higgs masses so that the direct production bound on the Higgs mass and the EWPD fit of the Higgs mass can be in better agreement.

Implications for the tension between leptonic and hadronic asymmetries

Although the SM produces a good quality global fit to EWPD, there exists a mild tension in the data between the leptonic and hadronic asymmetries. In particular A_{FB}^b deviates from the SM predicition by 2.5σ and favours a heavy Higgs ~ 400GeV, while A_e differs from the SM by $\sim 2\sigma$ and favours a Higgs mass far below the direct production bound. Here we address the question of whether the oblique contributions of octet scalars can change this tension.

To this end we calculate χ^2 for the hadronic asymmetries A_{FB}^b, A_{FB}^c, A_b, A_c, and for the leptonic asymmetries using A_τ and the A_e values given in Table 5.A. The results are shown in Figure 5.9, where the solid curves plot χ^2 with the SM Higgs alone and the dashed curves include the octets for a particular mass spectrum allowed by EWPD. The two panels compare results for relatively light and relatively heavy octet scalars.

The figure shows that the preferred value of the Higgs mass is strongly dependent

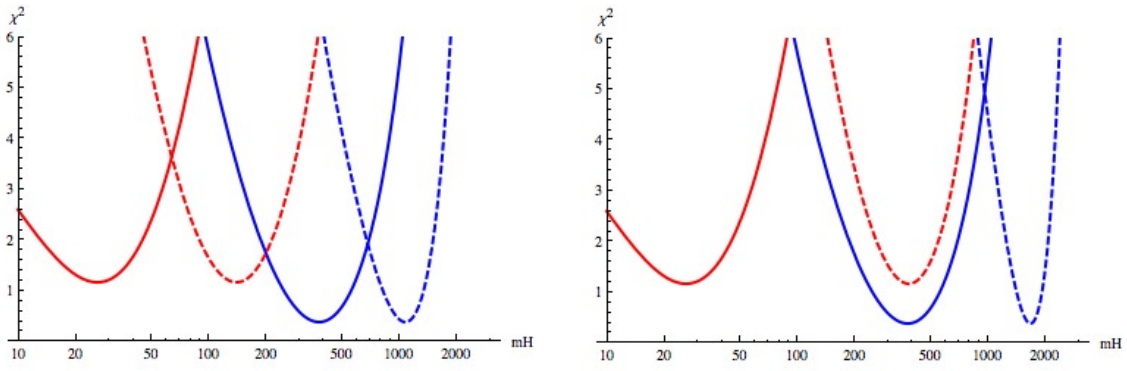

Figure 5.9: The χ^2 of the leptonic asymmetries (red) and hadronic asymmetries (blue) as a function of Higgs mass in GeV. The solid curves show the contribution of the Higgs alone and the dashed curves are for the Higgs and the octets. The figure on the left is for octet masses $(M_\pm, M_R, M_I) = (300, 400, 330)$GeV and on the right is for $(M_\pm, M_R, M_I) = (900, 1000, 940)$GeV.

on the mass splitting of the octets. As discussed in Section 5.3.1, the octets, unlike the Higgs, give a positive contribution to ΔT, which depends on the mass splitting in the doublet. This increases the allowed value of the Higgs mass. The octets can change the pull of A_e, for example, to favour large Higgs masses, however they also do the same to A^b_{FB}. As can be seen from Figure 5.9, although the leptonic and hadronic asymmetries can now both prefer a Higgs masses above the direct production bound of 114.4 GeV, they are not brought in to closer agreement in their predictions for the value of M_H.

We see from this that the octet oblique contributions do not in themselves remove the tension between the leptonic and hadronic asymmetries. However, because the octets are coloured it is possible that their non-oblique corrections to A^b_{FB} might be able to bring together the leptonic and hadonic observables. We leave this observation to a more complete calculation, which lies beyond the scope of this chapter.

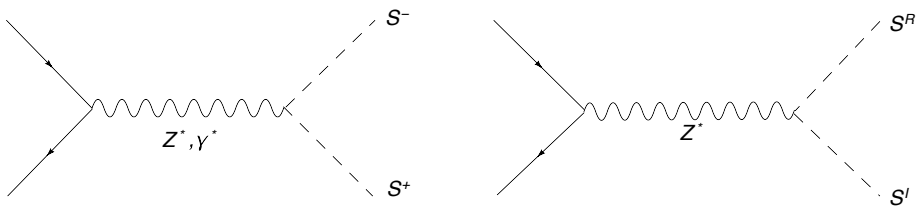

Figure 5.10: The tree level production mechanism for $S^+ + S^-$ and $S^0_R + S^0_I$ at LEPII.

5.3.2 Direct-production constraints from LEP

The octets would have been directly produced at LEP2 if they were light enough through the processes in Figure 5.10.

The production cross sections are given by

$$\begin{aligned}\sigma_{S^+S^-} &= \frac{d_A}{4}\left(\frac{4\pi\alpha^2}{3s}\right)\lambda^{3/2}\left(1,\frac{M_+^2}{s},\frac{M_+^2}{s}\right) \\ &\times \left\{1+2v_+v_e\mathrm{Re}\left[\left(1-\frac{M_Z^2}{s}+\frac{iM_Z\Gamma_Z}{s}\right)^{-1}\right]+v_+^2(v_e^2+a_e^2)\left|1-\frac{M_Z^2}{s}+\frac{iM_Z\Gamma_Z}{s}\right|^{-2}\right\},\end{aligned} \tag{5.32}$$

$$\sigma_{S^0_RS^0_I} = \frac{d_A}{4}\left(\frac{4\pi\alpha^2}{3s}\right)\lambda^{3/2}\left(1,\frac{M_R^2}{s},\frac{M_I^2}{s}\right)v_0^2(v_e^2+a_e^2)\left|1-\frac{M_Z^2}{s}+\frac{iM_Z\Gamma_Z}{s}\right|^{-2}, \tag{5.33}$$

where we have defined $d_A = 8$, $a_e = -(4s_Wc_W)^{-1}$

$$\lambda(x,y,z) = x^2+y^2+z^2-2xy-2xz-2yz, \tag{5.34}$$

$$v_+ = \frac{s_W^2-c_W^2}{2s_Wc_W}, \qquad v_0 = \frac{1}{2s_Wc_W}, \qquad v_e = \frac{-1+4s_W^2}{4s_Wc_W} \tag{5.35}$$

The highest COM energy at which LEP2 operated was $\sqrt{s} = 209$ GeV, where approximately $\int \mathcal{L}dt \sim 0.1$ fb^{-1} of integrated luminosity was collected. We give a rough estimate of the sensitivity of LEP2 to light octets by requiring less than 10 total events for a given set of masses, $\sigma \times \int \mathcal{L}dt < 10$. Note that these limits are essentially kinematic limits for production, and more accurate exclusions in the mass parameter space are possible, but these will be dependent on the detailed decays of the octets and SM backgrounds and be weaker constraints. The LEP2 production bounds are shown in Figure 5.11.

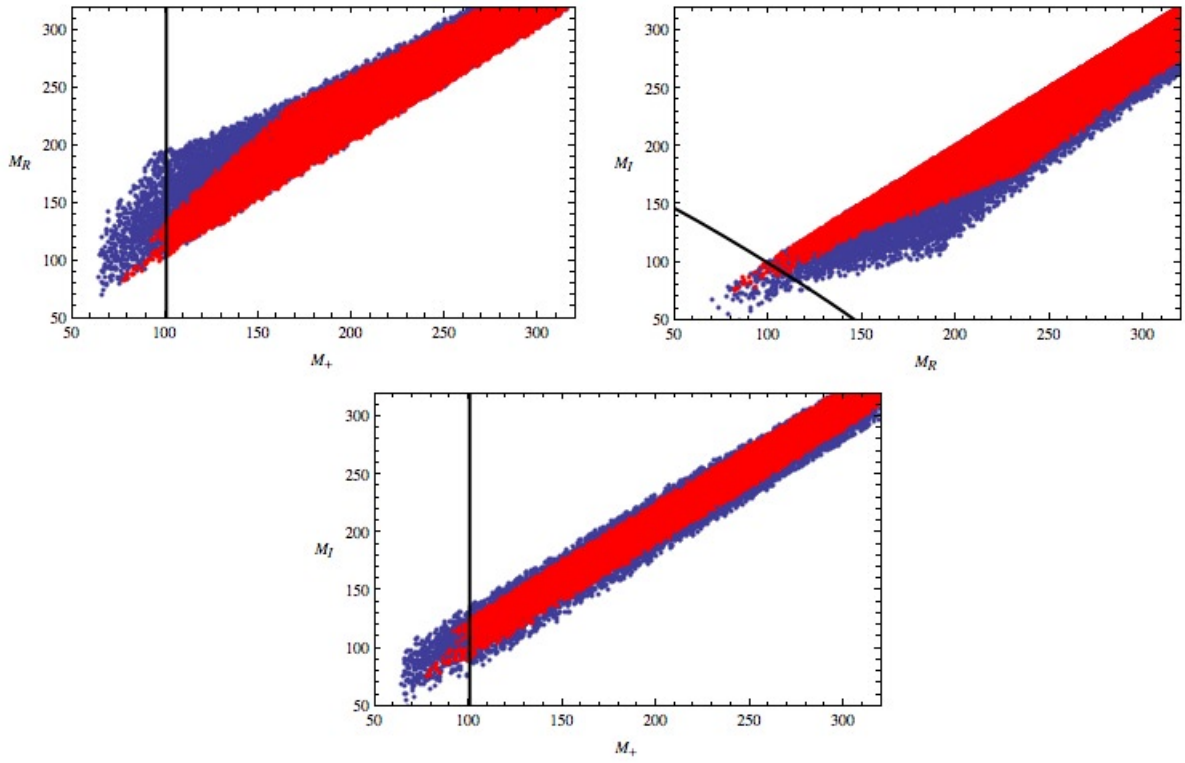

Figure 5.11: Comparison of the 68% (red or light) and 95% (blue or dark) confidence regions when $\lambda_i < 1$. The LEP2 production bound for ten events is the black line.

5.3.3 Tevatron constraints

Dijet constraints on the production cross section.

Heavy octet production via gluon fusion has been examined in some detail in the literature see [27, 109, 96]. We use the results of [27, 109, 96] to determine the production cross sections for light octets and consider the relevant bounds on the model in this region from the Tevatron. The single production cross section we use, [109], neglects for simplicity the scalar mass splitting and assumes that η_U, λ_4 and λ_5 are real. However, note that this is partially justified for light masses as EWPD selects for an approximately degenerate mass spectrum with an approximate $\mathrm{SU}(2)_\mathrm{C}$ symmetry in the underlying potential, giving $\lambda_4 = \lambda_5^\star$ and one need only assume one of the couplings are real. [9] For the sake of simplicity we will also neglect the effects of mixing of the S_I, S_R states that can occur if the effective yukawa couplings of the octet carries a phase as discussed in the Appendix. The pair production cross section for the charged scalars is twice that for the real scalars [27] and so is not shown.

The tree level pair production dominates the loop suppressed single production in the low mass region for small $\lambda_{4,5}$. However as $\lambda_{4,5}$ increase the single production contribution takes over, which occurs at $\lambda_{4,5} \sim 2$ for the neutral scalar, S_R, with a mass of 200 GeV.

A direct search strategy to find octets is to look for narrow resonance structures above the QCD background for states that decay into dijets. CDF has recently performed such a search [114] with $1.13\, fb^{-1}$ of data that could discover octet bound states [110] or single S_i that decay to dijets above the QCD background. The cross sections for the production of these states at the Tevatron, leading to dijet resonance structures, are orders of magnitude below the QCD background in the regions of parameter space we consider, this is shown in Fig. 5.12

The low mass region is not directly ruled out, although a dedicated study to refine the

[9] Note that setting λ_4 and λ_5 to real values removes the scalar loop contributions to the single production of S_I, which can become large as the values of $\lambda_{4,5}$ increases.

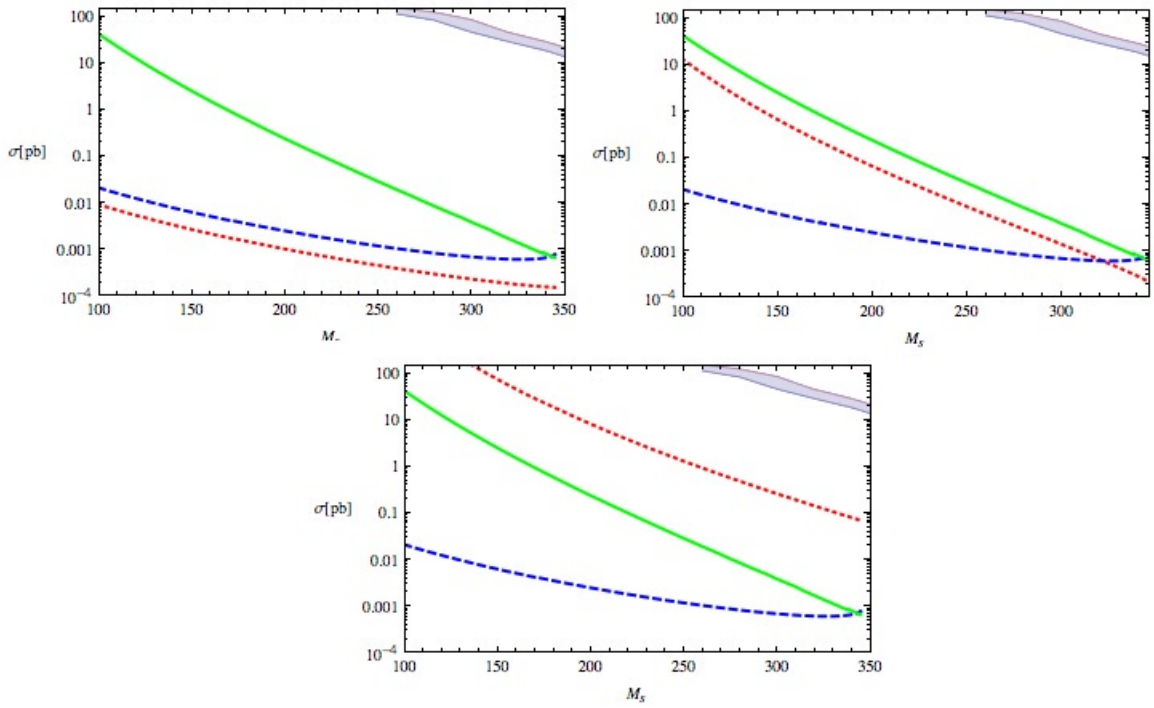

Figure 5.12: Shown is the production cross section of $\sigma(g\,g \to S_R)$ red short dashed line, $\sigma(g\,g \to S_I)$ blue long dashed line, and the $\sigma(g\,g \to S_R\,S_R)$ given by the solid green line. The results are for Tevatron with $\sqrt{s} = 1.96\,\text{TeV}$, $\alpha_s(M_Z) = 0.1217$, $m_t = 173.1\,\text{GeV}$, $M_Z = 91.1876\,\text{GeV}$ and the NLO CTEQ5 pdfs. The values of (λ_4, λ_5) chosen are $(0, 0)$ upper left, $(1, 1)$ upper right and $(10, 10)$ for the bottom graph. In all three graphs we have set $\eta_U = 0.2$. The dependence on η_U is weak and as η_U decreases the production cross sections decrease. Also shown is a 95% confidence limit band (the shaded region) derived from [114] that places an upper bound on new physics that decays to dijets. The region is defined by the upper limit on $\sigma(X)\mathcal{B}(X \to jj) * A(|y| < 1)$ where the difference between the W' and RS graviton $G^\star$ 95% confidence upper bounds are taken and the acceptance fraction requires the leading jets to have rapidity magnitude $|y| < 1$. The exclusion region depends weakly on the shape of the resonance, so a dedicated study is required to exactly bound the octet decay to dijets, however, the octet signal is orders of magnitude below the exclusion regions obtained from Tevatron before branching and acceptance ratios further reduce the signal. A resummation of large threshold logarithms for single S production was performed in [96]. The K factors for single S production was found to be ~ 2 for $500\,\text{GeV}$ a octet mass and this K factor falls as the mass decreases. This indicates that threshold enhancements will not raise the cross section enough to

lower mass bound is warranted due to the shape dependence of the exclusion bound.[10]

Gauge boson decays and Lepton Signatures

The decays of the octets involving gauge bosons

$$\begin{aligned} S_{R,I} &\to W^{\pm} S^{\mp}, \quad S_{R,I} \to Z\, S_{I,R} \\ S^{\pm} &\to W^{\pm} S_{R,I}, \quad S^{\pm} \to Z\, S^{\pm}. \end{aligned} \tag{5.36}$$

were studied in some detail in [27, 97]. These decays are of phenomenological interest as the gauge bosons can be a source of leptons to trigger on at LHC and Tevatron. The EWPD constraints $|M_{\pm} - M_I| < 50\,\text{GeV}$ and for most of the allowed parameter space $|M_i - M_j| < M_W, M_Z$, as the mass splitting of the doublets scale as v^2/M_s for large masses. This causes the decays to proceed through an offshell gauge boson for most of the allowed parameter space. In this case an effective local operator can be used to approximate the decays.

For example consider $S_R \to S^- \ell^+ \nu$ through an off shell W. The effective Lagrangian at leading order is given by the product of scalar octet and left handed lepton currents

$$\mathcal{L}_{\text{eff}} = \frac{-i\, g_1^2}{\sqrt{2}\, M_W^2} \left(S_R\, \partial_\mu S_+\right) \left(\bar{\nu}_L\, \gamma^\mu\, \ell_L\right). \tag{5.37}$$

Exact formula for three body decays such as this exist in the literature [112]. For the masses allowed by EWPD[11] generally the energy release is $\Delta = M_R - M_{\pm} < M_R, M_-, M_W$. The resulting decay width at leading order in Δ/M_R is

$$\Gamma_\ell = \frac{\alpha^2\, \Delta^5}{60\, \pi\, s_W^4\, M_W^4}. \tag{5.38}$$

[10] Other possible indirect search strategies for the effects of octet scalars include determining the effect of the octets on the A_{fb}^t. In a similar manner to axigluons [116], these new exotic coloured states could contribute to A_{fb}^t as they are coloured, couple strongly to tops, and are not a vectorlike state. Interestingly, A_{fb}^t has recently been measured [117, 118] to be $A_{FB}^t = 0.19 \pm 0.065(stat) \pm 0.024(syst)$ which is a deviation larger than 2 sigma from its SM value [116] of $A_{FB}^t = 0.05 \pm 0.015$.

[11] This assumes that the initial state that is eventually triggered on is not highly boosted. This is generally the case due to the kinematic reach of the Tevatron and LHC.

When $M_R > 2\,m_t$ the decays to leptons through an offshell W, Z are suppressed decay channels. The dominant decay widths are to $t\,\bar{b}$, $t\,\bar{t}$ unless $\eta_U \ll \eta_D$. The ratio of Γ_ℓ to this decay, in the limit $M_R \gg 2\,m_t$, is given by

$$\frac{\Gamma_\ell}{\Gamma_{S_R^0 \to t\,\bar{t}}} \simeq \frac{0.005\text{GeV}}{M_R\,|\eta_U|^2}\,\left(\frac{\Delta}{50\,\text{GeV}}\right)^5 \tag{5.39}$$

for $\alpha = 1/128$, $s_W = 0.48$ and $m_t = 173\,\text{GeV}$.

When $M_R < 2\,m_t$ the offshell W, Z will be dominant decay channels for light masses for much of the parameter space. Taking $m_b = 4.23\,\text{GeV}$, and the other factors as before, the ratio of the offshell decay to the $S_R^0 \to b\,\bar{b}$ decay is given by

$$\begin{aligned}\frac{\Gamma_\ell}{\Gamma_{S_R^0 \to b\,\bar{b}}} &\simeq \frac{4\alpha^2}{15\,s_W^4 |\eta_D|^2}\,\left(\frac{\Delta^5\,v^2}{m_W^4\,m_b^2\,M_R}\right), \\ &\simeq \frac{8\,\text{GeV}}{M_R\,|\eta_D|^2}\,\left(\frac{\Delta}{50\,\text{GeV}}\right)^5 .\end{aligned} \tag{5.40}$$

If the dominant fermionic decays are to charm quarks due to a mild hierarchy of $\eta_U > (m_b/m_c)\,\eta_D$, then taking $m_c = 1.3\,\text{GeV}$ gives the branching ratio

$$\frac{\Gamma_\ell}{\Gamma_{S_R^0 \to c\,\bar{c}}} \simeq \frac{82\,\text{GeV}}{M_R\,|\eta_U|^2}\,\left(\frac{\Delta}{50\,\text{GeV}}\right)^5 . \tag{5.41}$$

Thus when quark decays are suppressed through $M_R < 2\,m_t$ the dominant decay mode will be through an offshell W, Z for much of the parameter space of η_U, η_D allowed by other constraints, notably the constraints due to R_b. This sets a lower bound on the decay width of the heavier octet species given parametrically by Eqn. 5.38. This sets an upper bound on the lifetime of these components of the octet doublet of $4.5/\Delta^5\ ps$ which yields a upper bound on the decay length of the form $10^{-3}/\Delta^5\ m$.[12] Thus the heavier octet species will decay promptly inside the detector and not leave a long lived charged track signature.

[12]Here we have converted units assuming that Δ is given in GeV as a pure number, ie for $\Delta = 50\,\text{GeV}$ we have a upper bound on the lifetime of $1.2 \times 10^{-2}\ as$.

As dominant decay modes of the heavy components of the octet doublet (when $M_i < 2\,m_t$) can be three body decays, the final state signature would be excess monojet or dijet (depending on the boost of the final state octet) events in association with a lepton and missing energy, or enhancements of dilepton signatures with a monojet or dijet. Dedicated studies of these signatures are warranted. The lifetime of the lightest component of the octet doublet is dictated by its decay to fermion pairs.

Constraints from $t\,\bar{t}$ decays.

For neutral octet masses above $2\,m_t$, decays into top quark pairs can be dominant. These were previously considered in [109]. The observed limits on excess $\sigma_X \cdot B(X \to t\,\bar{t})$ at Tevatron with $0.9\,fb^{-1}$ of data [115] do not rule out octets in the intermediate mass region $350 - 1000\,\mathrm{GeV}$. The production cross section for single $gg \to S_R$ production can become large enough for the bound on $t\,\bar{t}$ to be relevant, however this requires $\lambda_4 \sim \lambda_5 \sim 75$ which is well into a nonperturbative region of the potential making any conclusion suspect. We illustrate these limits in Fig. 5.13

Constraints from $\bar{b}\,b\,\bar{b}\,b$ decays.

The dominant decays for light masses will be to quarks $S_+ \to t\bar{b}$, $S_{R,I} \to b\bar{b}$ below the $t\bar{t}$ threshold for $\eta_{U,D} \sim \mathcal{O}(1)$. In this regime [97] places a lower bound on the scalar mass of approximately 200 GeV from the CDF search for a scalar particle decaying dominantly to $b\bar{b}$ when produced in association with b quarks [113] This bound is avoided for almost all of the available parameter space for light octet masses. $S_{I,R}$ can decay preferentially to charms, which corresponds to a mild hierarchy of couplings

$$\frac{|\eta_D|^2}{|\eta_U|^2} < \frac{m_c^2}{m_b^2} \sim \frac{1}{10} \tag{5.42}$$

when neglecting $\mathcal{O}(m_{b,c}^2/M_S^2)$ terms. Neutral scalar masses below 200GeV are allowed for $\eta_D \lesssim 0.1$, given an upper limit of $\eta_U \sim 0.3$ from [109] for masses in this range. The

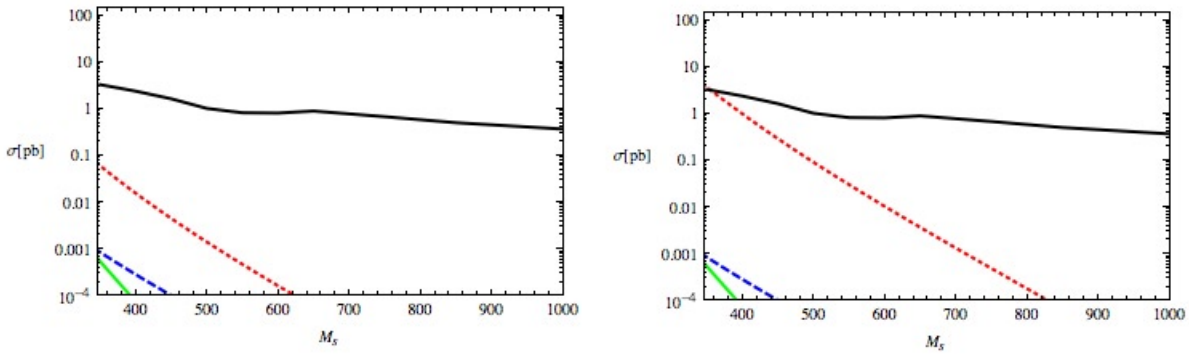

Figure 5.13: Shown is the production cross section of $\sigma(g\,g \to S_R)$ red short dashed line, $\sigma(g\,g \to S_I)$ blue long dashed line, and the $\sigma(g\,g \to S_R\,S_R)$ given by the solid green line. The results are for Tevatron with $\sqrt{s} = 1.96\,\text{TeV}$, $\alpha_s(M_Z) = 0.1217$, $m_t = 173.1\,\text{GeV}$, $M_Z = 91.1876\,\text{GeV}$ and the NLO CTEQ5 pdfs are used. The D0 95% confidence limit on $\sigma(X)\Gamma(X \to t\,\bar{t})$ is the upper solid black line [115]. The values of (λ_4, λ_5) are $(10, 10)$ for the left hand figure and $(75, 75)$ for the right hand figure. $\eta_U = 0.2$ for both figures. For perturbative $\lambda_i \lesssim 10$, current Tevatron production bounds on resonances in $t\,\bar{t}$ do not rule out octets of mass $350 - 1000\,\text{GeV}$.

three body decays discussed in Section 5.3.3 are actually dominant over quark decays for much of the parameter space allowed by EWPD for light octet masses, invalidating the assumptions of [97] for most of the remaining parameter space.

Constraints from $\gamma\,\gamma$ decays.

A promising signature for octets at hadron colliders is the annihilation of a pair of charged octets to photons, $gg \to S^+\,S^- \to \gamma\,\gamma$. We can use the recent results of DO [120, 119] that utilize 4.2 fb^{-1} of date to place 95% confidence upper limits on $\sigma(h) \times BR(h \to \gamma\,\gamma)$ compared to the SM Higgs signal to directly constrain octet annihilation into $\gamma\,\gamma$. We must consider annihilation decays of octet bound states, octetonia, studied in [110], as the contribution from virtual octets will be a non-resonant signal and the Tevatron Higgs search would not apply. Due to the fact that the results are reported only up to Higgs masses of 150 GeV we are only able to exclude octets up to 75 GeV, which is already disfavoured by LEP2. If the experimental study of $h \to \gamma\,\gamma$ is extended to higher Higgs masses at the Tevatron or LHC, this signal is likely to be a significant constraint on the model.

We utilize the fact that this signature has been studied for octetonia in [110] to demonstrate the potential of this signal to raise the mass limit on octets. The ratio we are interested in is that of the octetonia $\sigma(gg \to O^+) \times BR(O^+ \to \gamma\,\gamma)$ to the SM rate for $\sigma(gg \to h) \times BR(h \to \gamma\,\gamma)$. We take [110]

$$\sigma(gg \to O^+) \times BR(O^+ \to \gamma\,\gamma) \approx \frac{9\,\pi^3\,\alpha^2 |\psi(0)|^2}{2\,M_S\,\hat{s}^2} \delta(1 - m_O^2/\hat{s}) \tag{5.43}$$

where $\hat{s}$ is the partonic center of mass energy squared and $|\psi(0)|$ is the wavefunction at the origin. We have used the approximation $\mathrm{BR(O^+ \to \gamma\,\gamma) \sim \alpha^2/\alpha_s^2(2M_S)}$. For the Higgs, we take the approximation

$$\sigma(gg \to h) \times BR(h \to \gamma\,\gamma) \approx \frac{G_F}{\sqrt{2}} \frac{M_H^2\,\alpha_s^2}{8\,\pi\,\hat{s}} \left(\frac{m_t^4}{M_H^4}\right) 10^{-3}\,\delta(1 - M_H^2/\hat{s}) \tag{5.44}$$

Neglecting order one factors the ratio of these two signals scales as

$$R \approx 10^6 \, \frac{\alpha^2}{\alpha_s^2} \, \frac{|\psi(0)|^2}{\hat{s}} \, \left(\frac{M_H^2}{M_S \, m_t^4 \, G_F} \right) \tag{5.45}$$

This ratio must be less than ~ 35 [120, 119] for $M_h = (100, 150)\,\text{GeV}$ or $M_\pm = (50, 75)\,\text{GeV}$. Unless the wavefunction at the origin was much smaller than its approximate expected value given by [110]

$$|\psi(0)|^2 = \frac{N_c^3 \, \alpha_s^3 (m_S \, v) \, M_S^3}{8 \, \pi}, \tag{5.46}$$

this bound will likely be violated for this entire mass range. Extending this analysis to higher Higgs masses is expected to raise the lower mass bound on octet states for this reason. For a recent comprehensive study of octetonia signals in gamma gamma for octets from $\sim 200 - 500$ GeV see [110].

5.3.4 Flavour constraints reexamined for light scalars

Flavour constaints on $(\mathbf{8}, \mathbf{2})_{1/2}$ scalars were examined in some detail in linear MFV[13] in [27] when the masses of the octet scalars were considered to be $\sim$ TeV. However, although MFV suppresses flavour changing effects and ensures the vanishing of tree level flavour changing neutral currents in linear MFV, when one goes beyond leading order in the Yukawa couplings problematic flavour changing neutral currents are possible [109]. The correct way to examine such flavour issues is to utilize a nonlinear representation of MFV[14] such as formulated in [81, 82, 83] which is beyond the scope of this work.

We have reexamined the flavour constraints that were examined in [27] in linear MFV for the light octet masses allowed by EWPD and not ruled out by direct production bounds. Flavour constraints are largely irrelevant for $|\eta_U|$ once the far more restrictive constraint from R_b is known. To quantitatively demonstrate this consider $K^0 - \bar{K}^0$ mixing for relatively light masses $M_s = 300\,(400)\text{GeV}$. We use the results

[13] Where one only utilizes a linear yukawa coupling for the scalars.
[14] We thanks J. Zupan for discussions on this point.

of [27] for the contribution of the octets to the wilson coefficient (C_s) of the operator $(V_{td}^\star V_{ts})(d_L\,\gamma^\nu\,s_L)(d_L\,\gamma^\nu\,s_L)$ and use the SM expression of [121] for the contribution of this operator to $K^0-\bar{K}^0$ mixing and hence $|\epsilon_K|$. One finds that the contribution of the octets to $|\epsilon_K|$ is given by

$$\Delta|\epsilon_K| = |C_\epsilon\, B_K\, \mathrm{Im}[V_{td}^\star V_{ts}]\, \mathrm{Re}[V_{td}^\star V_{ts}]\, C_S| \tag{5.47}$$

Using the measured values $m_K = 497.6\,\mathrm{MeV}$, $f_K = (156.1 \pm 0.8)\mathrm{MeV}$, $(\Delta M_K)_{exp} = 3.483 \pm 0.006) \times 10^{-12}\mathrm{MeV}$ one obtains

$$C_\epsilon = \frac{G_F^2\, F_K^2\, m_K\, M_W^2}{6\sqrt{2}\,\pi^2\,\Delta M_K} = 3.65 \times 10^4. \tag{5.48}$$

Further, Lattice QCD [122] gives the input $B_K(2\,\mathrm{GeV}) = 0.54 \pm 0.05$, and using the central values of fitted values for the CKM parameters $A, \bar{\eta}, \bar{\rho}, \lambda$ from the PDG we find that the shift in $|\epsilon_K|$ is given by

$$\Delta|\epsilon_K| = 1.5\,(1.6) \times 10^{-12}(|\eta_U|^2 + 6\,(3)|\eta_U|^4) \tag{5.49}$$

for $M_s = 300\,(400)\mathrm{GeV}$. Considering $|\epsilon_K|_{exp} = (2.229 \pm 0.010) \times 10^{-3}$ while the same values employed above gives the central value $|\epsilon_K|_{theory} = 1.70 \times 10^{-3}$ one can set an upper limit on $|\eta_U|$ from $K^0-\bar{K}^0$ mixing by conservatively assigning one tenth of the discrepency between theory and experiment to the effect of octets. This gives an upper bound on $|\eta_U|$ of $48\,(56)$ for $M_s = 300\,(400)\mathrm{GeV}$. The weak mass dependence of the bound allows one to neglect Kaon mixing constraints for low masses, compared to R_b constraints on $|\eta_U|$, for light masses $M_s \ll 1\,\mathrm{TeV}$, in linear MFV.

The $B \to X_s\,\gamma$ decay rate constrains the combination $|\eta_U\,\eta_D|$, in the limit η_U is small, and was calculated in [27] . Using their result and the upper bound on $|\eta_U|$ from R_b, we determine the strongest upper bound on $|\eta_D|$ for light masses by requiring that the octet contribution to $B \to X_s\,\gamma$ is less than the $\sim 10\%$ SM theoretical and experimental errors. For $M_\pm = (75, 100, 200)$ and the corresponding maximum $|\eta_U| = (0.26, 0.27, 0.33)$, one

obtains an upper bound on $|\eta_D|$ of $(0.36, 0.39, 0.50)$. As $|\eta_U|$ decreases, the upper bound on $|\eta_D|$ is relaxed.

Finally, the electric dipole moment of the neutron constrains the imaginary part of the η_i and using [27] we find for light masses that $\mathrm{Im}[\eta_U^\star \, \eta_D^\star] < 1/10$ for $m_S = 100\,\mathrm{GeV}$.

5.4 Conclusions

We have considered the phenomenological constraints of the general scalar sector that contains one $(\mathbf{1}, \mathbf{2})_{1/2}$ Higgs doublet and a one $(\mathbf{8}, \mathbf{2})_{1/2}$ colour octet scalar doublet. To this end we have performed a modern fit in the STU and STUVWX approaches to EWPD and used these results to determine the allowed masses for light octets. We have demonstrated that, somewhat surprisingly, the six parameter fit formalism is more restrictive for light states due to strong correlations amongst the fit observables. We find that the octet doublet masses can be in the 100 GeV range. Such light octets can significantly effect the discovery strategies for a light Higgs by modifying the Higgs production mechanism through a one loop contribution to $gg \to h$ that is not well approximated by a local operator. Octets will also induce a further effective coupling at one loop between h and $\gamma\,\gamma$, ZZ and W^+W^- and would significantly effect Higgs discovery at LHC [123]. Despite this, we have shown that current production bounds on light octets at LEP2 and Tevatron do not rule out the low mass region and further studies for narrow resonances in the dijet invariant mass distribution and $h \to \gamma\,\gamma$ signal are required. Currently, octets are another example of physics beyond the SM that can significantly effect the properties of the Higgs and yet are otherwise relatively unconstrained experimentally.[15] For light octets, one possible alternate search strategy is to utilize the Higgs p_T distribution [126] to find indirect evidence for onshell octet scalars that have eluded direct detection.

We have also performed a joint fit for the Higgs and the octets by varying the Higgs

[15] For further studies of the modification of the properties of the Higgs through otherwise experimentally elusive new physics see [124, 125].

mass oblique corrections at one loop while allowing the masses of the octets to vary. Doing so we have demonstrated a mechanism that is quite general in its effect of giving a positive contribution to the T parameter when an extra doublet is present and fit to in EWPD. This allows the Higgs and octet to be simultaneously heavy and the Higgs can be as massive as its unitarity bound. For the parameter space where the Higgs mass is raised, h decaying to pairs of octets is kinematically suppressed. The search strategy for the heavy Higgs remains substantially the same with difficulties in constructing a mass peak due to the width of the Higgs resonance and large irreducible backgrounds to SM processes producing W^+W^- decays such as from $\bar{t}\,t$, and large Wj backgrounds. Likewise very heavy octets are also very broad resonances for large masses and are difficult to discover at hadron colliders with decays to $\bar{t}t$ dominating, and large SM backgrounds. Further dedicated studies of LHC phenomenology of this scenario are warranted, as are further dedicated studies to attempt to raise the lower mass bounds on octet scalar doublets.

5.A EWPD fit

The data and theory predictions used in constructing the fit are given in Table 2.

The numbers we use for the theory predictions are based on the 2008 PDG results of a global fit to the EWPD. The input values used in the theory predictions are

$$\begin{aligned} M_Z &= 91.1876 \pm 0.0021\text{GeV}, \qquad M_H = 96^{+29}_{-24}\text{GeV}, \\ m_t &= 173.1 \pm 1.4\text{GeV}, \qquad \alpha_s(M_Z) = 0.1217 \pm 0.0017\text{GeV}, \\ \hat{\alpha}(M_Z)^{-1} &= 127.909 \pm 0.0019, \qquad \Delta\,\alpha^{(5)}_{had} \approx 0.02799 \pm 0.00014. \end{aligned} \tag{5.50}$$

Observable	Data Used	Theory Prediction
M_W [GeV]	80.428 ± 0.039	80.380 ± 0.015
	80.376 ± 0.033	80.380 ± 0.015
M_Z [GeV]	91.1876 ± 0.0021	91.1874 ± 0.0021
Γ_Z [GeV]	2.4952 ± 0.0023	2.4954 ± 0.0009
Γ_{had} [GeV]	1.7444 ± 0.0020	1.7419 ± 0.0009
Γ_{inv} [MeV	499.0 ± 1.5	501.68 ± 0.07
$\Gamma_{l^+l^-}$ [MeV]	83.984 ± 0.086	84.002 ± 0.016
σ_{had} [nb]	41.541 ± 0.037	41.483 ± 0.008
R_e	20.804 ± 0.050	20.736 ± 0.010
R_μ	20.785 ± 0.033	20.736 ± 0.010
R_τ	20.764 ± 0.045	20.736 ± 0.010
R_b	0.21629 ± 0.00066	0.21578 ± 0.00005
R_c	0.1721 ± 0.0030	0.17224 ± 0.00003
A^e_{FB}	0.0145 ± 0.0025	0.01627 ± 0.00023
A^μ_{FB}	0.0169 ± 0.0013	0.01627 ± 0.00023
A^τ_{FB}	0.0188 ± 0.0017	0.01627 ± 0.00023
A^b_{FB}	0.0992 ± 0.0016	0.1033 ± 0.0007
A^c_{FB}	0.0707 ± 0.0035	0.0738 ± 0.0006
$\bar{s}^2_l(A^q_{FB})$	0.2316 ± 0.0018	0.2315 ± 0.0001
A_e	0.15138 ± 0.00216	0.1473 ± 0.0010
	0.1544 ± 0.0060	0.1473 ± 0.0010
	0.1498 ± 0.0049	0.1473 ± 0.0010
A_μ	0.142 ± 0.015	0.1473 ± 0.0010
A_τ	0.136 ± 0.015	0.1473 ± 0.0010
	0.1439 ± 0.0043	0.1473 ± 0.0010
A_b	0.923 ± 0.020	0.9347 ± 0.0001
A_c	0.670 ± 0.027	0.6679 ± 0.0004
g^2_L	0.3010 ± 0.0015	0.3039 ± 0.0002
g^2_R	0.0308 ± 0.0011	0.03000 ± 0.00003
$g^{\nu e}_V$	-0.040 ± 0.015	-0.0397 ± 0.0003
$g^{\nu e}_A$	-0.507 ± 0.014	-0.5064 ± 0.0001
$Qw(Cs)$	-73.16 ± 0.35	-73.16 ± 0.03
$Qw(Tl)$	-116.4 ± 3.6	-116.8 ± 0.04
Γ_W [GeV]	2.141 ± 0.041	2.0902 ± 0.0009

Table 5.2: Observables used in fit to oblique parameters.

The definitions of the oblique corrections we use are

$$\begin{aligned}
\frac{\alpha S}{4 s_W^2\, c_W^2} &= \left[\frac{\delta\Pi_{ZZ}(M_Z^2)-\delta\Pi_{ZZ}(0)}{M_Z^2}\right] - \frac{(c_W^2-s_W^2)}{s_W\, c_W}\delta\Pi'_{Z\,\gamma}(0) - \delta\Pi'_{\gamma\,\gamma}(0),\\
\alpha T &= \frac{\delta\Pi_{WW}(0)}{M_W^2} - \frac{\delta\Pi_{ZZ}(0)}{M_Z^2},\\
\frac{\alpha U}{4 s_W^2} &= \left[\frac{\delta\Pi_{WW}(M_W^2)-\delta\Pi_{WW}(0)}{M_W^2}\right] - c_W^2\left[\frac{\delta\Pi_{ZZ}(M_Z^2)-\delta\Pi_{ZZ}(0)}{M_Z^2}\right]\\
&\quad -s_W^2\,\delta\Pi'_{\gamma\,\gamma}(0) - 2\,s_W\,c_W\,\delta\Pi'_{Z\,\gamma}(0),\\
\alpha V &= \delta\Pi'_{ZZ}(M_Z^2) - \left[\frac{\delta\Pi_{ZZ}(M_Z^2)-\delta\Pi_{ZZ}(0)}{M_Z^2}\right],\\
\alpha W &= \delta\Pi'_{WW}(M_W^2) - \left[\frac{\delta\Pi_{WW}(M_W^2)-\delta\Pi_{WW}(0)}{M_W^2}\right],\\
\alpha X &= -s_W\,c_W\left[\frac{\delta\Pi_{Z\,\gamma}(M_Z^2)}{M_Z^2} - \delta\Pi'_{Z\,\gamma}(0)\right]
\end{aligned} \tag{5.51}$$

The self energies to determine these results are given by the following in terms of PV functions that match the definitions in [111] and are

$$16\,\pi^2\,\mu^{4-n}\int\frac{d^n\,q}{i\,(2\,\pi)^n}\,\frac{1}{q^2-m^2+i\,\epsilon} = A_0(m^2) \tag{5.52}$$

$$\begin{aligned}
16\,\pi^2\,\mu^{4-n}\int\frac{d^n\,q}{i\,(2\,\pi)^n}\,\frac{1}{[q^2-m_1^2+i\,\epsilon]\,[(q-p)^2-m_2^2+i\,\epsilon]} &= B_0(p^2,m_1^2,m_2^2)\\
16\,\pi^2\,\mu^{4-n}\int\frac{d^n\,q}{i\,(2\,\pi)^n}\,\frac{q_\mu}{[q^2-m_1^2+i\,\epsilon]\,[(q-p)^2-m_2^2+i\,\epsilon]} &= p_\mu\,B_1(p^2,m_1^2,m_2^2)\\
16\,\pi^2\,\mu^{4-n}\int\frac{d^n\,q}{i\,(2\,\pi)^n}\,\frac{q_\mu\,q_\nu}{[q^2-m_1^2+i\,\epsilon]\,[(q-p)^2-m_2^2+i\,\epsilon]} &= p_\mu\,p_\nu\,B_{21}(p^2,m_1^2,m_2^2),\\
&\quad +g_{\mu\,\nu}\,B_{22}(p^2,m_1^2,m_2^2)
\end{aligned}$$

Our results are

$$\begin{aligned}
\delta\Pi_{WW}(p^2) &= \frac{g_1^2}{2\pi^2}\Big[B_{22}(p^2,M_I^2,M_+^2) + B_{22}(p^2,M_R^2,M_+^2)\\
&- \frac{1}{2}A_0(M_+^2) - \frac{1}{4}A_0(M_R^2) - \frac{1}{4}A_0(M_I^2)\Big] \qquad (5.53)\\
\delta\Pi_{ZZ}(p^2) &= \frac{g_1^2}{2\pi^2 c_W^2}\Big[(1-2s_W^2)^2\left(B_{22}(p^2,M_+^2,M_+^2) - \frac{1}{2}A_0(M_+^2)\right)\\
&+ B_{22}(p^2,M_R^2,M_I^2) - \frac{1}{4}A_0(M_R^2) - \frac{1}{4}A_0(M_I^2)\Big] \qquad (5.54)\\
\delta\Pi_{\gamma\gamma}(p^2) &= \frac{2e^2}{\pi^2}\Big[B_{22}(p^2,M_+^2,M_+^2) - \frac{1}{2}A_0(M_+^2)\Big] \qquad (5.55)\\
\delta\Pi_{\gamma Z}(p^2) &= \frac{e g_1(1-2s_W^2)}{\pi^2 c_W}\Big[B_{22}(p^2,M_+^2,M_+^2) - \frac{1}{2}A_0(M_+^2)\Big] \qquad (5.56)
\end{aligned}$$

For $p^2 = 0$ these expressions become

$$\delta\Pi_{WW}(0) = \frac{g_1^2}{8\pi^2}\left(\frac{1}{2}f(M_+, M_R) + \frac{1}{2}f(M_+, M_I)\right) \tag{5.57}$$

$$\delta\Pi_{ZZ}(0) = \frac{g_1^2}{8\pi^2 c_W^2}\left(\frac{1}{2}f(M_R, M_I)\right) \tag{5.58}$$

where

$$f(m_1, m_2) = m_1^2 + m_2^2 - \frac{2m_1^2 m_2^2}{m_1^2 - m_2^2}\log\frac{m_1^2}{m_2^2} \tag{5.59}$$

The derivatives of the vacuum polarizations are

$$\delta\Pi'_{\gamma\gamma}(0) = -\frac{e^2}{6\pi^2}B_0(0, M_+^2, M_+^2) \tag{5.60}$$

$$\delta\Pi'_{\gamma Z}(0) = -\frac{e g_1(1 - 2s_W^2)}{12\pi^2 c_W}B_0(0, M_+^2, M_+^2) \tag{5.61}$$

5.B Renormalization

We use dim reg in $d = 4 - 2\,\epsilon$ dimensions. We introduce wavefunction renormalization and mass renormalization constants for the octet fields as usual

$$S_i = \frac{S_i^{(0)}}{\sqrt{Z_i}}, \qquad M_i = \frac{M_i^{(0)}}{\sqrt{Z_{Mi}}}. \tag{5.62}$$

However, in choosing renormalization conditions, we note that to define the masses and the mass splittings one cannot use $\overline{\rm MS}$, as in $\overline{\rm MS}$ the mass is defined to have only the divergence subtracted from the bare mass. The resulting renormalized mass in $\overline{\rm MS}$ is not shifted by the finite components of the loop corrections that we have determined. The renormalization prescription we use is the zero-momentum subtraction scheme [127], where we require that the self energy and its derivative with respect to external momentum, p^2, vanishes at $p^2 \to 0$. Note that the second derivative term in the Taylor expansion of the self energy does not contribute until two loop order and therefore can be neglected here. The counter terms in the lagrangian are given by

$$\sum_i \left[(Z_i - 1)(\partial^\mu S_i\, \partial_\mu S_i) - (Z_i\; Z_{Mi} - 1)M_i^2\; S_i^2\right]. \tag{5.63}$$

With this prescription the wavefunction renormalization and the mass counterterm are of the form

$$\begin{aligned} Z_i &= 1 - \frac{a}{\epsilon} - \frac{d\,\Sigma_i(p^2)}{d\,p^2}\mid_{p^2\to 0} \\ Z_{Mi} &= 1 + \frac{b}{\epsilon} + \Sigma_i(p^2)\mid_{p^2\to 0} + (1 - Z_i) \end{aligned} \tag{5.64}$$

where a, b are the coefficients of the p^2, M^2 dependent one loop divergences respectively and the Σ_i are the finite terms of the one loop self energy.

Using this scheme and the divergence properties of the PV functions, the wavefunction renormalization factors are determined to be

$$\begin{aligned} Z_I &= 1 - \frac{y_t^2\,|\eta_U|^2 + y_b^2\,|\eta_D|^2}{64\,\pi^2\,\epsilon} + \frac{g_1^2}{32\,\pi^2\,\epsilon}\left[1 + \frac{1}{2\,c_W^2}\right] + \frac{y_t^2|\eta_U|^2\,\log\left[\frac{m_t^2}{\mu^2}\right] + y_b^2|\eta_D|^2\,\log\left[\frac{m_b^2}{\mu^2}\right]}{32\,\pi^2} \\ &\quad + \frac{y_t^2\,\mathrm{Im}[\eta_U]^2 + y_b^2\,\mathrm{Im}[\eta_D]^2}{48\,\pi^2} + \frac{g_1^2}{16\,\pi^2}\left[b_0(0, M_W^2, m_\pm^2) + \frac{b_0(0, M_Z^2, M_R^2)}{2\,c_W^2}\right] \\ Z_R &= 1 - \frac{y_t^2\,|\eta_U|^2 + y_b^2\,|\eta_D|^2}{64\,\pi^2\,\epsilon} + \frac{g_1^2}{32\,\pi^2\,\epsilon}\left[1 + \frac{1}{2\,c_W^2}\right] + \frac{y_t^2|\eta_U|^2\,\log\left[\frac{m_t^2}{\mu^2}\right] + y_b^2|\eta_D|^2\,\log\left[\frac{m_b^2}{\mu^2}\right]}{32\,\pi^2} \\ &\quad + \frac{y_t^2\,\mathrm{Re}[\eta_U]^2 + y_b^2\,\mathrm{Re}[\eta_D]^2}{48\,\pi^2} + \frac{g_1^2}{16\,\pi^2}\left[b_0(0, M_W^2, M_\pm^2) + \frac{b_0(0, M_Z^2, M_I^2)}{2\,c_W^2}\right] \\ Z_\pm &= 1 - \frac{y_t^2\,|\eta_U|^2 + y_b^2\,|\eta_D|^2}{64\,\pi^2\,\epsilon} + \frac{g_1^2}{32\,\pi^2\,\epsilon}\left[1 + \frac{(1 - 2\,s_W^2)^2}{2\,c_W^2} + 2\,s_W^2\right] \\ &\quad + \frac{g_1^2}{32\,\pi^2}\left[b_0(0, M_W^2, M_I^2) + b_0(0, M_W^2, M_R^2) + \frac{(1 - 2s_W^2)^2 b_0(0, M_Z^2, M_\pm^2)}{c_W^2} - 4s_W^2\left(\log\left[\frac{M_\pm^2}{\mu^2}\right] - 1\right)\right] \\ &\quad - \frac{(y_b^2|\eta_D|^2 + y_t^2|\eta_U|^2)}{32\,\pi^2}\,b_0(0, m_b^2, m_t^2) \end{aligned} \tag{5.65}$$

Using these results the mass renormalization factors are determined to be

$$
\begin{aligned}
Z_{MI} &= (2 - Z_I) - \frac{v^2}{32\,\pi^2\,M_I^2}\left[y_t^4\,(\mathrm{Re}[\eta_U]^2 + 3\,\mathrm{Im}[\eta_U]^2)\left(\frac{1}{2\,\epsilon} - \log\left[\frac{m_t^2}{\mu^2}\right]\right)\right. \\
&\left. + y_b^4\,(\mathrm{Re}[\eta_D]^2 + 3\,\mathrm{Im}[\eta_D]^2)\left(\frac{1}{2\,\epsilon} - \log\left[\frac{m_b^2}{\mu^2}\right]\right)\right] - \frac{v^2\,(y_t^4|\eta_U|^2 + y_b^4|\eta_D|^2)}{32\pi^2\,M_I^2} \\
&+ \frac{g_1^2}{64\,\pi^2\,M_I^2\,\epsilon}\left[3\,M_W^2 - M_\pm^2 + \frac{(3\,M_Z^2 - M_R^2)}{2\,c^2}\right] \\
&+ \frac{g_1^2}{32\,\pi^2\,M_I^2}\left[(M_W^2 - 2M_\pm^2)\,b_0[0, M_W, M_\pm] + \frac{(M_Z^2 - 2\,M_R^2)\,b_0[0, M_Z, M_R]}{2c_W^2}\right. \\
&+ M_\pm^2\left(1 - \log\left[\frac{M_\pm^2}{\mu^2}\right]\right) + M_W^2\left(1 - 2\,\log\left[\frac{M_W^2}{\mu^2}\right]\right) + \frac{M_Z^2}{2\,c_W^2}\left(1 - 2\,\log\left[\frac{M_Z^2}{\mu^2}\right]\right) \\
&\left. + \frac{M_R^2}{2\,c_W^2}\left(1 - \log\left[\frac{M_R^2}{\mu^2}\right]\right)\right] \\
Z_{MR} &= Z_{MI}\,|_{M_R^2 \to M_I^2, Z_I \to Z_R, \mathrm{Re}\leftrightarrow\mathrm{Im}} \\
Z_{M\pm} &= (2 - Z_\pm) - \frac{v^2\,y_b^4\,|\eta_D|^2}{64\,\pi^2\,M_\pm^2}\left[\frac{1}{\epsilon} + b_0[0, m_b, m_t] - \log\left[\frac{m_b^2}{\mu^2}\right] + 1\right] \\
&- \frac{v^2\,y_t^4\,|\eta_U|^2}{64\,\pi^2\,M_\pm^2}\left[\frac{1}{\epsilon} + b_0[0, m_b, m_t] - \log\left[\frac{m_t^2}{\mu^2}\right] + 1\right] \\
&- \frac{y_b^2\,y_t^2 v^2}{64\,\pi^2\,M_\pm^2}\left[|\eta_D|^2\left(\frac{1}{\epsilon} - \log\left[\frac{m_t^2}{\mu^2}\right] + 1 + b_0[0, m_b, m_t]\right)\right. \\
&\left. + |\eta_U|^2\left(\frac{1}{\epsilon} - \log\left[\frac{m_b^2}{\mu^2}\right] + 1 + b_0[0, m_b, m_t]\right) - (\eta_D\,\eta_U + \eta_D^\star\,\eta_U^\star)\left(\frac{1}{\epsilon} + 2\,b_0[0, m_b, m_t]\right)\right] \\
&+ \frac{g_1^2}{32\,\pi^2\,\epsilon}\left[\frac{6\,M_W^2 - M_R^2 - M_I^2}{4\,M_\pm^2} + \frac{(1 - 2s_W^2)^2}{4\,c_W^2}\,\frac{(3\,M_Z^2 - M_\pm^2)}{M_\pm^2} - s_W^2\right] \\
&+ \frac{g_1^2}{64\,\pi^2\,M_\pm^2}\left[(M_W^2 - 2\,M_I^2)\,b_0[0, M_W, M_I] + (M_W^2 - 2\,M_R^2)\,b_0[0, M_W, M_R]\right. \\
&+ (M_Z^2 - 2\,M_\pm^2)\frac{(1 - 2s_W^2)^2}{c_W^2} b_0[0, M_Z, M_\pm] + M_I^2\left(1 - \log\left[\frac{M_I^2}{\mu^2}\right]\right) \\
&+ M_R^2\left(1 - \log\left[\frac{M_R^2}{\mu^2}\right]\right) + 2\,M_W^2\left(1 - 2\log\left[\frac{M_W^2}{\mu^2}\right]\right) \\
&\left. + \frac{M_Z^2\,(1 - 2s_W^2)^2}{c_W^2}\left(1 - 2\log\left[\frac{M_Z^2}{\mu^2}\right]\right) + M_\pm^2\,\frac{8s_W^4 - 8s_W^2 + 1}{c_W^2}\left(1 - \log\left[\frac{M_\pm^2}{\mu^2}\right]\right)\right]
\end{aligned}
\tag{5.66, 5.67}
$$

The remaining renormalization is for the mixing operator $S_R\,S_I$ which is renormalized as usual by introducing a further counter term to subtract the only divergences of composite operators as in $\overline{\mathrm{MS}}$

$$
\frac{\sqrt{Z_I}\,\sqrt{Z_R}\,(v^2\,S_R\,S_I)}{Z_{RI}} \tag{5.68}
$$

where

$$Z_{RI} = 1 + \frac{Z_R - 1}{2} + \frac{Z_I - 1}{2} + \frac{y_t^4 \,\mathrm{Re}[\eta_U]\,\mathrm{Im}[\eta_U] - y_b^4 \,\mathrm{Re}[\eta_D]\,\mathrm{Im}[\eta_D]}{32\,\pi^2\,\epsilon} \tag{5.69}$$

5.C Mixing of S_R and S_I

For completeness in examining one loop effects we determine the mixing between S_R and S_I. The mass matrix is given by

$$M_{RI} = \begin{pmatrix} M_I^2 + \delta\langle T\{S^I\,S^I\}\rangle_G + \delta\langle T\{S^I\,S^I\}\rangle_Y & \delta\langle T\{S^R\,S^I\}\rangle_Y \\ \delta\langle T\{S^R\,S^I\}\rangle_Y & M_R^2 + \delta\langle T\{S^R\,S^R\}\rangle_G + \delta\langle T\{S^R\,S^R\}\rangle_Y \end{pmatrix}. \tag{5.70}$$

We diagonalize the mass matrix by introducing a mixing angle and rotating the S_R, S_I fields to a diagonal mass basis S'_R, S'_I via

$$\begin{pmatrix} S_I \\ S_R \end{pmatrix} = \begin{pmatrix} \cos(\theta) & \sin(\theta) \\ -\sin(\theta) & \cos(\theta) \end{pmatrix} \begin{pmatrix} S'_I \\ S'_R \end{pmatrix}. \tag{5.71}$$

The mixing angle is given by

$$\sin(\theta) = \frac{|y_t^4\,B_0^\star(p^2, m_t^2, m_t^2)\mathrm{Re}(\eta_U)\,\mathrm{Im}(\eta_U) - y_b^4\,B_0^\star(p^2, m_b^2, m_b^2)\mathrm{Re}(\eta_D)\,\mathrm{Im}(\eta_D)|}{8\,\pi^2\,\lambda_2} \tag{5.72}$$

where $B_0^\star$ is the usual PV function with the divergence subtracted given by

$$B_0^\star(p^2, m_i^2, m_i^2) = -2 + \log\left(\frac{m_i^2}{\mu^2}\right) - \beta\,\log\left(\frac{1+\beta}{1-\beta}\right) \tag{5.73}$$

where $\beta = \sqrt{1 - 4m_i^2/p^2}$, which would be the velocity of the scalar produced in the CM frame which was subsequently to mix into another state with mass m_j. We take $p^2 = m_s^2$ as the mass splittings are a small perturbation in a radiatively induced mixing. If we take $\mu \simeq 1\,\mathrm{TeV}$ as the scale at which we impose exact $\mathrm{SU}(2_\mathrm{C})$ on our scalar potential, this gives a mixing angle

$$\sin(\theta) \simeq 0.04\,\frac{|\mathrm{Re}(\eta_U)|\,|\mathrm{Im}(\eta_U)|}{\lambda_2}, \tag{5.74}$$

which depends weakly on the value of m_s as the numerical coefficient changes by 25% for m_s varying between $0.01 - 300$ GeV. This mixing angle, if non zero, will effect the production cross section of the S_I, S_R states at LHC and Tevatron, and introduce mixing between the octetonia states discussed in [110].

Chapter 6

Conclusion

We have addressed two classes of questions in this thesis. The first aimed at improving our understanding of a variety of SM quantities, namely the CKM matrix element $|V_{ub}|$ and the production of final state jets. The second line of investigation determines constraints on an extension of the SM scalar sector using a range of current data, including electroweak precision measurements and flavour constraints.

It is important to over-constrain the SM unitarity triangle to test the consistency of this picture. $|V_{ub}|$ is of particular interest since it is the side opposite the well measured angle $\sin 2\beta$. It is theoretically challenging to obtain due to cuts on the large background from $b \to c$ processes, which give rise to a nonperturbative shape function at leading order. The shape function is universal in B decays and can be eliminated by relating different spectra. We consider the relation between the $B \to X_u \ell \nu_\ell$ P_+ spectrum and the $B \to X_s \gamma$ photon energy spectrum, given by a weight function, $W(\Delta, P_\gamma)$. We study the perturbative behaviour of this relation using a renormalon analysis and calculate the weight function to order $\alpha_s^n \beta_0^{n-1}$. We confirm the leading renormalon is at $u = 1/2$, corresponding to non-perturbative corrections at $\mathcal{O}(\Lambda_{QCD}/m_b)$, where we know there to be subleading shape functions present. We use a model of the photon spectrum to assess the importance of terms in the expansion of the weight function. Our results can be used

to estimate the perturbative uncertainty in the extraction of $|V_{ub}|$, which we find to be at the percent level.

Jet production tests QCD over a wide range of scales and is also important as a background to new physics searches. Factorization of perturbatively calculable hard interactions and jet functions from nonperturbative low-energy effects is critical to gaining control over such QCD processes. SCET is a useful tool with which to study jets since it separates physics associated with the jet and soft scale at the level of the Lagrangian, making the proof of all orders factorization much more tractable. In order to begin to address this problem, we show how to properly implement jet algorithms in the effective theory, clarifying the connection between cutoffs in SCET and phase space limits. By considering several jet algorithms at next-to-leading order, we show the consistency of this approach with a non-trivial zero-bin subtraction, which properly accounts for double counting in SCET. By studying the $k_\perp$ algorithm, we show the dependence of factorization on the ultraviolet cutoff.

If we view the SM as a low energy effective theory of an underlying theory that has $\mathrm{SU}(3)_{U_R} \times \mathrm{SU}(3)_{D_R} \times \mathrm{SU}(3)_{Q_L}$ flavour symmetry, which is broken to generate the Yukawa matrices, we are led to the idea of MFV. Manohar and Wise showed that only one type of exotic scalar can Yukawa couple to quarks consistently with MFV, a colour octet electroweak doublet. We consider an extension of the SM with one additional octet scalar and ask how light it can be, what the constraints on it are, and what the implications are for the Higgs mass. We carry out an up-to-date fit to electroweak precision data with an extended set of oblique parameters relevant for light states and find that the new scalars can be light, $\mathcal{O}(100\,\mathrm{GeV})$. We show that direct production bounds from LEPII and the Tevatron do not rule out light octet scalars and find that a promising signal is the octet decay to two photons. In order to investigate the impact of the new scalar on the Higgs mass from electroweak precision data, we perform a joint fit. Mass splitting in the exotic scalar doublet allows both the Higgs and octet scalar masses to be large and consistent

with electroweak precision data.

6.1 Future Directions

Efforts to improve the determination of $|V_{ub}|$ continue, for example through the Analysis of B-Meson Inclusive Spectra (SIMBA) project where a fit to charmless inclusive B meson decay spectra is to be carried out using all available information. Our study of the higher order perturbative corrections to the extraction of $|V_{ub}|$ based on relating the semi-leptonic and radiative B meson decays can be used as inputs to such a fit and to improve the accuracy of theoretical error estimates.

The work on final state jet production in SCET, in particular the consistent approach developed to implement a given jet algorithm with arbitrary parameters in the effective theory, has been used by other groups to study for example jet shape observables [128]. A future direction of this work is to apply the SCET approach to further study non-global observables, beginning with ones with fewer scales such as the left hemisphere mass distribution, which has been considered using perturbative QCD techniques [17].

Minimal flavour violation continues to be an interesting and actively explored idea by which flavour changing neutral currents can be suppressed in extensions of the SM. The phenomenology of coloured scalars at LHC also continue to be investigated. Our work demonstrates that the colour-octet electroweak-doublet scalars can be light and we strongly constrain their mass splitting using EWPD. This highlights possible phenomenologically interesting search strategies.

Bibliography

[1] L. Wolfenstein, Phys. Rev. Lett. **51**, 1945 (1983).

[2] C. Amsler et al. (Particle Data Group), Physics Letters B667, 1 (2008)

[3] C. W. Bauer, Z. Ligeti, M. Luke, A. V. Manohar and M. Trott, Phys. Rev. D **70**, 094017 (2004) [arXiv:hep-ph/0408002].

[4] C. W. Bauer, Z. Ligeti and M. E. Luke, Phys. Rev. D **64**, 113004 (2001) [arXiv:hep-ph/0107074].

[5] B. O. Lange, M. Neubert and G. Paz, Phys. Rev. D **72**, 073006 (2005) [arXiv:hep-ph/0504071].

[6] C. W. Bauer, S. Fleming and M. E. Luke, Phys. Rev. D **63**, 014006 (2000) [arXiv:hep-ph/0005275].

[7] J. C. Collins, D. E. Soper and G. Sterman, Adv. Ser. Direct. High Energy Phys. **5**, 1 (1988) [arXiv:hep-ph/0409313].

[8] G. Sterman, hep-ph/9606312.

[9] S. Catani, Y. L. Dokshitzer, M. Olsson, G. Turnock and B. R. Webber, Phys. Lett. B **269**, 432 (1991).

[10] C. W. Bauer, F. J. Tackmann and J. Thaler, JHEP **0812**, 010 (2008) [arXiv:0801.4026 [hep-ph]];

C. W. Bauer, F. J. Tackmann and J. Thaler, JHEP **0812**, 011 (2008) [arXiv:0801.4028 [hep-ph]].

[11] A. Hornig, C. Lee and G. Ovanesyan, JHEP **0905**, 122 (2009) [arXiv:0901.3780 [hep-ph]]; A. Hornig, C. Lee and G. Ovanesyan, Phys. Lett. B **677**, 272 (2009) [arXiv:0901.1897 [hep-ph]].

[12] C. W. Bauer and M. D. Schwartz, Phys. Rev. D **76** (2007) 074004 [arXiv:hep-ph/0607296].

[13] C. W. Bauer, S. Fleming, D. Pirjol and I. W. Stewart, Phys. Rev. D **63**, 114020 (2001) [arXiv:hep-ph/0011336].

[14] C. W. Bauer and I. W. Stewart, Phys. Lett. B **516**, 134 (2001) [arXiv:hep-ph/0107001].

[15] C. W. Bauer, D. Pirjol and I. W. Stewart, Phys. Rev. D **65**, 054022 (2002) [arXiv:hep-ph/0109045].

[16] C. W. Bauer, S. Fleming, D. Pirjol, I. Z. Rothstein and I. W. Stewart, Phys. Rev. D **66**, 014017 (2002) [arXiv:hep-ph/0202088].

[17] M. Dasgupta and G. P. Salam, Phys. Lett. B **512**, 323 (2001) [arXiv:hep-ph/0104277];
R. B. Appleby and G. P. Salam, arXiv:hep-ph/0305232;
A. Banfi, M. Dasgupta, K. Khelifa-Kerfa and S. Marzani, arXiv:1004.3483 [hep-ph].

[18] G. Sterman and S. Weinberg, Phys. Rev. Lett. **39** (1977) 1436.

[19] R. Barbieri and A. Strumia, arXiv:hep-ph/0007265.

[20] R. S. Chivukula and H. Georgi, Phys. Lett. B **188** (1987) 99.

[21] L. J. Hall and L. Randall, Phys. Rev. Lett. **65**, 2939 (1990).

[22] G. D'Ambrosio, G. F. Giudice, G. Isidori and A. Strumia, Nucl. Phys. B **645** (2002) 155 [arXiv:hep-ph/0207036].

[23] V. Cirigliano, B. Grinstein, G. Isidori and M. B. Wise, Nucl. Phys. B **728** (2005) 121 [arXiv:hep-ph/0507001].

[24] A. J. Buras, Acta Phys. Polon. B **34** (2003) 5615 [arXiv:hep-ph/0310208].

[25] G. C. Branco, A. J. Buras, S. Jager, S. Uhlig and A. Weiler, JHEP **0709** (2007) 004 [arXiv:hep-ph/0609067].

[26] S. L. Glashow and S. Weinberg, Phys. Rev. D **15**, 1958 (1977).

[27] A. V. Manohar and M. B. Wise, Phys. Rev. D **74** (2006) 035009 [arXiv:hep-ph/0606172].

[28] F. Campanario, M. Luke and S. Zuberi, Phys. Rev. D **79**, 094007 (2009) [arXiv:0811.1787 [hep-ph]].

[29] W. Y. Cheung, M. Luke and S. Zuberi, Phys. Rev. D **80**, 114021 (2009) [arXiv:0910.2479 [hep-ph]].

[30] C. P. Burgess, M. Trott and S. Zuberi, JHEP **0909**, 082 (2009) [arXiv:0907.2696 [hep-ph]].

[31] A. V. Manohar and M. B. Wise, Heavy Quark Physics, Cambridge Monographs on particle physics, nuclear physics, and cosmology (Cambridge University Press, 2000) and the references therein.

[32] B. Grinstein, R. P. Springer and M. B. Wise, Phys. Lett. B **202**, 138 (1988).

[33] J. Chay, H. Georgi and B. Grinstein, Phys. Lett. B **247**, 399 (1990).

[34] S. W. Bosch, B. O. Lange, M. Neubert and G. Paz, Nucl. Phys. B **699** (2004) 335 [hep-ph/0402094];

S. W. Bosch, B. O. Lange, M. Neubert and G. Paz, Phys. Rev. Lett. **93** (2004) 221801 [hep-ph/0403223].

[35] I. Bizjak *et al.* [Belle Collaboration], Phys. Rev. Lett. **95**, 241801 (2005) [arXiv:hep-ex/0505088].

[36] M. Neubert, Phys. Rev. D **49** (1994) 3392 [hep-ph/9311325];
M. Neubert, Phys. Rev. D **49** (1994) 4623 [hep-ph/9312311].

[37] A. K. Leibovich, I. Low and I. Z. Rothstein, Phys. Rev. D **61** (2000) 053006 [hep-ph/9909404];
A. K. Leibovich, I. Low and I. Z. Rothstein, Phys. Lett. B **486** (2000) 86 [hep-ph/0005124].

[38] A. H. Hoang, Z. Ligeti and M. Luke, Phys. Rev. D **71** (2005) 093007 [hep-ph/0502134].

[39] M. Beneke, A. P. Chapovsky, M. Diehl and T. Feldmann, Nucl. Phys. B **643**, 431 (2002) [arXiv:hep-ph/0206152].

[40] A. V. Manohar and I. W. Stewart, Phys. Rev. D **76** (2007) 074002 [arXiv:hep-ph/0605001].
B. Aubert *et al.* [BABAR Collaboration], Phys. Rev. Lett. **100**, 171802 (2008) [arXiv:0708.3702 [hep-ex]].

[41] J. Chay, H. Georgi and B. Grinstein, Phys. Lett. B **247** (1990) 399;
M. A. Shifman and M. B. Voloshin, Sov. J. Nucl. Phys. **41** (1985) 120;
I. I. Y. Bigi, N. G. Uraltsev and A. I. Vainshtein, Phys. Lett. B **293** (1992) 430 [Erratum-ibid. B **297** (1993) 477] [hep-ph/9207214];
I. I. Y. Bigi, M. A. Shifman, N. G. Uraltsev and A. I. Vainshtein, Phys. Rev. Lett. **71** (1993) 496 [hep-ph/9304225];
A. V. Manohar and M. B. Wise, Phys. Rev. D **49** (1994) 1310 [hep-ph/9308246].

[42] A. F. Falk, Z. Ligeti and M. B. Wise, Phys. Lett. B **406** (1997) 225 [hep-ph/9705235];
R. D. Dikeman and N. G. Uraltsev, Nucl. Phys. B **509** (1998) 378 [hep-ph/9703437].

[43] I. I. Y. Bigi, M. A. Shifman, N. G. Uraltsev and A. I. Vainshtein, Int. J. Mod. Phys. A **9** (1994) 2467 [hep-ph/9312359].

[44] C. W. Bauer, M. E. Luke and T. Mannel, Phys. Rev. D **68** (2003) 094001 [hep-ph/0102089];
C. W. Bauer, M. Luke and T. Mannel, Phys. Lett. B **543** (2002) 261 [hep-ph/0205150]

[45] S. W. Bosch, M. Neubert and G. Paz, JHEP **0411** (2004) 073 [hep-ph/0409115].

[46] B. O. Lange, M. Neubert and G. Paz, JHEP **0510** (2005) 084 [hep-ph/0508178].

[47] K.S.M. Lee and I.M. Stewart, Nucl. Phys. B **721** (2005) 325 [hep-ph/0409045].

[48] M. Beneke, F. Campanario, T. Mannel and B. Pecjak, JHEP **06** (2005) 071 [hep-ph/0411395].

[49] S. J. Lee, M. Neubert and G. Paz, Phys. Rev. D **75** (2007) 114005 [hep-ph/0609224].

[50] B. O. Lange, JHEP **0601** (2006) 104 [hep-ph/0511098].

[51] M. Beneke and V. M. Braun, [hep-ph/0010208].

[52] P. Ball, M. Beneke and V. M. Braun, Nucl. Phys. B **452** (1995) 563 [hep-ph/9502300].

[53] G. 't Hooft, in *The Whys of Subnuclear Physics*, edited by A. Zichichi (Plenum, New York, 1978).

[54] J. R. Andersen and E. Gardi, JHEP **0701** (2007) 029 [hep-ph/0609250];
E. Gardi, JHEP **0404** (2004) 049 [hep-ph/0403249].

[55] P. Gambino, E. Gardi and G. Ridolfi, JHEP **0612** (2006) 036 [hep-ph/0610140];
V. Aquila, P. Gambino, G. Ridolfi and N. Uraltsev, Nucl. Phys. B **719** (2005) 77 [hep-ph/0503083].

[56] M. Neubert, Eur. Phys. J. C **40** (2005) 165 [hep-ph/0408179].

[57] C. W. Bauer and A. V. Manohar, Phys. Rev. D **70** (2004) 034024 [hep-ph/0312109].

[58] Z. Ligeti, M. E. Luke, A. V. Manohar and M. B. Wise, Phys. Rev. D **60** (1999) 034019 [hep-ph/9903305].

[59] U. Aglietti, G. Ricciardi and G. Ferrera, Phys. Rev. D **74** (2006) 034004 [hep-ph/0507285];
U. Aglietti, G. Ricciardi and G. Ferrera, Phys. Rev. D **74** (2006) 034006 [hep-ph/0509271].

[60] K. Melnikov and A. Mitov, Phys. Lett. B **620** (2005) 69 [hep-ph/0505097].

[61] M. Misiak, arXiv:0808.3134 [hep-ph].

[62] C.W. Bauer, A.V. Manohar and M.B. Wise, Phys. Rev. Lett. **91** (2003) 122001 [arXiv:hep-ph/0212255].

[63] C.W. Bauer, C. Lee, A.V. Manohar and M.B. Wise, Phys. Rev. D **70** (2004) 034014 [arXiv:hep-ph/0309278].

[64] C. W. Bauer, S. P. Fleming, C. Lee and G. Sterman, Phys. Rev. D **78**, 034027 (2008) [arXiv:0801.4569 [hep-ph]].

[65] S. Fleming, A. H. Hoang, S. Mantry and I. W. Stewart, Phys. Rev. D **77**, 074010 (2008) [arXiv:hep-ph/0703207].

[66] C.W. Bauer, A. Hornig and F.J. Tackmann, arXiv:0808.2191 [hep-ph].

[67] M. Trott, Phys. Rev. D **75** (2007) 054011 [arXiv:hep-ph/0608300].

[68] JADE Collaboration, S. Bethke *et al.*, Phys. Lett. B **213** (1988) 235.

[69] A. V. Manohar, Phys. Rev. D **68** (2003) 114019 [arXiv:hep-ph/0309176].

[70] A. Idilbi and T. Mehen, Phys. Rev. D **75** (2007) 114017 [arXiv:hep-ph/0702022].

[71] A. Idilbi and T. Mehen, Phys. Rev. D **76** (2007) 094015 [arXiv:hep-ph/0707.1101].

[72] J.-Y. Chiu, A. Fuhrer, A. H. Hoang, R. Kelley and A. V. Manohar, arXiv:hep-ph/0901.1332.

[73] G. Kramer and B. Lampe, Z. Phys. C **34** (1987) 497 [Erratum-ibid. C **42** (1989) 504].

[74] N. Brown and W. J. Stirling, Z. Phys. C **53**, 629 (1992).

[75] N. Brown and W. J. Stirling, Phys. Lett. B **252** (1990) 657-662.

[76] S. Mukhi and G. Sterman, Nucl. Phys. B **206**, 221 (1982).

[77] J. Y. Chiu, A. Fuhrer, R. Kelley and A. V. Manohar, arXiv:0909.0012 [hep-ph].

[78] L. Susskind, Phys. Rev. D **20** (1979) 2619.

[79] S. Weinberg, Phys. Rev. D **19** (1979) 1277.

[80] P. Sikivie, L. Susskind, M. B. Voloshin and V. I. Zakharov, Nucl. Phys. B **173** (1980) 189.

[81] T. Feldmann and T. Mannel, Phys. Rev. Lett. **100** (2008) 171601 [arXiv:0801.1802 [hep-ph]].

[82] A. L. Kagan, G. Perez, T. Volansky and J. Zupan, arXiv:0903.1794 [hep-ph].

[83] T. Feldmann, M. Jung and T. Mannel, arXiv:0906.1523 [hep-ph].

[84] J. Erler, P. Langacker, S. Munir and E. R. Pena, arXiv:0906.2435 [hep-ph].

[85] T. Plehn and T. M. P. Tait, J. Phys. G **36**, 075001 (2009) [arXiv:0810.3919 [hep-ph]].

[86] S. Y. Choi, M. Drees, J. Kalinowski, J. M. Kim, E. Popenda and P. M. Zerwas, Phys. Lett. B **672**, 246 (2009) [arXiv:0812.3586 [hep-ph]].

[87] C. T. Hill, Model," Phys. Lett. B **266** (1991) 419.

[88] B. A. Dobrescu, K. Kong and R. Mahbubani, Phys. Lett. B **670**, 119 (2008) [arXiv:0709.2378 [hep-ph]].

[89] B. A. Dobrescu, K. Kong and R. Mahbubani, JHEP **0707**, 006 (2007) [arXiv:hep-ph/0703231].

[90] P. Y. Popov, A. V. Povarov and A. D. Smirnov, Mod. Phys. Lett. A **20**, 3003 (2005) [arXiv:hep-ph/0511149].

[91] I. Dorsner and I. Mocioiu, Nucl. Phys. B **796** (2008) 123 [arXiv:0708.3332 [hep-ph]].

[92] P. Fileviez Perez, R. Gavin, T. McElmurry and F. Petriello, Phys. Rev. D **78** (2008) 115017 [arXiv:0809.2106 [hep-ph]].

[93] P. Fileviez Perez, H. Iminniyaz and G. Rodrigo, Phys. Rev. D **78** (2008) 015013 [arXiv:0803.4156 [hep-ph]].

[94] P. Fileviez Perez and M. B. Wise, arXiv:0906.2950 [hep-ph].

[95] P. H. Frampton and S. L. Glashow, Phys. Lett. B **190** (1987) 157.

[96] A. Idilbi, C. Kim and T. Mehen, arXiv:0903.3668 [hep-ph].

[97] M. Gerbush, T. J. Khoo, D. J. Phalen, A. Pierce and D. Tucker-Smith, Phys. Rev. D **77** (2008) 095003 [arXiv:0710.3133 [hep-ph]].

[98] C. P. Burgess, S. Godfrey, H. Konig, D. London and I. Maksymyk, Phys. Lett. B **326** (1994) 276 [arXiv:hep-ph/9307337].

[99] I. Maksymyk, C. P. Burgess and D. London, Phys. Rev. D **50** (1994) 529 [arXiv:hep-ph/9306267].

[100] B. Holdom and J. Terning, Phys. Lett. B **247** (1990) 88, M. E. Peskin and T. Takeuchi, Phys. Rev. Lett. **65**, 964 (1990). M. Golden and L. Randall, Nucl. Phys. B **361**(1991)3,

[101] M. E. Peskin and T. Takeuchi, Phys. Rev. D **46** (1992) 381.

[102] G. Altarelli and R. Barbieri, Phys. Lett. B **253** (1991) 161. G. Altarelli, R. Barbieri and S. Jadach, Nucl. Phys. B **369** (1992) 3 [Erratum-ibid. B **376** (1992) 444].

[103] M. B. Einhorn, D. R. T. Jones and M. J. G. Veltman, Nucl. Phys. B **191**, 146 (1981).

[104] M. E. Peskin and J. D. Wells, Phys. Rev. D **64**, 093003 (2001) [arXiv:hep-ph/0101342].

[105] P. H. Chankowski, T. Farris, B. Grzadkowski, J. F. Gunion, J. Kalinowski and M. Krawczyk, Phys. Lett. B **496** (2000) 195 [arXiv:hep-ph/0009271].

[106] R. Barbieri, L. J. Hall and V. S. Rychkov, Phys. Rev. D **74**, 015007 (2006) [arXiv:hep-ph/0603188].

[107] N. G. Deshpande and E. Ma, Phys. Rev. D **18**, 2574 (1978).

[108] C. Amsler et al. (Particle Data Group), Physics Letters B667, 1 (2008)

[109] M. I. Gresham and M. B. Wise, Phys. Rev. D **76** (2007) 075003 [arXiv:0706.0909 [hep-ph]].

[110] C. Kim and T. Mehen, arXiv:0812.0307 [hep-ph].

[111] J. D. Wells, arXiv:hep-ph/0512342.

[112] M. Pospelov and M. Trott, JHEP **0904**, 044 (2009) [arXiv:0812.0432 [hep-ph]].

[113] The CDF Collaboration, CDF Note 8954 v1.0

[114] T. Aaltonen *et al.* [CDF Collaboration], arXiv:0812.4036 [hep-ex].

[115] V. M. Abazov *et al.* [D0 Collaboration], Phys. Lett. B **668**, 98 (2008) [arXiv:0804.3664 [hep-ex]].

[116] O. Antunano, J. H. Kuhn and G. Rodrigo, Phys. Rev. D **77** (2008) 014003 [arXiv:0709.1652 [hep-ph]].

[117] T. Aaltonen *et al.* [CDF Collaboration], Phys. Rev. Lett. **101**, 202001 (2008) [arXiv:0806.2472 [hep-ex]].

[118] The CDF Collaboration, CDF Note 9724 v1.0

[119] The D0 Collaboration, D0 Note 5858-CONF

[120] V. M. Abazov *et al.* [D0 Collaboration], arXiv:0901.1887 [hep-ex].

[121] G. Buchalla, A. J. Buras and M. E. Lautenbacher, Rev. Mod. Phys. **68**, 1125 (1996) [arXiv:hep-ph/9512380].

[122] V. Lubicz and C. Tarantino, Nuovo Cim. **123B**, 674 (2008) [arXiv:0807.4605 [hep-lat]].

[123] A. V. Manohar and M. B. Wise, Phys. Lett. B **636**, 107 (2006) [arXiv:hep-ph/0601212].

[124] S. Mantry, M. Trott and M. B. Wise, Phys. Rev. D **77**, 013006 (2008) [arXiv:0709.1505 [hep-ph]].

[125] S. Mantry, M. J. Ramsey-Musolf and M. Trott, Phys. Lett. B **660**, 54 (2008) [arXiv:0707.3152 [hep-ph]].

[126] C. Arnesen, I. Z. Rothstein and J. Zupan, arXiv:0809.1429 [hep-ph].

[127] N. N. Bogoliubov and O. S. Parasiuk, Acta Math. **97**, 227 (1957).

[128] S. D. Ellis, C. K. Vermilion, J. R. Walsh, A. Hornig and C. Lee, arXiv:1001.0014 [hep-ph].